6-2021

# Adaptive-Optimal Control of Spacecraft near Asteroids

Madhur Tiwari

# ADAPTIVE-OPTIMAL CONTROL OF SPACECRAFT NEAR ASTEROIDS

By

Madhur Tiwari

A Dissertation Submitted to the Faculty of Embry-Riddle Aeronautical University

In Partial Fulfillment of the Requirements for the Degree of

Doctor of Philosophy in Aerospace Engineering

June 2021

Embry-Riddle Aeronautical University

Daytona Beach, Florida

ADAPTIVE-OPTIMAL CONTROL OF SPACECRAFT
NEAR ASTEROIDS

By

Madhur Tiwari

This Dissertation was prepared under the direction of the candidate's Dissertation Committee Chair, Dr. Troy Henderson, Department of Aerospace Engineering, and has been approved by the members of the Dissertation Committee. It was submitted to the Office of the Senior Vice President for Academic Affairs and Provost, and was accepted in the partial fulfillment of the requirements for the Degree of Philosophy in Aerospace Engineering.

DISSERTATION COMMITTEE

Troy A. Henderson Digitally signed by Troy A. Henderson Date: 2021.07.12 15:58:02 -04'00'

Chairman, Dr. Troy Henderson

Richard J. Prazenica Digitally signed by Richard J. Prazenica Date: 2021.07.12 16:26:34 -04'00'

Member, Dr. Richard Prazenica

Eric Coyle Digitally signed by Eric Coyle Date: 2021.07.13 10:07:15 -04'00'

Member, Dr. Eric Coyle

Morad Nazari Digitally signed by Morad Nazari Date: 2021.07.12 19:06:59 -04'00'

Member, Dr. Morad Nazari

Sirish Namilae Digitally signed by Sirish Namilae Date: 2021.07.13 11:28:34 -04'00'

Graduate Program Coordinator,
Dr. Sirish Namilae

07/13/2021

Date

Maj Mirmirani Digitally signed by Maj Mirmirani Date: 2021.07.13 09:04:21 -07'00'

Dean of the College of Engineering,
Dr. Maj Mirmirani

07/13/2021

Date

Lon Moeller Digitally signed by Lon Moeller Date: 2021.07.13 12:59:48 -04'00'

Senior Vice President for Academic Affairs and Provost,
Dr. Lon Moeller

07/13/2021

Date

## ACKNOWLEDGEMENTS

First and foremost, I would like to thank my mom and dad for their continuous support throughout my life. I want to thank my wife, Kanika, for all her sacrifices and being there during all the ups and downs. Without you, this wouldn't have happened. I want to thank my brothers, Varad and Veeru. My friends for life.

I want to thank Dr. Troy Henderson for giving me an opportunity when no one else did. Thank you for believing in me and being there for me whenever I needed it. Special thanks to Dr. Richard Prazenica, who is not only a great mentor but a very good friend. Thank you for taking the time out for our long conversations and sharing your part of life with me. I want to thank Dr. Eric Coyle for being such a fantastic advisor and being available for our discussions whenever I needed it. I look forward to our future works. I would also like to thank Dr. Morad Nazari for being there as someone I strive to be. Your discipline and work ethic is something I try to incorporate in my academic life. Honestly, I couldn't have asked for a better group of gentlemen to guide me through my academic journey. I am so thankful to all of you that no words can describe.

Nothing can be accomplished without a team. I want to thank all my friends throughout my academic life. Thank you, Naveen, Anu, Krishna, Audrey, Sharath, David, Chris, Daniel, Suma, Peter, for all the good times.

I want to thank everyone in the Aerospace Department for giving me this opportunity and for always supporting me throughout my Ph.D. I want to acknowledge the grant from Defense Advanced Research Projects Agency (DARPA) under Contract No. D16PC00110 for partly funding my Ph.D.

## ABSTRACT

Spacecraft dynamics and control in the vicinity of an asteroid is a challenging and exciting problem. Currently, trajectory tracking near asteroid requires extensive knowledge about the asteroid and constant human intervention to successfully plan and execute proximity operation. This work aims to reduce human dependency of these missions from a guidance and controls perspective. In this work, adaptive control and model predictive control are implemented to generating and tracking obstacle avoidance trajectories in asteroid's vicinity.

Specifically, direct adaptive control derived from simple adaptive control is designed with $e$ modification to track user-generated trajectories in the presence of unknown system and sensor noise. This adaptive control methodology assumes no information on the system dynamics, and it is shown to track trajectories successfully in the vicinity of the asteroid. Then a nonlinear model predictive control methodology is implemented to generate obstacle avoidance trajectories with minimal system information namely mass and angular velocity of the asteroid.

Ultimately, the adaptive control system is modified to include feed-forward control input from the nonlinear model predictive control. It is shown through simulations that the new control methodology names direct adaptive model predictive control (DAMPC), is able to generate sub-optimal trajectories. A comparative study is done with Asteroid Bennu, Kleopatra and Eros to show the benefits of DAMPC over adaptive control and MPC. A study on effect of noisy measurements and model is also conducted on adaptive control and direct adaptive model predictive control.

# TABLE OF CONTENTS

## LIST OF FIGURES

Figure Page

Figure Page

Figure Page

# LIST OF TABLES

# NOMENCLATURE

| | | |
|---|---|---|
| r | position | m |
| $\dot{r}$ | velocity | m/s |
| $\ddot{r}$ | Acceleration | m/$s^2$ |
| t | time | s |
| $K_e$ | Time-varying control gain matrix | |
| $K_e$ | Tme-varying feedforward control gains | |
| $K_x$ | Time-varying feedforward control gains | |
| Q | Gain matrix for state | |
| R | Gain matrix for control | |
| $e_y$ | Output error | |
| $e_x$ | State error | |
| u | Control input | m/$s^2$ |
| a, b, c | Principal axes of the ellipsoid | km |
| m | mass | kg |
| x, y, z | Positions in 3-D coordinate frame | km |
| F(r) gp | Force due to polyhedral gravity | N |
| f(r, σ) gg | Force due to gravity gradient | N |
| f(σ) srp | Force due to solar radiation pressure | N |
| σ | Modified Rodriguez parameter | |

| | | |
|---|---|---|
| Tgg | Torque due to gravity gradient | Nm |
| Φ | Principal rotation vector | |
| e | Principal unit vector | |
| q | Quaternion | |
| σ̇ | MRP rate of change | MRP/s |
| $\sigma^x$ | Skew symmetric matrix | |
| $C_{DCM}$ | Direction cosine matrix | |
| I | Inertia matrix | kg$m^2$ |
| $\hat{n}$ | Normal unit vector | |
| agp | Acceleration due to polyhedral gravity | m/$s^2$ |
| $s^{SC}$ | Sun-pointing vector | |
| Tsrp | Torque due to solar radiation pressure | Nm |
| P | Positive definite matrix | |
| $\widetilde{K}$ | Ideal gain matrix | |
| $\dot{z}$ | Zero dynamics | |
| A | State matrix | |
| x(t) | States | |
| V(t) | Lyapunov function | |
| Γ | Gain | |
| $I_x, I_y, I_z$ | Principal axes of inertia | |

# 1. Introduction

Autonomous spacecraft trajectory tracking near asteroids is a challenging and exciting problem that has received considerable attention from researchers and scientists. The problem presents several challenges, but one of the main issue is the unknown dynamical environment near asteroids. Before missions to these asteroids, very little is known about the asteroid characteristics, especially for close proximity missions. This is because the asteroids are usually very small and distant, and earth-based technologies cannot capture precise details of the asteroid environment.

Another big challenge is a delay in communication. Currently, it takes around 15-20 minutes to send a one-way signal to spacecrafts orbiting around asteroids due to large distances (Shea, 2018). This delay causes significant issues as real-time control of spacecraft becomes impossible, and the scientists have to rely on old data for estimating spacecraft trajectories and parameters. This is a significant problem for missions to asteroids where the dynamical environment is rapidly changing and real-time communication is necessary (Tsuda et al., 2013).

With communication delays and lack of knowledge, the spacecraft has to rely on an earth-based ground station to perform mission objectives like orbiting, proximity missions, landing, and sample collection (Scheeres, 2006). In the future, the goal would be to minimally rely on ground stations and perform various aspects of missions like trajectory generation and tracking autonomously.

The main objective of this work is to design and implement a control methodology that does not rely on knowledge of an asteroid's dynamical environment and can generate and track sub-optimal/optimal trajectories around asteroids. This is achieved by

designing and implementing adaptive control techniques based on simple adaptive control (Kaufman et al., 1997a). The adaptive controller is further modified to include model predictive control to the control system while generating obstacle avoidance trajectories around the asteroid.

### 1.1. Adaptive Control

In this work, a direct adaptive controller based on simple adaptive control methodology is considered. This is an output feedback controller with two feed-forward terms as follows:

$$\mathbf{u} = \mathbf{K}_e(t)\mathbf{e}_y + \mathbf{K}_x(t)\mathbf{x}_m + \mathbf{K}_u(t)\mathbf{u}_m \tag{1.1}$$

In Equation 1.1, $\mathbf{e}_y$ is the output tracking error, defined as,

$$\mathbf{e}_y(t) = \mathbf{y}_m(t) - \mathbf{y}(t) \tag{1.2}$$

$$\mathbf{e}_y(t) = \mathbf{C}\mathbf{x}_m(t) - \mathbf{C}\mathbf{x}(t) \tag{1.3}$$

where $\mathbf{y}_m \in R^m$ and $\mathbf{y} \in R^m$ are the output vectors of the reference and system models respectively. $\mathbf{K}_e(t) \in R^{m\times m}$ is the time-varying control gain matrix, $\mathbf{K}_x(t) \in R^{m\times n}$ and $\mathbf{K}_u(t) \in R^{m\times m}$ are time-varying feedforward control gains, and $\mathbf{x}_m v \in R^n$ and $\mathbf{u}_m \in R^m$ are the states and control vectors of the reference model.

This form of adaptive control is very advantageous to our mission scenarios as it does not require any dynamical parameters such as asteroid's gravity, rotation rate, inertia, solar radiation pressure, or spacecraft parameters. The adaptive control also does not require full state feedback, but only the states are being tracked.

The adaptive controller above requires a user-given trajectory to track and cannot generate obstacle-avoidance trajectories to achieve full control autonomy. Also, the

adaptive control is not optimal, which could be an issue for long-term missions with limited fuel capacity.

Therefore, to address the shortcomings of adaptive control, a nonlinear model predictive controller (NMPC) is designed and implemented. Initially, the NMPC is studied as a standalone controller to generate trajectories, but later the adaptive control law is modified to include NMPC as a feed-forward term. The ultimate goal is to design a controller that combines the adaptive control and nonlinear model predictive control advantages while using minimal information about the asteroid parameters.

### 1.2. Model Predictive Control

Model predictive control is currently being extensively studied and implemented in various applications such as autonomous driving, unmanned aerial vehicles, and spacecrafts. MPC works by optimizing a cost function to generate trajectories over a finite time horizon (Mehrez Said, 2018). The trajectories generated could be optimal or sub-optimal depending on the convexity or non-convexity of the system or constraints. One of the main advantages of the MPC is that a nonlinear system with nonlinear system constraints can be considered for optimization.

This work aims to implement a feed-forward nonlinear model predictive control methodology to generate sub-optimal trajectories that can be tracked by implementing the adaptive controller (Andersson et al., 2019). The NMPC designed in this work will use only the least amount of available information, such as the mass of the asteroid and approximated rotation rate, which is readily available by light curve analysis.

Clearly, the feedfoward NMPC designed with a two-body approximation will not able to handle the disturbances produced from the non-spherical gravity and other forces

acting on the spacecraft. In that case, the adaptive control works as a disturbance rejecting control while tracking sub-optimal/optimal trajectories from the NMPC. Even though a feedback NMPC control can be applied in this case which inheritably rejects disturbances, the stability of the NMPC cannot be guaranteed and the system is computationally expensive.

Therefore, an NMPC is implemented as a feed-foward control which is augmented by the direct adaptive control. The nonlinear model predictive control implemented is a discrete control system which is discretized by the fourth order Runge-Kutta scheme and the multiple shooting method is implemented with an interior point numerical solver known as Casadi (Andersson et al., 2019). In the section, the modified adaptive control with the feed-forward NMPC is presented where the control law takes the adavante of the optimality of the NMPC and the robust of the direct adaptive control system. The formulation of NMPC is given as follows:

$$\min_{\mathbf{u}_k,..,\mathbf{u}_{k+N-1},\mathbf{x}_k,..,\mathbf{x}_{k+N-1}} \quad F(\mathbf{x}_N) + \sum_{k=0}^{N-1} [\mathbf{x}(k) - \mathbf{x_r}(k)]^T \mathbf{Q} [\mathbf{x}(k) - \mathbf{x_r}(k)] + \mathbf{u}(k)^T \mathbf{R} \mathbf{u}(k) \tag{1.4}$$

subjected to:

$$\mathbf{x}_{k+1} = \mathbf{f}(\mathbf{x}_k, \mathbf{u}_k),\ \mathbf{x} \in R^6,\ k = 0, ..., N \tag{1.5}$$

$$\mathbf{u}_{min}(k) \leq \mathbf{u}(k) \leq \mathbf{u}_{max}(k),\ k = 0, ..., N-1 \tag{1.6}$$

$$1 - \left[ \left( \frac{x_k}{a} \right)^2 + \left( \frac{y_k}{b} \right)^2 + \left( \frac{z_k}{c} \right)^2 \right] \leq 0 \tag{1.7}$$

Here Equation 1.4 defines the cost function to be minimized. The dynamical constraints are given in Equation 1.5 and control constraints are given in Equation 1.6 where $\mathbf{u}_{min}$ and $\mathbf{u}_{max}$ are the lower and upper-bound of the control effort. The safety ellipsoid

constraint is given in Equation 1.7. The term $F(\mathbf{x}_N)$ is the cost on the final state and is defined as,

$$F(\mathbf{x}_N) = [\mathbf{x}_N - \mathbf{r}_N]^T \mathbf{P} [\mathbf{x}_N - \mathbf{r}_N] \quad \mathbf{x}_N, \mathbf{r}_N \in R^6, \quad \mathbf{P} \in R^{6\times 6} \tag{1.8}$$

### 1.3. Direct-Adaptive Model Predictive Control

A control methodology that takes advantage of the adaptive control and the model predictive control is designed such that adaptive control is implemented as a feedback control law while the NMPC is implemented as a feed-forward control law. The resulting control system computationally efficient and sub-optimal while being robust to the unknown dynamical parameters and noise. The direct-adaptive model predictive control (DAMPC) is defined as follows,

$$\mathbf{u}_{DAMPC} = \mathbf{K}_e(t)\mathbf{e}_y + \mathbf{u}_{MPC} \tag{1.9}$$

Here $\mathbf{K}_e(t) \in R^{n\times n}$ is the adaptive control law, $\mathbf{e}_y \in R^n$ is the error term between the actual and ideal reference model and $\mathbf{u}_{MPC}$ is the feed-forward model predictive control.

The direct adaptive-model predictive control (DAMPC) has a few major advantages:

- The adaptive control component adds robustness to the MPC since the system model for the MPC is a low-fidelity simplified version of the gravitational field, and the unmodeled forces are missing.
- The MPC adds optimality to the control system via the feed-forward control inputs and generates sub-optimal trajectories for the adaptive control to track.
- MPC also adds better noise handling to the adaptive control system by the addition of feed-forward control. This especially helps since the adaptive control is

initialized by zero initial condition.

### 1.4. Contributions of this dissertation

The main objective of this work is to design and implement adaptive control and model predictive control systems to increase the autonomy of spacecraft proximity operations near asteroids. Three different asteroids are considered for simulation purposes. A summary of the contributions is outlined as follows:

- A detailed spacecraft orbital and attitude dynamical model in asteroid body frame is implemented with solar radiation pressure, polyhedral gravitational model, and gravity gradient force and torques.
- An adaptive control system with a simple adaptive control methodology is implemented and studied.
- The adaptive control system is modified using an $e$ modification for robustness to system and sensor noise. A Lyapunov stability analysis is presented with robustness modification terms. Several simulation studies are done to show the adaptability of the control system.
- A nonlinear model predictive control framework with obstacle avoidance is designed and implemented. Trajectory tracking and point-to-point trajectory generation cases are discussed.
- A novel control system based on adaptive control and model predictive control is designed and implemented. The control system is studied in detail with various simulations, and the performance and robustness of the control system is compared to both the MPC and adaptive control systems.

# 2. Literature Review

There has been a growing interest in exploring near-earth asteroids for scientific, threat avoidance, and future industrial projects. Due to these recent developments, the scientific community is actively working to devise innovative technologies that can make accessing asteroids easy, autonomous and safe. This chapter will present state of the art in spacecraft dynamics and control in the vicinity of asteroids and other small solar system bodies.

## 2.1. Spacecraft Dynamics

Spacecraft dynamical modeling in the small bodies' vicinity is an ongoing research area in the aerospace community. This topic is not fully explored because each mission to these bodies presents different challenges. The main factors that influence the dynamical uncertainty include:

(1) Irregular and unknown shape: precise estimation of small bodies' shape is difficult, if not impossible, with earth-based technologies. Therefore, an accurate gravitational model cannot be generated, resulting in poor dynamical modeling. The irregular shape of the asteroids results in an irregular gravitational field, which results in unknown forces and torques acting on the spacecraft (Scheeres & Schweickart, 2004).

(2) Solar radiation pressure (SRP): Usually, SRP cannot be fully modeled, as it is dependent on the spacecraft's position, attitude, shape, and reflective properties. This introduces uncertainty in the dynamics and usually needs to be resolved with active control methodologies (Kikuchi et al., 2017).

(3) Asteroid rotation: Small bodies like asteroids rotate at a high rate. Earth-based methodologies such as light curve methods are used to estimate the rotation. However,

the precise and the axis of rotation is unknown. Nearly half of the asteroids are known to rotate on a time-varying axis, and many of them have a periodic rotation axis (Scheeres, 2006).

(4) Other factors: There are several other known and unknown factors that affect the motion of the spacecraft near asteroids such as, variable inertia due to rover and solar panel deployment, mass change due to fuel consumption, solar winds, n-body gravitational effects (Tsuda et al., 2013).

Theoretical analysis of the gravitational field of the asteroids is studied in vast detail. A polyhedral gravity model for irregularly shaped bodies is presented by Werner and Scheeres (1996). This model is the benchmark for simulating the asteroid's gravitational field due to its accuracy and validity for irregularly shaped bodies. However, this model could be computationally expensive, especially for online implementation. Triaxial ellipsoidal gravity models are used in several studies to study the effect of gravity. These models are computationally efficient and can be easily implemented online. Even though these models suffer from inaccuracies, they could be sufficient for short-term proximity missions to asteroids and other small bodies.

Another extensively used gravity model is the spherical harmonic gravitational model (SHM). This model is beneficial for shapes that differ from a perfect sphere. Several studies have been conducted using this model for asteroid proximity missions; however, due to the fact that the SHM fails to converge inside the Brillouin sphere, they are not suitable for estimating gravity for proximity operations.

Recently, more precise and detailed models are being considered that treat asteroids and spacecraft as point masses. This model fills the asteroid with several finite point

masses, and the gravitational field at a specific location is calculated from the effect of all the point masses. Even though this model captures a better picture of the gravitational field at a large distance, this model fails to provide an accurate estimate. To precisely capture the gravitational field's effect on the spacecraft, it is necessary to model the orbit-attitude coupling effects. One of the early works by Sincarsin and Hughes (1982) shows the impact of orbit-attitude coupling via Taylor series expansion. The authors conclude that the attitude is affected by orbital motions depending on the size of the spacecraft.

In Scheeres (2006), the author highlights the effect of orbit-attitude coupling the proximity of a small asteroid. The paper concludes that a non-negotiable mass of the small body can significantly perturb the spacecraft's orbital path due to coupling effects. This is specifically important if the spacecraft is required to deflect the asteroid via mechanical attachments (Scheeres & Schweickart, 2004) or tugging (Lu & Love, 2005). The problem of studying the coupled effects is reviewed by several researchers (Sanyal et al., 2004; Wang, Krishnaprasad, et al., 1990).

Recently, a lot of effort is put into capturing this effect to precisely model the spacecraft dynamics in the proximity of the asteroid and other small bodies. In Wang Yue and Xu Shijie (2014), the authors model a spheroid planet's gravity field by considering the spacecraft as 36 point masses, and gravity is represented using an SHM. The paper concludes that the spacecraft is severely affected by coupled effects. The effects are largely dependent on the parameter $\rho/r$ (Bolatti & de Ruiter, 2020; Sincarsin & Hughes, 1982; Wang, Zhong, et al., 2018), where $\rho$ is the largest dimension (characteristic dimension) of the spacecraft and $r$ is the orbit radius. Therefore, as the proximity to the

asteroid increases, so does the effect of orbit-attitude coupling. In (Kikuchi et al., 2017) the authors model gravity using a tri-axial ellipsoidal model. The spacecraft is treated as a rigid body, and the force due to gravity is up to fourth-order while the torque acting the spacecraft due to its shape is up to second order. Effect of solar radiation pressure (SRP) is also included. This model, however, is not appropriate for proximity missions, especially inside the Brillouin sphere.

In Bolatti and de Ruiter (2016), as well as Bolatti and de Ruiter (2020), the authors present a novel formulation by considering a polyhedral gravity model for the asteroid and treating the spacecraft as a combination of several points masses. This model can effectively capture a very precise dynamical model for spacecraft at proximity.

In Misra (2016), the authors present another coupled orbit-attitude model that captures the effects of SRP and solar tides. The gravity is modeled using a uniformly rotating tri-axial model up to second degree and order.

### 2.2. Spacecraft Control Around Small Bodies

Currently, the spacecraft control for proximity asteroid operations is a combination of autonomous and ground-in-loop systems. Most of the control strategy is tediously designed offline and uploaded to the spacecraft. As an example, Hayabusa2's GNC system consists of PD control and a sliding mode control strategy. PD control is deployed when the spacecraft is close to the asteroid (under 5 km), and the sliding mode control is deployed at other times. PD control gains are calculated via a ground-based Monte-Carlo simulation, and the delta-v commands are calculated onboard the spacecraft.

In the case of the sliding mode control, after receiving the commands (image-based navigation) from the spacecraft (20 mins), the ground team calculates the required delta-v

commands and uploads them to the spacecraft (Ono et al., 2020). The complete process requires a team of scientists and 65 min to send a velocity command. The process is repeated after acquiring additional images. Therefore, a more autonomous navigation and control methodology is needed for future missions.

Recently, spacecraft control in an asteroid's vicinity has been studied in quite some detail. The problem of orbital control is a primary concern for most asteroid missions. However, attitude control is also essential for several applications such as mapping, photography, and other scientific experiments. There are several control objectives for spacecraft missions near asteroids. Near inertial hovering focuses on tracking a fixed point in inertial space. This is helpful in studying asteroid properties. Asteroid body-fixed hovering is another important maneuver where the spacecraft tracks a fixed location with respect to the asteroid. This is essential, especially during the landing and sampling phase of the mission.

Thirdly, circumnavigation and orbital tracking maneuvers are implemented to guide the spacecraft to the desired location. In this section, a literature review on spacecraft control in the asteroid's vicinity is presented. Broschart and Scheeres (2005) designed a feedback control for spacecraft hovering with application to asteroid Itokawa. First, an open-loop control with a combination of deadband control is designed. The open-loop control cancels the nominal acceleration and centrifugal acceleration. In contrast, deadband control is enabled whenever the spacecraft loses altitude outside the band defined by $h_o \pm \delta$ where $h_o$ is the altitude with a tolerance factor $\delta$. The controller assumes the gravity and rotational information of the asteroid.

Second, feedback control is designed that estimates the nominal and centrifugal

accelerations at the required altitude. This improves the performance and saves fuel because the estimation of the accelerations is more accurate in this case. In Kumar and Shah (2007), authors designed an invariance based feedback control. The controller is designed to follow an ideal attitude trajectory, and a PD type of tracking controller is designed with a feedforward term that cancels nominal and centrifugal accelerations. The controller inherently assumes the orbital and gravitational properties of the asteroid.

Guelman (2014) designed an elegant feedback orbital control law. The control is designed to achieve a circular orbit around asteroids with the desired radius, inclination, and right ascension of the ascending node (RAAN). The gravitational field is modeled using McCullagh's approximation. Again, the controller assumes rotational and gravitational information of the asteroid.

Reyhanoglu (2012) presented a Lyapunov-based nonlinear feedback control law to control the rotational and translational motion of the spacecraft. The orbital controller is designed to reach a desired circular orbit, while the attitude control is designed to track a nadir pointing attitude. A finite-time control law for body-fixed hovering is designed by (Lee, Sanyal, et al., 2015). The dynamics are expressed in exponential coordinates. A Lyapunov stability analysis is presented. The controller is able to hover at the desired location successfully.

Liu (2015) presented a controller based on a combination of PD and terminal sliding mode control. The PD control is implemented for the descending phase, while the sliding mode controller for the landing phase. Open-loop sub-optimal fuel trajectories are designed for tracking. It is shown that the controller can successfully perform the desired maneuvers.

Li (2019) presented a novel attitude control law for trajectory tracking near small bodies. The controller exploits gravitational coupling arising from the irregular gravitational field of the asteroid and the shape of the spacecraft. A polyhedral model of the asteroid is implemented, and the spacecraft is modeled using a distributed point-mass model. The results show successful tracking using only attitude control. However, a detailed polyhedral shape model of the spacecraft is required to implement the control law.

### 2.3. Adaptive Control

In Lee and Vukovich (2015), as well as, Lee and Vukovich (2016), authors design an adaptive sliding mode control scheme for autonomous body-fixed hovering in an asteroid's vicinity. The controller does not assume upper and lower uncertainty bounds. The controller requires an online estimation of gravitational parameters and upper bound disturbances. The paper shows successful hovering maneuvers. However, in the case of trajectory tracking, the estimation of parameters will be more complex due to the irregular gravity of the asteroid.

Tiwari and Henderson (2020) authors present a direct adaptive control strategy to track a hovering trajectory in an asteroid's vicinity. The controller does not require a system model of the spacecraft or the asteroid. The adaptive control law can successfully track the given trajectory in the presence of uncertain parameters.

In Tiwari and Prazenica (2020), the spacecraft is required to follow an ellipsoidal trajectory around an asteroid, an adaptive control law based on simple adaptive control (SAC) is designed and implemented. The spacecraft is modeled using a point mass, and the asteroid's gravity field is modeled using McCullagh's gravity approximation. The

adaptive control is successfully able to track the trajectory with an unknown system model and disturbances. In Stackhouse (2020), authors present an adaptive control design using Udwadia-Kalaba (UK) formulation to perform a hovering maneuver over an asteroid. The gravity is modeled using spherical harmonics. An indirect adaptive control law is designed where the gravitational parameters are estimated online. The UK formulated is fed with adaptive estimates from the adaptive control. The results show effective tracking over asteroid Bennu. However, the UK formulation required exact dynamics to output control accelerations which ultimately relies on the choice of gravitational model.

Non-Certainty-equivalence based indirect adaptive control law is designed by Lee (2019) for attitude control of the spacecraft around an asteroid. It does not assume spacecraft inertial and asteroid gravitational parameters. The control is required to track reference attitude trajectories for precise nadir pointing in elliptical prograde and retrograde orbits. The control system comprises a control module and a parameter identifier. The results show successful attitude tracking with unknown system parameters. Another paper by the same authors (Lee 2019) presents a super twisting adaptive control law for translational trajectory tracking around asteroids.

Silva (2020) present an indirect adaptive control law for spacecraft control for trajectory tracking around asteroids. The certainty equivalence-based adaptive control law is designed to estimate the unknown system parameters using an extended Kalman filter. Estimated states and the parameters are then fed into the adaptive control. The adaptive control law is simply a nonlinear version of LQR. However, the error dynamics are linearized using Taylor series expansion, and the resulting system is a time-varying LQR

problem. The optimal gains are calculated by solving the differential Riccati equation for each time step. Even though the control is inherently adaptive due to its time-varying nature, it's still dependent on the assumed dynamical model of the asteroid and spacecraft.

In Li (2018), authors designed a self-adaptive control for orbit maintenance. The control law is designed using Lyapunov theory, and the stability is shown using Barbalat's lemma. The spacecraft is successfully able to maintain the orbit with added system disturbances. A numerical analysis is shown on binary asteroids.

### 2.4. Optimal Control and Model Predictive Control

Model predictive control (MPC), also known as receding horizon control, is currently being implemented in several spacecraft GNC applications. Unlike traditional LQR, MPC can be linear or nonlinear, adaptive to disturbances online, and offer superior constraint handling.

In Nazari (2014), authors designed an observer-based optimal control for spacecraft hovering in a body-fixed frame. A time-varying LQR based on Lyapunov-Floquet transformation (LFT) and a time-invariant LQR are considered. The gravity is modeled using a tri-axial gravity model, and the states are estimated using an EKF. The rotation of the asteroid is considered periodic in nature. The controller can successfully hover over a tumbling asteroid. However, the controller requires gravitational and rotational estimates.

Authors Yang and Baoyin (2015) design a fuel optimal control problem for a soft landing on an asteroid. The optimal trajectory designed is taken as a reference trajectory for sliding mode control. Monte-Carlo simulations are done to show the controller's performance numerically.

Researchers have designed a multiple-horizon multiple-model predictive control for

a soft landing on an asteroid (AlandiHallaj & Assadian, 2017). The MPC is designed such that it uses multiple models for prediction. A polyhedral gravity model is used in the near time horizon, while a spherical harmonic model is used for a far future. This is based on studies that show that the control effort is not affected by the dynamical model in the distant future in the prediction horizon. The methodology requires a very detailed shape model of the asteroid for successful application.

A convex model predictive control is implemented by Reynolds and Mesbahi (2017) where authors convexify the soft landing problem and the system constraints. A collision avoidance method using an optimal separating hyperplane is designed. Spherical harmonics expansion is used to model the asteroid's gravity, which required a-prior for fast online estimation. It is numerically shown that the spacecraft is successfully able to circumnavigate and land on the asteroid.

Liao and McPherson (2016), authors present multiple optimal strategies to tackle the problem of soft landing on an asteroid using MPC. An extended command governer (ECG), convex model predictive controller (CMPC), and a nonlinear model predictive control (NMPC) are employed. The results show that an NMPC has superior performance for disturbance rejection and constraint handling.

Authors present a solar radiation pressure based optimal orbit control strategy in Oguri and McMahon 2020. The orbit-attitude coupling due to SRP is exploited to design an optimal feedback controller. The control strategy is designed such that the optimal control problem reduces a Lyapunov function.

### 2.5. Direct Adaptive Control

In this section, we present the literature review on the direct adaptive control methodology implemented in our work. A direct adaptive controller based on simple adaptive control (SAC) (Kaufman et al., 1997a) is modified and implemented. SAC is a model reference adaptive control (MRAC) which can track desired trajectories from a low-order reference model in the presence of system uncertainty and disturbance. In fact, SAC does not require a system at all for implementation, making it suitable for applications where it is difficult or impossible to estimate system models.

There have been several developments and applications related to SAC. Researchers have implemented a modified version of the controller for trajectory tracking for UAVs (Prabhakar et al., 2018). The control has been added for disturbance rejection. In Shi (), authors present an application of SAC for spacecraft attitude control in the presence of added disturbances and system uncertainties. Ulrich and Saenz-Otero (2012) use SAC for adaptive control flexible joint manipulator. The adaptive control is successfully able to track desired trajectories in the presence of uncertainties in the model.

Simple adaptive control (SAC) is used for application to spacecraft proximity maneuvers in the presence of system uncertainties in Ulrich (2016). Experimental and numerical results are presented to show that the adaptive control is able to track desired trajectories. Tiwari and Prabhakar (2020), as well as, Tiwari (2016) presented space-related applications of SAC. It can be noted that the most of the work disscussed here do not assume a system model for the spacecraft and shows that the simple adaptive control (SAC) is able to handle system uncertainty.

### 2.6. Nonlinear Model Predictive Control

In this work, a modified nonlinear predictive control (NMPC) is implemented in conjunction with an adaptive control. NMPC is a sub-optimal finite-horizon control that can handle nonlinear systems models and constraints.

Schlipf (2013) presented an NMPC to control wind turbines using light detection and ranging (LiDAR). It shows that an NMPC is able to optimize the performance in the presence of disturbances. Lee (2018) presented an NMPC scheme using direct collocation. A learning-based nonlinear model predictive control for robot path tracking by (Ostafew et al., 2016). The algorithm uses a simple vehicle model and learned disturbances model. The disturbances are modeled using a Gaussian process. The results show that controllers can learn to reduce tracking errors over time based on experience.

Rybus (2017) implement an NMPC for a free-floating space manipulator. The NMPC is used to track end-effectors in the presence of uncertainties. The NMPC is then compared with a modified simple adaptive control (Ulrich & de Lafontaine, 2007). The results show superior tracking with NMPC as compared to SAC-based control. Starek and Kolmanovsky (2014) implement NMPC for low thrust spacecraft missions. The NMPC is used to solve a low thrust rendezvous problem.

It is shown that the NMPC can handle control objectives even in the presence of system uncertainties. However, (Grimm et al., 2004) showed that a nonlinear model predictive control with nonlinear states and constraint does not guarantee asymptotic stability and may have no robustness to external disturbances.

# 3. Spacecraft Dynamics Near Small Bodies

In this chapter, we discuss the formulation of dynamics, forces, and coordinate frames. The dynamical model presented here is then implemented as a true to numerically verify the performance of adaptive control and direct adaptive model predictive control methodology. The model is numerically propagated using fourth order Runge-Kutta formulation in MATLAB and Simulink.

Polyhedral model implemented in this dissertation is from (Bolatti & de Ruiter, 2020). The system is dynamics is represented in the usual two-body form as well as Euler-Lagrange form. Euler-Lagrange form is used to prove the stability of the direct adaptive control. The coupling between translational and attitude dynamics arising from gravity gradient and solar radiation pressure is also shown. The attitude dynamics is parametrized via modified Rodriguez parameters.

## 3.1. Dynamics

This section presents the dynamical formulation and the forces acting on the spacecraft in small bodies' (asteroid') vicinity. First, we discuss the coordinate frames and coordinate transformations applied in this work. Next, we provide the details on gravitational forces, external forces, coupled forces, and the SRP.

In this work, a hybrid approach is taken to model the forces due to gravity and coupled translational-rotational motion. A polyhedral gravity model is considered to model the asteroid's gravity for the spacecraft's point mass model. However, the gravity gradient torque and translational-rotational coupling for the rigid body spacecraft are modeled using the asteroid's point mass gravity model.

This hybrid approach captures the dominant forces due to the asteroid's irregular shape while keeping the rigid body spacecraft model relatively simple.

### 3.1.1. Coordinate Frames

In this research, we have implemented five-coordinate frames to describe the spacecraft's orbital and attitude states. It is conventional to write the orbital dynamics in the small body-fixed frame. Simultaneously, it is conventional to write the attitude dynamics in spacecraft fixed body frame. The approach taken here is similar to (Kikuchi et al., 2017).

The coordinate frames are given as follows:

1. Inertial coordinate system ($x^I, y^I, z^I$): A right-handed coordinate system inertially fixed at the center of the sun.

2. Asteroid fixed coordinate system (SB) ($x^{SB}, y^{SB}, z^{SB}$): The origin is at the center of mass of the asteroid. $z^{SB}$ axis is in the direction of the angular velocity of the asteroid. The asteroid is assumed to be rotating with a constant angular velocity about the $z^{SB}$ axis.

3. Spacecraft fixed body frame (SC) ($x^{SC}, y^{SC}, z^{SC}$): The origin is at the spacecraft center. The axes are aligned along the principal axes of the moment of inertia.

4. Orbit Fixed Frame (Hill Frame) ($x^H, y^H, z^H$): The origin is fixed at the center of the asteroid. The $x^H$ axis is parallel to the sun direction but points in the opposite direction. The $z^H$ axis is in the direction of the angular velocity of the asteroid around the sun, and the $y^H$ axis completes the triad. See Figure 3.1.

5. Sun-pointing coordinate frame ($x^{SP}, y^{SP}, z^{SP}$): The coordinate frame is at the center of the spacecraft. The $z^{SP}$ axis is fixed to point at the sun, $x^{SP}$ points parallel to

the plane formed by $x^H$ and $y^H$. The attitude of the spacecraft is defined with respect to this frame. See Figure 3.2.

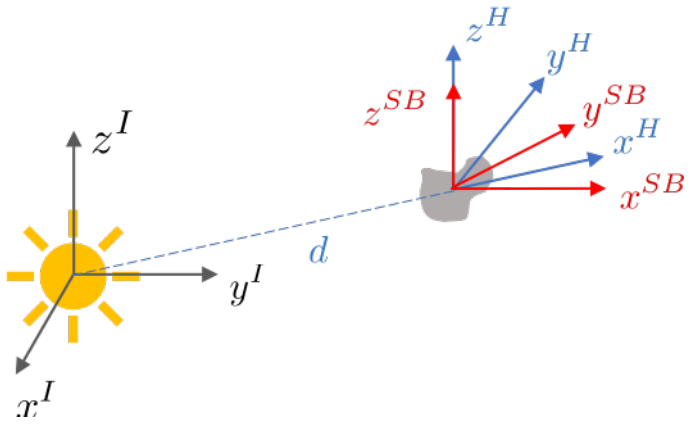


*Figure 3.1* Asteroid body frames with respect to sun.

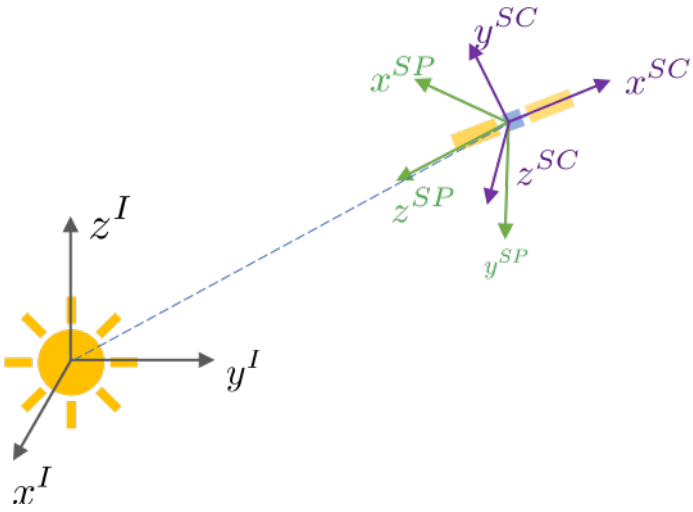


*Figure 3.2* Spacecraft body frames with respect to sun.

### 3.1.2. Orbital Dynamics

The controlled spacecraft dynamics relative to the asteroid is expressed in the rotating asteroid body fixed frame ($SB$) is given as,

$$m\ddot{\mathbf{r}} + 2m(\boldsymbol{\Omega} \times \dot{\mathbf{r}}) + m(\boldsymbol{\Omega} \times (\boldsymbol{\Omega} \times \mathbf{r})) = \mathbf{F}(\mathbf{r})_{gp} + \mathbf{f}(\mathbf{r}, \boldsymbol{\sigma})_{gg} + \mathbf{f}(\boldsymbol{\sigma})_{srp} + \mathbf{u} \qquad (3.1)$$

where $m$ is the mass of the spacecraft, $\mathbf{r} = [x\ y\ z]^T$ is the position vector from the center of mass of the asteroid to the center of mass of the spacecraft expressed in the asteroid body frame ($SB$) as shown in Figure 3.3. The angular velocity vector $\mathbf{\Omega} = [0\ 0\ \omega]^T$ is considered constant, where $\omega$ is the magnitude of the angular velocity. The vector $\mathbf{\Omega}$ is aligned with the unit vector $\hat{\mathbf{z}}_{SB}$ and $\boldsymbol{\sigma} = [\sigma_1\ \sigma_2\ \sigma_3]^T$ are the modified Rodrigues parameters (MRPs).

Here $\mathbf{F}(\mathbf{r})_{gp} = [F_{gp_x}\ F_{gp_y}\ F_{gp_z}]^T$ is the force due to the polyhedral gravity model of the asteroid and $\mathbf{f}(\mathbf{r}, \boldsymbol{\sigma})_{gg} = [f_{gg_x}\ f_{gg_y}\ f_{gg_z}]^T$ is the gravitational gradient force arsing from the interaction between point mass gravity model of the asteroid and the rigid body model of the spacecraft.

Here $\mathbf{f}(\boldsymbol{\sigma})_{SRP} = [f_{srp_x}\ f_{srp_y}\ f_{srp_z}]^T$ is the force due to solar radiation pressure which is dependent on the attitude of the spacecraft. Here $\mathbf{u} = [u_x\ u_y\ u_z]^T$ is the thrust control vector assumed to be aligned with the principal axes of the asteroid.

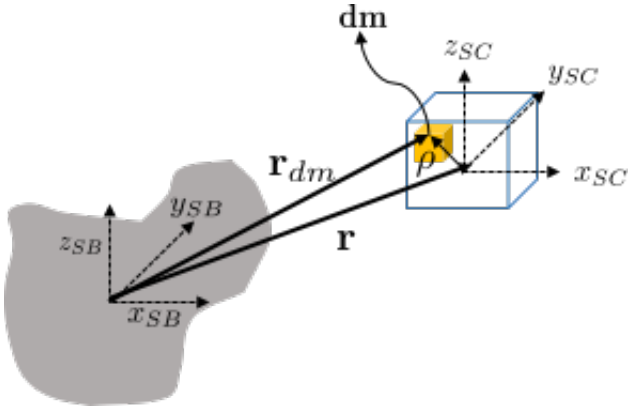


*Figure 3.3* Spacecraft rigid body with respect to asteroid

It can be noted that the functions $\mathbf{f}(\mathbf{r}, \boldsymbol{\sigma})_{gg}$ and $\mathbf{f}(\boldsymbol{\sigma})_{SRP}$ shows the coupling between translational and attitude dynamics through SRP and gravitational gradient effects. These

forces are derived in the subsequent sections.

For this research, and without loss of generality, the asteroid's angular velocity vector is aligned with the $z$ axis of the asteroid. The state-space formulation for the orbital dynamics with state vector $\mathbf{x} = [\mathbf{r}(t) \;\; \dot{\mathbf{r}}(t)]^T$is given as,

$$\begin{aligned} \dot{\mathbf{x}} &= \mathbf{F}(\mathbf{x}) + \mathbf{B}\mathbf{u} \\ \mathbf{y} &= \mathbf{C}\mathbf{x} \end{aligned} \tag{3.2}$$

where $\mathbf{F}(\mathbf{x})$, $\mathbf{B}$ and $\mathbf{C}$ are given as,

$$\mathbf{F}(\mathbf{x}) = \frac{1}{m}\begin{bmatrix} \dot{x} \\ \dot{y} \\ \dot{z} \\ 2m\omega\dot{y} + m\omega^2 x + F_{gp_x} + f_{gg_x} + f_{SRP_x} \\ -2m\omega\dot{x} + m\omega^2 y + F_{gp_y} + f_{gg_y} + f_{SRP_y} \\ F_{gp_z} + f_{gg_z} + f_{SRP_z} \end{bmatrix}, \mathbf{B} = \frac{1}{m}\begin{bmatrix} \mathbf{0}_{3\times3} \\ \mathbf{I}_{3\times3} \end{bmatrix}, \mathbf{C} = [\mathbf{I}_{3\times3} \;\; \mathbf{I}_{3\times3}] \tag{3.3}$$

For the sake of stability analysis, higher order forces can be considered as both low frequency and low magnitude perturbations, which can be handled by the robustness of the adaptive controller. The adaptive controller implemented in this work requires the system to be in square state-space form to satisfy the almost strictly passive conditions (ASP) (see section III). The square state-space form, with a point mass gravity model is given as,

$$\dot{\mathbf{x}} = \mathbf{A}_{ss}\mathbf{x} + \mathbf{B}\mathbf{u} + \frac{1}{m}\mathbf{F}_\mathbf{e} \tag{3.4}$$

$$\mathbf{y} = \mathbf{C}\mathbf{x} \tag{3.5}$$

where $\mathbf{F_e} = \mathbf{F}(\mathbf{r})_{ghot} + \mathbf{f}(\mathbf{r}, \boldsymbol{\sigma})_{gg} + \mathbf{f}(\boldsymbol{\sigma})_{srp}$ are the sum of disturbance forces to higher order gravity terms $\mathbf{F}(\mathbf{r})_{ghot}$, SRP, and gravity gradient and $\mathbf{A}_{ss} \in R^{n \times n}$ is a square matrix given as,

$$\mathbf{A}_{ss} = \begin{bmatrix} & \mathbf{0}_{3\times3} & & & \mathbf{I}_{3\times3} & \\ \omega^2 - \frac{\mu}{|\mathbf{r}|^3} & 0 & 0 & 0 & 2\omega & 0 \\ 0 & \omega^2 - \frac{\mu}{|\mathbf{r}|^3} & 0 & -2\omega & 0 & 0 \\ 0 & 0 & -\frac{\mu}{|\mathbf{r}|^3} & 0 & 0 & 0 \end{bmatrix} \tag{3.6}$$

Equation (3.4) is exploited to study the stability of the adaptive controller in subsequent sections, which is derived from the theoretical results presented by Barkana (Barkana, 2010). It can be noted here that $\mathbf{C}$ from Equation (5.10) outputs the states as the summation of position and velocity, also known as blended output, which has shown to significantly improve the controller performance by adding damping effects on the control thrust, and it assists in satisfying the minimum phase conditions.

### 3.1.3. Attitude Dynamics

The attitude dynamics of the spacecraft are expressed in the spacecraft fixed body frame ($x^{SC}, y^{SC}, z^{SC}$). The frame is fixed at the center of mass of the spacecraft and is aligned with the principle axes of the spacecraft. The attitude dynamics is expressed using Euler rotational equations as follows:

$$\mathbf{I}\dot{\boldsymbol{\omega}} = -\boldsymbol{\omega}^{\times}\mathbf{I}\boldsymbol{\omega} + \boldsymbol{\tau} + \mathbf{T}_{SRP}(\boldsymbol{\sigma}) + \mathbf{T}_{GG}(\boldsymbol{\sigma}, \mathbf{r}) \tag{3.7}$$

where $\mathbf{I} \in R^{3\times3}$ is the inertia of the spacecraft written in the SC frame and, $\boldsymbol{\omega} \in R^3$ is the angular velocity vector of the spacecraft with respect to the orbit fixed frame (H).

Here, $\boldsymbol{\tau} \in R^3$ is the attitude control thrust vector, $\boldsymbol{T}_{SRP}(\boldsymbol{\sigma}) \in R^3$ is the torque due to solar radiation pressure, $\boldsymbol{T}_{GG}(\boldsymbol{\sigma}, \mathbf{r}) \in R^3$ is the torque due to gravity gradient. It can be noted that the function $\boldsymbol{T}_{GG}(\boldsymbol{\sigma}, \mathbf{r})$ shows the coupling between translational and rotational dynamics. $\boldsymbol{\omega}^{\times} \in R^{3\times3}$ is a skew symmetric matrix and $\mathbf{I}$ is the inertia tensor as given in Equation 3.8.

$$\boldsymbol{\omega}^{\times} = \begin{bmatrix} 0 & -\omega_3 & \omega_2 \\ \omega_3 & 0 & -\omega_1 \\ -\omega_2 & \omega_1 & 0 \end{bmatrix}, \quad \mathbf{I} = \begin{bmatrix} I_x & 0 & 0 \\ 0 & I_y & 0 \\ 0 & 0 & I_z \end{bmatrix} \tag{3.8}$$

#### 3.1.3.1. Attitude Kinematics

A brief overview of attitude kinematics is provided in this section. In this research, attitude kinematics is parameterized using modified Rodrigues parameters (MRPs). The MRPs are defined in terms of quaternions by applying a stereo-graphic projection and can be defined as follows:

$$\sigma_i = \frac{q_i}{1 + q_0}, \quad i = 1, 2, 3 \tag{3.9}$$

where $q$ is the quaternion and $\sigma$ is the MRP. The MRPs have few advantages over quaternions such as they are unique and non-redundant. However, MRPs do suffer from geometric singularity at $q_0 = -1$. Further, the MRPs can be expressed in terms of a principal rotation angle and principal axis vector as follows:

$$\boldsymbol{\sigma} = \tan\frac{\Phi}{4}\hat{\mathbf{e}} \tag{3.10}$$

where $\boldsymbol{\sigma} \in R^3$ is the MRP vector, $\Phi$ is the principal rotation vector, and $\hat{\mathbf{e}} \in R^3$ is the principal axis vector. It can be seen from Equation (3.10) that the geometric singularity in terms of the principal rotation angle is at $\Phi = \pm 360\,\mathrm{deg}$. Therefore, in order to resolve

the singularity issue, shadow sets are defined as follows:

$$\sigma_i^s = \frac{-q_i}{1-q_0}, \quad i = 1, 2, 3 \tag{3.11}$$

Introducing a shadow set allows to switch and avoid discontinuities when working with MRPs. Hence, when the $\Phi = \pm 360\,\mathrm{deg}$, the MRP formulation is switched to the shadow set as given in Equation (3.11). It can be noted that shadow sets suffer from the singularity at $\Phi = 0\,\mathrm{deg}$.

#### 3.1.3.2. Attitude Kinematic Differential Equations

The kinematics differential equation using MRPs is given as follows:

$$\dot{\boldsymbol{\sigma}} = \frac{1}{4}\begin{bmatrix} 1-|\boldsymbol{\sigma}|^2+2\sigma_1^2 & 2(\sigma_1\sigma_2-\sigma_3) & 2(\sigma_1\sigma_3+\sigma_2) \\ 2(\sigma_2\sigma_1+\sigma_3) & 1-|\boldsymbol{\sigma}|^2+2\sigma_2^2 & 2(\sigma_2\sigma_3-\sigma_1) \\ 2(\sigma_3\sigma_1-\sigma_2) & 2(\sigma_3\sigma_2+\sigma_1) & 1-|\boldsymbol{\sigma}|^2+2\sigma_3^2 \end{bmatrix} \begin{pmatrix} \omega_1 \\ \omega_2 \\ \omega_3 \end{pmatrix}^{SC} \tag{3.12}$$

where $\boldsymbol{\omega}^{SC} = [\omega_1,\ \omega_2,\ \omega_3]^T$ are the angular velocities of the spacecraft in the spacecraft body fixed frame ($x^{SC}, y^{SC}, z^{SC}$), and $|\boldsymbol{\sigma}|$ is the magnitude of the MRP vector.

The MRP kinematics differential equation can be written in a more compact vector form as,

$$\dot{\boldsymbol{\sigma}} = \mathbf{S}(\boldsymbol{\sigma})\boldsymbol{\omega} \tag{3.13}$$

where,

$$\mathbf{S}(\boldsymbol{\sigma}) = \frac{1}{4}[(1-|\boldsymbol{\sigma}|^2)[I_{3\times 3}]] + 2\boldsymbol{\sigma}^{\times} + 2\boldsymbol{\sigma}\boldsymbol{\sigma}^T] \tag{3.14}$$

where $\boldsymbol{\sigma}^{\times} \in R^{3\times 3}$ is the skew symmetric matrix is given as,

$$\sigma^{\times} = \begin{bmatrix} 0 & -\sigma_3 & \sigma_2 \\ \sigma_3 & 0 & -\sigma_1 \\ -\sigma_2 & \sigma_1 & 0 \end{bmatrix} \tag{3.15}$$

Alternatively, the kinematics can be expressed in terms of angular velocity as,

$$\boldsymbol{\omega} = \mathbf{S}^{-1}(\boldsymbol{\sigma})\dot{\boldsymbol{\sigma}} \tag{3.16}$$

where $\mathbf{S}^{-1}(\boldsymbol{\sigma})$ is given as,

$$\mathbf{S}^{-1} = \frac{4}{(1+|\boldsymbol{\sigma}|^2)}[(1-|\boldsymbol{\sigma}|^2)\mathbf{I}_{3\times 3} - 2\boldsymbol{\sigma}^{\times} + 2\boldsymbol{\sigma}\boldsymbol{\sigma}^T]\dot{\boldsymbol{\sigma}} \tag{3.17}$$

The MRP kinematics differential equation for the shadow are given as,

$$\dot{\boldsymbol{\sigma}}^S = -\frac{\dot{\boldsymbol{\sigma}}}{|\boldsymbol{\sigma}|^2} + \frac{1}{2}\left(\frac{1+|\boldsymbol{\sigma}|^2}{|\boldsymbol{\sigma}|^4}\right)\boldsymbol{\sigma}\boldsymbol{\sigma}^T\boldsymbol{\omega}^{SC} \tag{3.18}$$

Shadow set switching is applied in this research to resolve the singularity issue. However, it has been shown in (Schaub & Junkins, 2018) that switching between original and shadow set at $|\boldsymbol{\sigma}| = 1$ or $\Phi = 180$ is more beneficial than switching when MRPs reach singularity. Therefore, in this research shadow set, switching is employed when MRPs reach $|\boldsymbol{\sigma}| = 1$.

For convenience, the square state-space form for attitude dynamics is formulated in Euler-Lagrange form (Shi et al., n.d., Wong et al., 2001).

$$\mathbf{J}(\boldsymbol{\sigma})\ddot{\boldsymbol{\sigma}}(\boldsymbol{\sigma}) + \mathbf{C}^*(\boldsymbol{\sigma}, \dot{\boldsymbol{\sigma}})\dot{\boldsymbol{\sigma}} = \mathbf{S}^{-1}(\boldsymbol{\sigma})\boldsymbol{\tau} \tag{3.19}$$

where $\mathbf{J}(\boldsymbol{\sigma})$ and $\mathbf{C}^*(\boldsymbol{\sigma}, \dot{\boldsymbol{\sigma}})$ are given as,

$$\mathbf{J} = \mathbf{S}^{-T}\mathbf{I}\mathbf{S}^{-1}, \quad \mathbf{C}^* = -\mathbf{J}\dot{\mathbf{S}}\mathbf{S}^{-1} - \mathbf{S}^{-T}(\mathbf{J}\mathbf{S}^{-\mathbf{1}}\dot{\boldsymbol{\sigma}})^{\times}\mathbf{S}^{-1} \tag{3.20}$$

The state-space formulation for attitude dynamics consists of state vector $\mathbf{x} = [\boldsymbol{\sigma}(t)\ \dot{\boldsymbol{\sigma}}(t)]^T$, where $\boldsymbol{\sigma}(t)$ and $\dot{\boldsymbol{\sigma}}(t)$ are the MRPs and rate of change of MRPs vector

respectively. Using the formulation from Equation (3.19), the square state-space form is given as,

$$\dot{\mathbf{x}} = \mathbf{A}_{att}\mathbf{x} + \mathbf{B}\mathbf{u} + \mathbf{T_e} \tag{3.21}$$

$$\mathbf{y} = \mathbf{C}\mathbf{x} \tag{3.22}$$

where $\mathbf{T_e} = \mathbf{T}_{GG}(\boldsymbol{\sigma}, \mathbf{r}) + \mathbf{T}_{SRP}(\boldsymbol{\sigma})$ is the sum of disturbances due to SRP and gravity gradient torques. The system matrices can be expressed as,

$$\mathbf{A}_{att} = \begin{bmatrix} \mathbf{0}_{3\times3} & \mathbf{I}_{3\times3} \\ \mathbf{0}_{3\times3} & -\mathbf{J}^{-1}\mathbf{C} \end{bmatrix},\ \mathbf{B} = \begin{bmatrix} \mathbf{0}_{3x3} \\ \mathbf{J^{-1}S^{-1}} \end{bmatrix},\ \ \mathbf{C} = [\mathbf{I}_{3\times3}\ \ \mathbf{I}_{3\times3}] \tag{3.23}$$

It may be noted that the output matrix $\mathbf{C}$ is the same for orbital and attitude dynamics; however, in general, the matrix $\mathbf{C}$ could be different. Again, in attitude dynamics, the out vector $\mathbf{y}$ is the blended output of MRPs and angular velocities. Also, the Euler-Lagrange form formulated in Equation (3.19) is not necessary for implementation. However, this form is exploited to study the stability of the attitude dynamics of the system.

#### 3.1.3.3. Direction Cosine Matrix (DCM)

Here we formulate the relationship between DCM and MRPs in order to implement coordinate frame transformations between various frames, as defined in the following section. The DCM can be paramterized in terms of MRPs as follows:

$$\mathbf{C}_{DCM} = \mathbf{I}_{3\times3} + \frac{8(\boldsymbol{\sigma}^{\times})^2 - 4(1 - |\boldsymbol{\sigma}|^2)\boldsymbol{\sigma}^{\times}}{(1 + |\boldsymbol{\sigma}|^2)^2} \tag{3.24}$$

where $\mathbf{C}_{DCM} \in R^{3\times3}$ is the DCM in terms of MRPs, and $\mathbf{I} \in R^{3\times3}$ is the identity matrix.

### 3.1.4. Coordinate Frame Transformations

This section discusses the various coordinate transformations required to implement the spacecraft's controlled coupled translational and rotational dynamics in the asteroid's vicinity. Let us define $\eta$ and $\psi$ to be any two arbitrary coordinate frames and let ${}^{\psi}\mathbf{C}_{\eta}$ be the DCM that transforms an arbitrary vector ${}^{\eta}\mathbf{r} \in R^3$ (not necessarily a position vector) defined in $\eta$-coordinate frame to the vector ${}^{\psi}\mathbf{r} \in R^3$ defined in $\psi$-coordinate frame. This transformation can be expressed as follows with various transformation:

$$ {}^{\psi}\mathbf{r} = {}^{\psi}\mathbf{C}_{\eta}\, {}^{\eta}\boldsymbol{r} \tag{3.25} $$

1. Spacecraft fixed frame to sun-pointing frame (${}^{SP}\mathbf{C}_{SC}$): This transformation defines the attitude of the spacecraft with respect to the spacecraft fixed sun-pointing frame. The DCM ${}^{SP}\mathbf{C}_{SC}$ is calculated via the attitude dynamics/kinematics of the spacecraft from Equation (3.24).
2. Sun-pointing frame to Hill frame (${}^{H}\mathbf{C}_{SP}$): The transformation between these frame is a time-invariant transformation since these frames are considered almost inertial due to the fact that $z << d$, i.e. the distance from the sun is large enough to consider this transformation time-invariant. The DCM to transform between the frames is given as,

$$ {}^{H}\mathbf{C}_{SP} = \begin{bmatrix} 0 & 1 & 0 \\ 0 & 0 & -1 \\ -1 & 0 & 0 \end{bmatrix} \tag{3.26} $$

3. Hill frame to asteroid body-frame(${}^{SB}\mathbf{C}_{H}$): This frame is the transformation between orbit fixed Hill frame and asteroid fixed body-frame. This results from

the asteroid's rotation with respect to the Hill frame. Since the angular velocity ($^{SB}\mathbf{\Omega} = [0,\ 0,\ \Omega]^T$(rad/s)) of the asteroid is constant with respect to the Hill frame, the transformation can be easily parametrized using single axis Euler angle rotation about the $z^{SB}$ axis. The transformation is given as,

$$^{SB}\mathbf{C}_H = \begin{bmatrix} \cos\theta(t) & \sin\theta(t) & 0 \\ -\sin\theta(t) & \cos\theta(t) & 0 \\ 0 & 0 & 1 \end{bmatrix} \tag{3.27}$$

where $\theta(t) = \Omega \times t$ (rad) is the angle of rotation, and $t$ is the time. It can be noted that an exception is made and Euler angles are used instead of MRPs. This is because the rotation is a single axis rotation and the singularity associated with Euler angles is avoided.

Finally, a complete transformation from spacecraft fixed frame to asteroid fixed frame ($^{SB}\mathbf{C}_{SC}$) can be formulated using the formulations mentioned above. It is convenient to calculate forces and torques in their original frame of references and then transforming them to their final frame. As an example, two transformations between SC and SB frame are shown as follows:

(a) Transformation of SRP force ($\mathbf{f}_{SRP}$) from SC frame to SB frame: Due to the dynamical coupling, the attitude of the spacecraft directly relates to the SRP force. This transformation sequence is given as,

$$^{SB}\mathbf{f}_{SRP} = {}^{SB}\mathbf{C}_H\, {}^{H}\mathbf{C}_{SP}\, {}^{SP}\mathbf{C}_{SC}\, {}^{SC}\mathbf{f}_{SRP} \tag{3.28}$$

where $^{SP}\mathbf{C}_{SC}$ is the attitude of the spacecraft with respect to the sun-pointing frame ($SP$), $^{H}\mathbf{C}_{SP}$ is a time-invariant transformation from the sun-pointing

frame to the Hill frame ($H$) and ${}^{SB}\mathbf{C}_H$ is the transformation from the Hill frame ($H$) to asteroid fixed body-frame ($SB$), which is dependent on the asteroid's rotation.

(b) Transformation of gravity gradient torque ($\mathbf{T}_{GG}$): Since the torque due to gravity gradient is dependent on the position of the spacecraft which is expressed in the asteroid body-frame, a transformation from for position is required from $SB$ to $SC$ frame. The sequence of rotation in this is simply the inverse sequence of Equation (3.29) and is given as,

$$ {}^{SC}\mathbf{T}_{GG} = {}^{SC}\mathbf{C}_{SP}\,{}^{SP}\mathbf{C}_{H}\,{}^{H}\mathbf{C}_{SB}\,{}^{SB}\mathbf{T}_{GG} \tag{3.29} $$

### 3.1.5. Forces and Moments

This section presents the formulation of the external forces and moments acting on the spacecraft due to gravity and solar radiation pressure. Mainly, the formulation of forces and moments appearing on the right-hand side of Equation 3.1 and 3.7 is presented.

#### 3.1.5.1. Polyhedral Point Mass Gravitational Model

This work has implemented a polyhedral gravitational model that was first proposed by Werner & Scheeres (1996). This gravity model has several advantages over conventional models, such as spherical harmonics and McCullagh's approximations, which are widely used in control-based applications.

The polyhedral model calculates the exact gravitational field for the given shape and density of the body (Werner & Scheeres, 1996). The model is valid up to the asteroid's surface, and unlike the spherical harmonics gravitational model, it does not diverge inside the Brillouin sphere. Generally, Spherical harmonics models are used to develop optimal

and robust control near the asteroid's vicinity due to its relatively simple formulation and because these controllers are model-dependent.

However, since a model-free direct adaptive control methodology is implemented in this work, a more complex but accurate gravitational model can be implemented. The polyhedral gravitational model assumes the spacecraft to be a point mass. In this work, we have modeled the coupled gravitational effects due to the rigid-body shape separately.

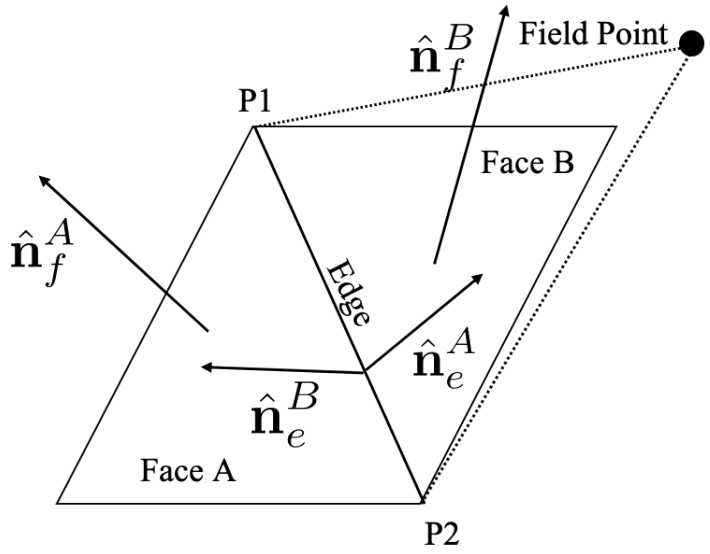


*Figure 3.4* Polyhedron facets and edges.

A polyhedral model is developed using a triangular facet with three vertices. Each edge of the facet is the boundary between two facets, as shown in Figure 3.4. Here $\mathbf{r}_f$ is the vector from the field point (spacecraft position in the asteroid body frame) to any point on the face plane. Vector $\hat{\mathbf{n}}_f$ is a unit vector normal to the face plane.

Each triangular facet is associated with its own coordinate frame ($\hat{\mathbf{i}},\ \hat{\mathbf{j}},\ \hat{\mathbf{k}}$) where the $\hat{\mathbf{k}}$ is aligned with the normal vector $\hat{\mathbf{n}}_f$. Vector $\mathbf{r}_e$ is a vector from the field point to any point at the edge $e$. Each edge has a normal edge vector, which is normal to the edge

vector $\mathbf{e}$ and the face normal vector $\hat{\mathbf{n}}_f$. Here, the edge vector $\mathbf{e}$ is the vector along the edge of the facet. Each edge is associated with two edge normal vectors (one for each face plane) namely $\mathbf{n}_e^A$ and $\mathbf{n}_e^B$. The edge and face dyads constants are given as,

$$\mathbf{E}_e = \hat{\mathbf{n}}_f^A \hat{\mathbf{n}}_e^A + \hat{\mathbf{n}}_f^B \hat{\mathbf{n}}_e^B \tag{3.30}$$

$$\mathbf{F}_f = \hat{\mathbf{n}}_f \hat{\mathbf{n}}_f^T \tag{3.31}$$

The potential due to the edge is denoted by $L_e$ and is given as,

$$L_e = \ln \frac{\|r_{e1}\| + \|r_{e2}\| + \|e\|}{\|r_{e1}\| + \|r_{e2}\| - \|e\|} \tag{3.32}$$

where $\|.\|$ is the magnitude of the vectors. Dimensionless factor $\omega_f$ is defined for each facet and is given as,

$$\omega_f = 2 \arctan \frac{\hat{\mathbf{r}}_{f1} \cdot \hat{\mathbf{r}}_{f2} \times \hat{\mathbf{r}}_{f3}}{1 + \hat{\mathbf{r}}_{f1} \cdot \hat{\mathbf{r}}_{f2} + \hat{\mathbf{r}}_{f2} \cdot \hat{\mathbf{r}}_{f3} + \hat{\mathbf{r}}_{f3} \cdot \hat{\mathbf{r}}_{f1}} \tag{3.33}$$

where the vectors $\mathbf{r}_{f1}$, $\mathbf{r}_{f1}$ and $\mathbf{r}_{f1}$ are the vectors from the field point to each vertex of the triangular facet. Given the above mentioned definitions, the acceleration due to the polyhedral shape of the body is given as,

$$\mathbf{a}_{gp} = -G\rho \sum_{e \in \text{edges}} \mathbf{E}_e \mathbf{r}_e \cdot L_e + G\rho \sum_{f \in \text{faces}} \mathbf{F}_f \mathbf{r}_f \cdot \omega_f \tag{3.34}$$

where $G$ and $\rho$ are the gravitational constant and density of the asteroid. The gravitational force ($\mathbf{F}_{gp}$) from due the polyhedral gravitational field of the asteroid on the spacecraft with mass $m$ is simply given as,

$$\mathbf{F}_{gp} = m\mathbf{a}_{gp} \tag{3.35}$$

Gravitational gradient force ($\mathbf{f}_{gg}$) is the force acting on the spacecraft due to the interaction between the shape of the spacecraft and the gravitational field of the asteroid. Figure 3.3 shows the rigid body spacecraft model in the vicinity of the asteroid. In this

work, gravitational gradient force is calculated using a point mass gravity model for the asteroid. It can be interpreted from (Bolatti & de Ruiter, 2020) that a point mass gravity model for the asteroid is sufficient in cases where the mission duration is short.

The force due to gravity gradient is given as,

$$\mathbf{f}_{gg}^{SB} = -\frac{3\mu}{\|r\|^5}\left[\mathbf{I} + \frac{1}{2}(tr(\mathbf{I}) - 5(\hat{\mathbf{r}}^T\mathbf{I}\mathbf{r})\,\mathbf{I}_{3\times 3}\right]\mathbf{r} \tag{3.36}$$

where, $tr(\mathbf{I})$ is the trace of the inertia tensor, $\mathbf{I}_{3\times 3}$ is a identity matrix and $\mathbf{r}$ is the position vector in expressed in the body-frame.

Again, the torque due to gravitational gradient results from the interaction of point mass gravity of the asteroid with the spacecraft. The mass closer to the asteroid experiences stronger force compared to the mass away from it, which results in a net torque. The torque due to gravity gradient in the spacecraft body frame ($SC$) is given as,

$$\mathbf{T}_{gg}^{SC} = -\frac{\mu}{\|\mathbf{r}_{dm}\|^3}\int \boldsymbol{\rho} \times \mathbf{r}_{dm}\, dm \tag{3.37}$$

where $\mathbf{r}_{dm} = \mathbf{r} + \boldsymbol{\rho}$ is the vector from center of the asteroid to the mass element in the spacecraft (SC) frame and, $\boldsymbol{\rho}$ is the vector from center of spacecraft to the mass element. See Figure 3.3.

The torque can be expressed in a more manageable form:

$$\mathbf{T}_{gg}^{SC} = \frac{3\mu}{\|r\|^5}\mathbf{r} \times \mathbf{I}\mathbf{r} \tag{3.38}$$

#### 3.1.5.2. Solar Radiation Pressure (SRP) Model

To model the acceleration due to the solar radiation pressure, a flat plate model is adopted. This model is used in (Kikuchi et al., 2017) to model Hayabusa2's SRP model. This model assumes that the effect of SRP is primarily due to the solar panels. Without the loss of generality, the solar panel is assumed to be perpendicular to the $z^{SC}$ axis. A

vector $\hat{\mathbf{n}}^{SC}$ is defined to be a unit vector parallel to the $z^{SC}$ axis. For maximum power output from the solar array, the goal would be to align $\hat{\mathbf{n}}^{SC}$ axis with the sun-pointing vector $\hat{\mathbf{s}}^{SC}$. The sun-pointing vector ($\hat{\mathbf{s}}^{SC}$) is given as,

$$\hat{\mathbf{s}}^{SC} = {}^{SC}\mathbf{C}_{SP}\hat{\mathbf{z}}^{SP} \tag{3.39}$$

Maximizing the power output from the solar panels results in maximizing the force due to SRP. This results $\hat{\mathbf{n}}^{SC} \cdot \hat{\mathbf{s}}^{SC} = 1$. In this work, the goal of the attitude adaptive control is to align the sun-pointing vector $\hat{\mathbf{s}}^{SC}$ with $\hat{\mathbf{n}}^{SC}$. The SRP force due to a flat plate model is given as,

$$\mathbf{f}_{SRP} = -PA(\hat{\mathbf{n}}^{SC} \cdot \hat{\mathbf{s}}^{SC})[(2(\hat{\mathbf{n}}^{SC} \cdot \hat{\mathbf{s}}^{SC})C_s + B_f C_d)\hat{\mathbf{n}}^{SC} + (C_d + C_a)\hat{\mathbf{s}}^{SC}] \tag{3.40}$$

where $B_f = \frac{2}{3}$ is the Lambertian coefficient, $A$ is the surface area of the flat plate, and $P = \frac{P_0}{d^2}$ is the SRP acting on the surface of the spacecraft. Also, $P_0 = 1 \times 10^{17} \frac{kg.m}{s^2}$ and $C_s, C_d, C_a$ correspond to optical constants of the spacecraft.

Torque due to SRP is given as,

$$\mathbf{T}_{SRP} = {}^{SC}\mathbf{L}_{SRP} \times m\mathbf{a}_{SRP} \tag{3.41}$$

where ${}^{SC}\mathbf{L}_{SRP}$ is the position vector from center of the spacecraft to the center of SRP force. This vector is defined to ${}^{SC}\mathbf{L}_{SRP} = [0, L, 0]^T$. Here, $L$ is the distance between the SRP force and center of mass of the spacecraft.

# 4. Direct Adaptive Control

A direct adaptive control strategy is implemented in this work. This form of model reference adaptive controller (MRAC) is based on the simple adaptive control (SAC) strategy (Kaufman et al., 1997a). This controller has several advantages over the conventional feedback controllers, such as it does not require a plant model, it is an output feedback controller, and it does not require a full state-feedback, and the estimation of system parameters is not required.

This gives this controller several advantages for spacecraft missions in unknown environments, such as asteroid proximity missions, where it is challenging to estimate system parameters in a short amount of time. SAC requires a reference model to track trajectories. A linear or low order reference model can be used as a reference model, making it simple to implement in real-world applications. In this section, the formulation of SAC and stability analysis of the orbit-attitude model is discussed.

## 4.1. Dynamical System

The nonlinear system dynamics are given as,

$$\dot{\mathbf{x}}(t) = \mathbf{A}\mathbf{x}(t) + \mathbf{B}\mathbf{u}(t) \tag{4.1}$$

$$\mathbf{y}(t) = \mathbf{C}\mathbf{x}(t) \tag{4.2}$$

where, $\mathbf{x}(t) \in \mathbf{R}^n, \mathbf{u}(t) \in \mathbf{R}^m, \mathbf{y}(t) \in \mathbf{R}^m$ are the state, control, and output vectors and $\mathbf{A} = \mathbf{A}(\mathbf{x}, t) \in \mathbf{R}^{n\times n}$, $\mathbf{B} = \mathbf{B}(\mathbf{x}, t) \in \mathbf{R}^{n\times m}$, and $\mathbf{C} \in \mathbf{R}^{m\times n}$. It should be noted that in SAC, it is necessary to maintain the square state-space form; that is, the number of control inputs ($\mathbf{u}$) must be equal to number of states being tracked ($\mathbf{y}$) (i.e. $dim(\mathbf{u}) = dim(\mathbf{y}) = m$).

The reference model to be tracked is given as,

$$\dot{\mathbf{x}}_m(t) = \mathbf{A}_m\mathbf{x}_m(t) + \mathbf{B}_m\mathbf{u}_m(t) \tag{4.3}$$

$$\mathbf{y}_m(t) = \mathbf{C}_m\mathbf{x}_m(t) \tag{4.4}$$

The order of reference model state and control vectors is independent of the system dynamics. However, the order of the output vector of the reference model ($\mathbf{y}_m \in \mathbf{R}^m$) must match the output vector of the system dynamics ($\mathbf{y} \in \mathbf{R}^m$) i.e. $dim(\mathbf{y}_m) = dim(\mathbf{y}) = m$.

### 4.2. Control Structure

SAC is an output feedback controller and only requires the measurement of the states to be tracked. The adaptive control is given as,

$$\mathbf{u} = \mathbf{K}_e(t)\mathbf{e}_y + \mathbf{K}_x(t)\mathbf{x}_m + \mathbf{K}_u(t)\mathbf{u}_m \tag{4.5}$$

In Equation (4.5), $\mathbf{e}_y(t)$ is the output tracking error, defined as,

$$\mathbf{e}_y(t) = \mathbf{y}_m(t) - \mathbf{y}(t) \tag{4.6}$$

$$\mathbf{e}_y(t) = \mathbf{C}\mathbf{x}_m(t) - \mathbf{C}\mathbf{x}(t) \tag{4.7}$$

where $\mathbf{y}_m(t)$ and $\mathbf{y}(t)$ are the output vectors of the reference and system models respectively. $\mathbf{K}_e(t) \in R^{m\times m}$ is the time-varying control gain matrix, $\mathbf{K}_x(t) \in R^{m\times n}$ and $\mathbf{K}_u(t) \in R^{m\times m}$ are time-varying feedforward control gains, and $\mathbf{x}_m$ and $\mathbf{u}_m$ are the states and control vectors of the reference model.

The adaptive gains $\mathbf{K}_e$(t), $\mathbf{K}_u(t)$ and $\mathbf{K}_u(t)$ from Equation (4.5) are the summation of integral adaptive gains $\mathbf{K}_I(t) = [\mathbf{K}_{Ie}\ \mathbf{K}_{Ix}\ \mathbf{K}_{Iu}]$ and proportional adaptive gains

$\mathbf{K}_P(t) = [\mathbf{K}_{Pe}\ \mathbf{K}_x\ \mathbf{K}_{Pu}]$ given as,

$$\begin{aligned} \mathbf{K}_e(t) &= \mathbf{K}_{Ie}(t) + \mathbf{K}_{Pe}(t) \\ \mathbf{K}_x(t) &= \mathbf{K}_{Ix}(t) + \mathbf{K}_{Px}(t) \\ \mathbf{K}_u(t) &= \mathbf{K}_{Iu}(t) + \mathbf{K}_{Pu}(t) \end{aligned} \tag{4.8}$$

To guarantee stability and achieve desired tracking performance, it has been shown that only the integral gains $\mathbf{K}_I(t)$ are necessary (Kaufman et al., 1997a). However, proportional adaptive gains $\mathbf{K}_P(t)$ have been shown to improve the rate of convergence of the SAC (**Ul**). Hence, they have been implemented in this work.

The integral control update law is given as,

$$\begin{aligned} \dot{\mathbf{K}}_{Ie}(t) &= \mathbf{e}_y(t)\mathbf{e}_y^T(t)\mathbf{\Gamma}_e \\ \dot{\mathbf{K}}_{Ix}(t) &= \mathbf{e}_y(t)\mathbf{x}_{ref}^T(t)\mathbf{\Gamma}_r \\ \dot{\mathbf{K}}_{Iu}(t) &= \mathbf{e}_y(t)\mathbf{u}(t)^T\mathbf{\Gamma}_u \end{aligned} \tag{4.9}$$

In Equation (4.9), $\mathbf{\Gamma}_e$, $\mathbf{\Gamma}_r$ and $\mathbf{\Gamma}_u$ are positive definite weighting matrices (tuning parameters) for the integral adaptive control law. It can be noted that these parameters must be manually tuned to adjust the rate of adaptation.

The proportional control update law is given as,

$$\begin{aligned} \mathbf{K}_{Pe}(t) &= \mathbf{e}_y(t)\mathbf{e}_y^T(t)\bar{\mathbf{\Gamma}}_e \\ \mathbf{K}_{Px}(t) &= \mathbf{e}_y(t)\mathbf{x}_{ref}^T(t)\bar{\mathbf{\Gamma}}_r \\ \mathbf{K}_{Pu}(t) &= \mathbf{e}_y(t)\mathbf{u}(t)^T\bar{\mathbf{\Gamma}}_u \end{aligned} \tag{4.10}$$

In Equation (4.10), $\bar{\mathbf{\Gamma}}_e$, $\bar{\mathbf{\Gamma}}_r$ and $\bar{\mathbf{\Gamma}}_u$ are positive semi-definite matrices used for the proportional adaptive gain laws.

The adaptive control law can be expressed in a compact form as,

$$\mathbf{u} = \mathbf{K}(t)\mathbf{r}(t) \tag{4.11}$$

where,

$$\begin{aligned} \mathbf{K}(t) &= [\mathbf{K}_e(t) \;\; \mathbf{K}_x(t) \;\; \mathbf{K}_u(t)] \\ \mathbf{r}(t) &= [\mathbf{e}_y(t)^T \;\; \mathbf{x}_m(t)^T \;\; \mathbf{u}_m(t)^T]^T \end{aligned} \tag{4.12}$$

### 4.3. SAC Modification for Orbital Dynamics

Adaptive controllers are designed separately for the orbital and attitude controller. The underlying assumption is that the spacecraft is equipped with thrusters, so the controllers can be decoupled, even though the system dynamics are coupled. In the case of orbital dynamics, the SAC is modified to exclude the feed-forward adaptive control law ($\mathbf{u}_m$). This is done because a user-defined reference model is designed such that the trajectories are directly generated without the need for reference control ($\mathbf{u}_m$).

The modified adaptive control is given as,

$$\mathbf{u} = \mathbf{K}_e(t)\mathbf{e}_y(t) + \mathbf{K}_x(t)\mathbf{x}_m(t) \tag{4.13}$$

It can be noted from (Kaufman et al., 1997b) that the feed-forward reference control is not required to guarantee stability. Also, in the case of attitude control, the full form of SAC, as given in Equation (4.5), is implemented.

### 4.4. Robustness Modification

The adaptive control gains can diverge during non-ideal tracking scenarios from the presence of noise as the tracking error continues to grow and the adaptive law (Equation (4.9)) struggles to compensate (Barkana, 2016). To address this issue, a $\sigma$ modification

was introduced by Ioannou and Kokotovic (Ioannou & Kokotovic, 1984). The sigma modification for the feedback integral control law ($\mathbf{K}_{Ie}$) can be given as,

$$\dot{\mathbf{K}}_{Ie}(t) = \mathbf{e}_y(t)\mathbf{e}_y^T(t)\mathbf{\Gamma}_e - \sigma\mathbf{K}_{Ie}(t) \tag{4.14}$$

The value for the $\sigma$ modification is set between 0 and 1 to avoid divergence (Ioannou & Kokotovic, 1983). It has also been shown in Reference (Barkana, 2016) that this modification is only needed for the feedback term i.e. $\mathbf{K}_{Ie}$. This modification has been applied in several applications (Ulrich, Saenz-Otero, et al., 2016b, Barkana, 2016, Ulrich, Sasiadek, et al., 2012).

Even though the $\sigma$ modification increases the robustness for noisy/non-ideal systems, it decreases robustness in case of ideal scenario. This is also known as bursting phenomenon. The $\sigma$ modification hinders the adaptive gains to tend to zero. Therefore, in order to resolve this issue, we have introduced an $e$ modification for SAC. This modification was initially introduced for adaptive control systems by Narendra and Annaswamy (Narendra & Annaswamy, 1987). The $e$ modification for SAC is defined as,

$$\dot{\mathbf{K}}_{Ie}(t) = \mathbf{e}_y(t)\mathbf{e}_y^T(t)\mathbf{\Gamma}_e - \mu\|\mathbf{e}_y\|\mathbf{K}_{Ie}(t) \tag{4.15}$$

Here $\mu$ is a constant, and $\|\mathbf{e}_y\|$ is the norm of the output tracking error. As the output tracking error tends to zero for an ideal tracking case, the $e$ modification term also tends to zero. This modification resolves the issue introduced due to the $\sigma$ modification.

A numerical comparison between $\sigma$ modification and $e$ modification is shown in Section 4.7.3.3. and the stability analysis is given in the following section. It can be noted that the robustness modification is given in Equation (4.15) is applied for numerical analysis in this work.

### 4.5. Stability Conditions

It is necessary to prove that the system is almost strictly passive (ASP) to guarantee SAC stability. A nonlinear system $(\mathbf{A}(\mathbf{x},t), \mathbf{B}(\mathbf{x},t), \mathbf{C})$ is called almost strictly passive if there exists a constant feedback gain $\tilde{\mathbf{K}}_e$ (unknown and not needed for implementation) such that the system is stable (Barkana, 2010). In this section, some necessary definitions are discussed that are required to prove stability for the SAC.

#### 4.5.1. Strictly Passive Systems

A nonlinear system as in Equation (4.1) is strictly passive (SP) if there exists two positive definite symmetric matrices $\mathbf{P}(\mathbf{x},t)$ and $\mathbf{Q}(\mathbf{x},t)$ such that the following two conditions are satisfied,

$$\dot{\mathbf{P}} + \mathbf{P}\mathbf{A} + \mathbf{A}^T\mathbf{P} = -\mathbf{Q} \tag{4.16}$$

$$\mathbf{P}\mathbf{B} = \mathbf{C}^T \tag{4.17}$$

The conditions in Equation (4.16)-(4.17) imply that a strictly passive (SP) system is an asymptotically stable system. This also implies that the system is a minimum phase system and the product $\mathbf{CB} > \mathbf{0}$.

#### 4.5.2. Almost Strictly Passive (ASP) System

A nonlinear system as in (4.1) is called as almost strictly passive (ASP) system if there exist positive definite matrices $\mathbf{P}$ and $\mathbf{Q}$, and constant output feedback gain $\tilde{\mathbf{K}}_e$ (unknown and not needed for implementation) such that the closed-loop system satisfies the following conditions,

$$\dot{\mathbf{P}} + \mathbf{P}(\mathbf{A} - \mathbf{B}\tilde{\mathbf{K}}_e\mathbf{C}) + (\mathbf{A} - \mathbf{B}\tilde{\mathbf{K}}_e\mathbf{C})^T\mathbf{P} = -\mathbf{Q} \tag{4.18}$$

$$\mathbf{PB} = \mathbf{C}^T \tag{4.19}$$

Satisfying the ASP property conditions in Equations (4.18) and (4.19) implies that the system is minimum phase and the product $\mathbf{CB} > \mathbf{0}$ and vice-versa, i.e. if the system is minimum-phase and the product $\mathbf{CB} > \mathbf{0}$, then the system is ASP.

In summary, a nonlinear system, as given in Equation (4.1), with the adaptive control input, is guaranteed to be stable if the system is minimum-phase and the product $\mathbf{CB} > \mathbf{0}$. The resulting system is also known as ASP. The proof is shown in the following section.

In case of orbital dynamics, the product $\mathbf{CB}$ is given as,

$$\mathbf{CB} = \frac{1}{m}[\mathbf{I}_{3\times3} \;\; \mathbf{I}_{3\times3}] \begin{bmatrix} \mathbf{0}_{3\times3} \\ \\ \mathbf{I}_{3\times3} \end{bmatrix} = \frac{1}{m}\mathbf{I}_{3\times3} > \mathbf{0} \tag{4.20}$$

where $\mathbf{C}$ and $\mathbf{B}$ are given from Equation (4.20). From Equation (4.20), the product $\mathbf{CB} > \mathbf{0}$ for orbital dynamics system.

In the case of attitude dynamics, the product $\mathbf{CB}$ is given as,

$$\mathbf{CB} = \mathbf{I}^{-1}[\mathbf{I}_{3\times3} \;\; \mathbf{I}_{3\times3}] \begin{bmatrix} \mathbf{0}_{3\times3} \\ \\ \mathbf{I}_{3\times3} \end{bmatrix} = \mathbf{I}^{-1}\mathbf{I}_{3\times3} > \mathbf{0} \tag{4.21}$$

where $\mathbf{C}$ and $\mathbf{B}$ are given from Equation (4.21) and the product $\mathbf{CB} > \mathbf{0}$ for attitude dynamics system. Therefore, one of the conditions for the system to be ASP is satisfied.

### 4.5.3. Minimum-Phase Systems

A linear system model is minimum-phase if the zero-dynamics of the transfer functions are stable. However, this cannot be shown for a nonlinear system since the transfer function is not defined for these systems. Therefore, Barkana (2010) provides an alternative set of conditions to determine if a nonlinear system is minimum phase.

If there exists $\mathbf{M} \in R^{n \times n-m}$ and $\mathbf{N} \in R^{n-m \times n}$ such that,

$$\mathbf{CM} = \mathbf{0} \tag{4.22}$$

$$\mathbf{NB} = \mathbf{0} \tag{4.23}$$

$$\mathbf{NM} = \mathbf{I}_{n-m} \tag{4.24}$$

then applying the transformation $\mathbf{x}(t) = \mathbf{M}\mathbf{z}(t)$ results in the zero-dynamics ($\dot{\mathbf{z}}(t)$), given as,

$$\dot{\mathbf{z}}(t) = (\dot{\mathbf{N}} + \mathbf{N})\mathbf{A}\mathbf{z}(t) \tag{4.25}$$

Defining appropriate $\mathbf{M}$ and $\mathbf{N}$ that satisfy the conditions from Equation (4.22) through Equation (4.24) results in a uniformly asymptotically stable zero-dynamics, and the system is defined to be minimum-phase.

For the orbital and attitude dynamics systems, the relationships from Equation (4.22) through Equation (4.24) are satisfied by defining $\mathbf{M}(\mathbf{x}, t)$ and $\mathbf{N}(\mathbf{x}, t)$ as,

$$\mathbf{M}(\mathbf{x}, t) = \begin{bmatrix} \mathbf{I}_{3\times3} \\ \\ -\mathbf{I}_{3\times3} \end{bmatrix}, \quad \mathbf{N}(\mathbf{x}, t) = \begin{bmatrix} \mathbf{I}_{3\times3} & -\mathbf{0}_{3\times3} \end{bmatrix} \tag{4.26}$$

Applying the transformation $\mathbf{x}(t) = \mathbf{M}\mathbf{z}(t)$, results stable in zero-dynamics for orbital and attitude given as,

$$\dot{\mathbf{z}}_{orb}(t) = \mathbf{N}\mathbf{A}_{orb}\mathbf{M}\mathbf{z}_{orb}(t) = -\mathbf{I}_{3\times3}\mathbf{z}_{orb}(t) \tag{4.27}$$

$$\dot{\mathbf{z}}_{att}(t) = \mathbf{N}\mathbf{A}_{att}\mathbf{M}\mathbf{z}_{att}(t) = -\mathbf{I}_{3\times3}\mathbf{z}_{att}(t) \tag{4.28}$$

here $\mathbf{I}_{3\times3}$ is the identity matrix.

Therefore, the controlled orbital and attitude dynamics systems are minimum-phase. Note that the choice of matrices $\mathbf{M}(\mathbf{x}, t)$ and $\mathbf{N}(\mathbf{x}, t)$ is non-unique, and any non-trivial and well-defined matrices can be chosen as long as the relationship given in Equation

(4.22) through Equation (4.24) are satisfied.

Therefore, it can be concluded that the orbital and attitude dynamics systems are almost strictly passive (ASP).

### 4.6. Stability Analysis

For MRAC, the stability of the system is defined on the error dynamics of the system. An ideal trajectory is defined such that $\mathbf{y}(t)^* = \mathbf{y}_m(t)$. Ideal trajectories $(\mathbf{x}^*(t), \mathbf{u}^*(t), \mathbf{y}^*(t))$ can be defined using the nonlinear system dynamics ($\mathbf{A}^* = \mathbf{A}^*(\mathbf{x}, t), \mathbf{B}^* = \mathbf{B}^*(\mathbf{x}, t)$) model as follows:

$$\dot{\mathbf{x}}^*(t) = \mathbf{A}^*\mathbf{x}^*(t) + \mathbf{B}^*\mathbf{u}^*(t) \tag{4.29}$$

$$\mathbf{y}^*(t) = \mathbf{C}\mathbf{x}^*(t) \tag{4.30}$$

In this application, $\mathbf{y}^* = \mathbf{y}_m$ such that the ideal trajectories correspond to tracking the reference output. The ideal state and control can be represented as a linear combination of reference states $\mathbf{x}_m(t)$ and control input $\mathbf{u}_m(t)$ as follows:

$$\mathbf{x}^*(t) = \mathbf{X}\mathbf{x}_m(t) + \mathbf{U}\mathbf{u}_m(t) \tag{4.31}$$

$$\mathbf{u}^*(t) = \tilde{\mathbf{K}}_{x_m}\mathbf{x}_m(t) + \tilde{\mathbf{K}}_{u_m}\mathbf{u}_m(t) \tag{4.32}$$

$$\mathbf{y}^*(t) = \mathbf{C}\mathbf{x}^*(t) \tag{4.33}$$

$$= \mathbf{C}\mathbf{x}_m(t) \tag{4.34}$$

where $\mathbf{X}$, $\mathbf{U}$, $\tilde{\mathbf{K}}_{x_m}$, $\tilde{\mathbf{K}}_{u_m}$ are constant unknown gains for the ideal system.

A condition for stability is such that the system states must converge to the ideal states. The error between the ideal and system states is given as,

$$\mathbf{e}_x(t) = \mathbf{x}^*(t) - \mathbf{x}(t) \tag{4.35}$$

Differentiating Equation (4.35) with respect to time results in error-dynamics equation, given as,

$$\dot{\mathbf{e}}_x(t) = \dot{\mathbf{x}}^*(t) - \dot{\mathbf{x}}(t) \tag{4.36}$$

The output tracking error ($\mathbf{e}_y$) is defined as,

$$\mathbf{e}_y(t) = \mathbf{y}_m(t) - \mathbf{y}(t) = \mathbf{C}\mathbf{x}^*(t) - \mathbf{C}\mathbf{x}(t) \tag{4.37}$$

The goal of the adaptive controller is to drive the error between the ideal states and the system states to zero (i.e. $\mathbf{e}_x(t) \rightarrow 0$).

The final form of error dynamics is given as (see Appendix for full derivation):

$$\dot{\mathbf{e}}_x(t) = \mathbf{A}\mathbf{e}_x(t) - \mathbf{B}\tilde{\mathbf{K}}_{e_y}\mathbf{e}_y(t) - \mathbf{B}[\mathbf{K}(t) - \tilde{\mathbf{K}}]\mathbf{r}(t) \tag{4.38}$$

The stability is proven using Lyapunov's direct method. The Lyapunov function is defined such that the dynamical gains resulting from the adaptive control laws are considered as the part function as well. The Lyapunov function is defined as follows:

$$V(t) = \mathbf{e}_x^T(t)\mathbf{P}\mathbf{e}_x(t) + tr[\mathbf{K}_I(t) - \tilde{\mathbf{K}}]\mathbf{\Gamma}^{-1}[\mathbf{K}_I(t) - \tilde{\mathbf{K}}]^T \tag{4.39}$$

where, $\mathbf{e}_x, \mathbf{P}, \mathbf{K}_I$ are functions of time and $\tilde{\mathbf{K}}$ is constant, and $\mathbf{\Gamma} > 0$ is a symmetric, positive definite matrix.

Using the ASP property and substituting (4.18) and (4.19) in (16), and rearranging the terms, the final form of derivative for the Lyapunov function is given as,

$$\dot{V}(t) = -\mathbf{e}_x^T(t)\mathbf{Q}(t)\mathbf{e}_x(t) - 2\mathbf{e}_y^T(t)\mathbf{e}_y(t)\mathbf{r}(t)^T\mathbf{\Gamma}\mathbf{r}(t) \tag{4.40}$$

From ASP property, the Lyapunov derivative negative definite with respect to $\mathbf{e}_x$ but only negative semi-definite with respect to the overall adaptive system. Thus, the system is bounded. From LaSalle's invariance principal for non-autonomous systems (LaSalle,

1976) it is shown from (Kaufman et al., 1997b) that the system asymptotically converges such that the tracking error $\mathbf{e}_x = 0$. Therefore, the Lyapunov function defined in Equation (4.39) reaches zero.

### 4.7. Simulation and Results

In this section, the SAC is implemented in simulation studies by formulating reference models for orbital, and attitude dynamics. There are two types of simulation scenarios chosen for this research: orbit-attitude coupled trajectory tracking for time-varying trajectories in the asteroid body-frame and orbit-attitude coupled trajectory tracking for the body-frame hovering.

Asteroid Kleopatra is chosen for the simulation as shown in Figure 4.1, the asteroid properties are taken from NASA's Planetary Data System (PDS) (NASA, 2020). The properties of asteroid Ida and the spacecraft can be found in Table 4.1 and Table 4.2. Asteroid Kleopatra is a metallic dog-bone shaped asteroid with a highly irregular gravitational field. The system dynamics are integrated with Runge-Kutta fourth-order (RK-4) with a time step of 0.01 seconds. Asteroid Kleopatra has the highest gravitational field amongst the three asteroids that are used to simulate the gravity in this work followed by asteroid Eros and asteroid Bennu.

Table 4.1

Asteroid 216 Kleopatra Parameters

| | |
|---|---|
| Body mass m | $5.1732 \times 10^{16}\ kg$ |
| $\omega$ | $3.77 \times 10^{-4}\ rad/s$ |
| Brillouin Radius | $138.24\ km$ |

Table 4.2

Spacecraft Parameters

| | |
|---|---|
| Mass (m) | 600 $kg$ |
| Moments of Inertia $(I_x, I_y, I_z)$ | 360,360,480 $kg.m^2$ |
| CS-CM distance | 0.2 $m$ |
| Optical elements $C_s, C_s, C_a$ | 0.1,0.1,0.8 |

### 4.7.1. Orbital-Attitude Trajectory Tracking

Here, we present the formulation of reference models and results for orbital dynamics. Time-varying trajectories for orbital and hovering scenarios are designed. First, we discuss the orbital reference trajectory modeling, followed by attitude reference trajectory modeling.

#### 4.7.1.1. Orbital Model

In this case, a closed time-varying trajectory is designed based on (Lee & Singh, 2019). Generally, any smooth reference time-varying trajectory can be considered. In this case a closed orbit trajectory $\mathbf{x}_m(t) = [\mathbf{r}_m,\ \dot{\mathbf{r}}_m]^T$ is given as,

$$\mathbf{x}_m(t) = \mathbf{x}_{in}e^{\alpha t^3} + \mathbf{x}_f(1 - e^{\alpha t^3}) \tag{4.41}$$

$$\mathbf{y}_m(t) = \mathbf{C}\mathbf{x}_m \tag{4.42}$$

where $\mathbf{x}_{in} = [\mathbf{r}_{in},\ \dot{\mathbf{r}}_{in}]^T$ is the initial condition of the the reference trajectory, and $\mathbf{x}_f = [\mathbf{r}_f(t),\ \dot{\mathbf{r}}_f(t)]^T$ is the final time-varying orbital reference trajectory. The tuning parameter $\alpha = -1 \times e^{-8}$ corresponds to the response characteristics and can be tuned depending on the dynamics of the system. The blended output $\mathbf{y}_m$ is the combination of reference position ($\mathbf{r}_m$) and velocity ($\dot{\mathbf{r}}_m$). The time-varying final orbital trajectory ($\mathbf{x}_f =$

$[\mathbf{r}_f(t),\ \dot{\mathbf{r}}_f(t)]^T$) is given as,

$$\mathbf{r}_f(t) = \begin{bmatrix} 0.5R_d \sin(\omega_e t) \\ R_d \cos(\omega_e t) \\ R_d \sin(\omega_e t) \end{bmatrix}, \quad \dot{\mathbf{r}}_f(t) = \begin{bmatrix} 0.5R_d\omega_e \cos(\omega_e t) \\ -R_d\omega_e \sin(\omega_e t) \\ Rd\omega_e \cos(\omega_e t) \end{bmatrix} \tag{4.43}$$

where $R_d$ is the desired final orbit radius and $\omega_e = 1.974\omega$, where $\omega$ is the angular velocity of the asteroid. It can be noted that the trajectory is designed such that, as time grows, the initial reference state ($\mathbf{x}_{in}$) converges to the final reference orbit ($\mathbf{x}_f$).

The initial condition for the reference model with $R_d = 60$ km is given as,

$$\mathbf{r}_{in} = [20\ 45\ 6\ ]^T \text{ km}, \quad \dot{\mathbf{r}}_{in} = [0\ 0\ 0]^T \times 10^{-3}\text{km/s} \tag{4.44}$$

The total simulation time is taken to be 20000 seconds. The integral adaptive gains are initialized with zero initial condition. The adaptive gains are chosen as $\mathbf{\Gamma}_e = \bar{\mathbf{\Gamma}}_e = 10^6\mathbf{I}_{3x3}$ and $\mathbf{\Gamma}_r = \bar{\mathbf{\Gamma}}_r = 0.001\mathbf{I}_{3x3}$. In this case, the modified adaptive control model from Equation (4.13) is implemented.

Spacecraft orbital tracking and the time-varying positions can be in seen Figures 4.1 and 4.2(a), respectively. The adaptive controller is able to successfully track the desired reference trajectory around asteroid Kleopatra in the body-frame of the asteroid. It can be noted that the spacecraft translates from close proximity of the asteroid to the final closed and time-varying trajectory. The position error between the actual and reference trajectory can be seen in Figure 4.2(c).

The control accelerations are given in Figure 4.2(b). It can be noted that a non-zero control effort is required to track the trajectories. Acceleration due to the polyhedral gravity model is shown in Figure 4.2(d). It can be noted that the gravity of asteroid

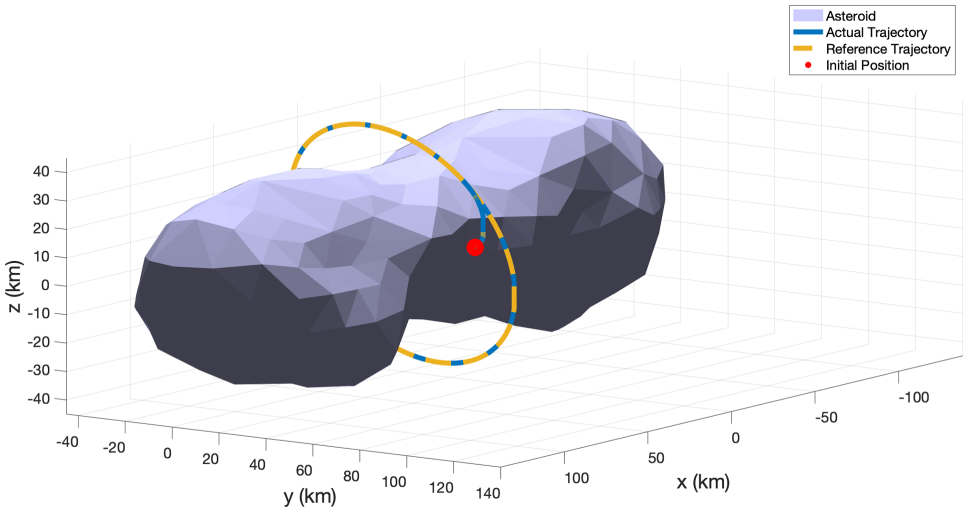


*Figure 4.1* Spacecraft trajectory of the spacecraft around asteroid Kleopatra in asteroid body-frame.

Kleopatra is highly time-variant and perturbed. The accelerations due to the solar radiation pressure (SRP) can be seen in Figure 4.2(e) and Figure 4.2(f). The SRP accelerations converge to a constant value when the attitude trajectory reaches the desired final orientation. This depicts the effect of orbit-attitude dynamical coupling. It can be noted that for a Hayabusa sized spacecraft, the magnitude of acceleration due to SRP is comparable to the gravity of the asteroid. The position tracking error (e) is shown in Figure 4.2(c). These figures show that the adaptive control is able track trajectories and while keeping the acceleration of the spacecraft to a realistic value (<240 N).

#### 4.7.1.2. Attitude Model

One of SAC's advantages is that a reference model independent of the system model dynamics can be implemented (Kaufman et al., 1997b). Therefore, the attitude reference model is designed based on a simple harmonic oscillator with damping. In this case, the full expression of SAC is implemented as given in Equation (4.5).

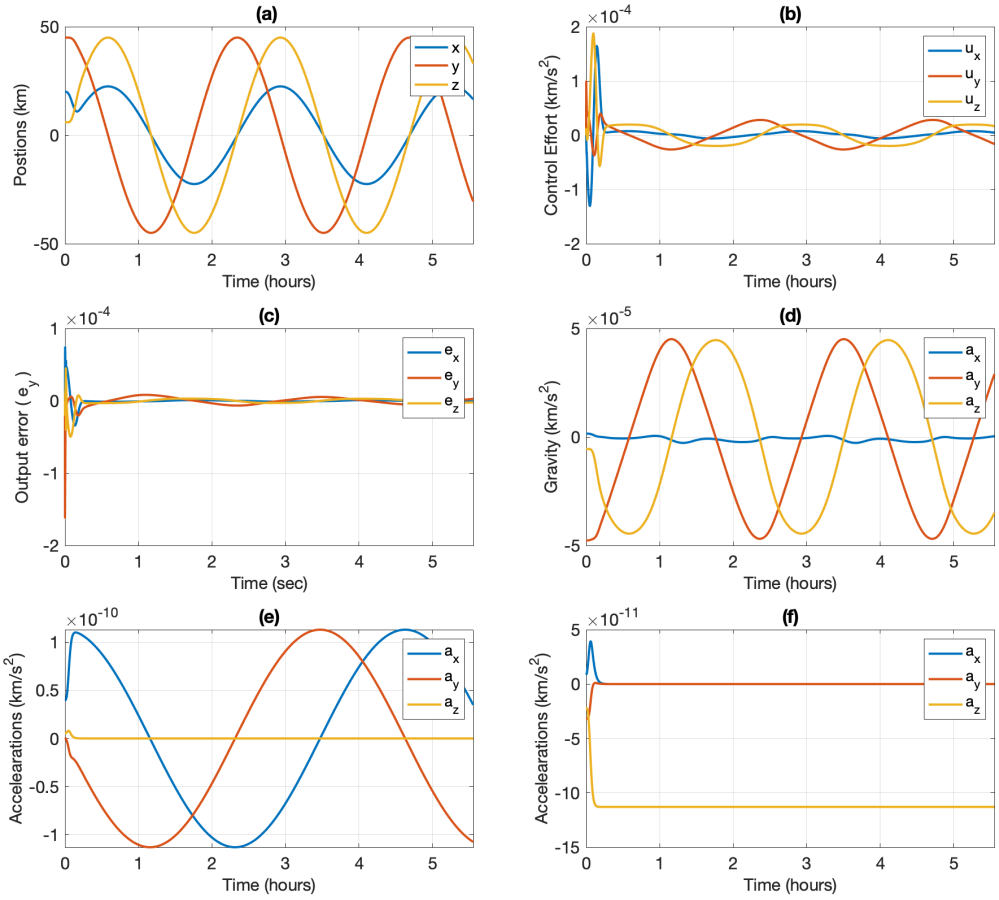


*Figure 4.2* Plots for asteoroid tracjectory tracking case for asteroid Kleopatra(a) position vs. time, (b) control effort vs. time, (c) output error vs. time, (d) acceleration due to gravity, (e) SRP vs. time in Sb frame, (f) SRP vs. time in SC frame.

The reference model is given as (Shi et al., n.d.):

$$\dot{\mathbf{x}}_m(t) = \mathbf{A}_m\mathbf{x}_m(t) + \mathbf{B}_m\mathbf{u}_m(t) \tag{4.45}$$

$$\mathbf{y}_m(t) = \mathbf{C}_m\mathbf{x}_m(t) \tag{4.46}$$

where the system matrices are given as,

$$\mathbf{A}_m = \begin{bmatrix} \mathbf{0}_{3x3} & \mathbf{I}_{3x3} \\ -\omega^2\mathbf{I}_{3x3} & -2\eta\omega\mathbf{I}_{3x3} \end{bmatrix}, \mathbf{B}_m = \begin{bmatrix} \mathbf{0}_{3x3} \\ \omega^2\mathbf{I}_{3x3} \end{bmatrix}, \mathbf{C}_m = \begin{bmatrix} \mathbf{I}_{3x3} & \mathbf{I}_{3x3} \end{bmatrix} \tag{4.47}$$

where $\eta = 1$ is the damping ratio and $\omega = 0.009\ rad/s$ is the natural frequency of

the linear reference model. The reference trajectories are generated by integrating the reference model dynamics. A rest-to-rest maneuver is designed for the attitude tracking problem. Therefore, the initial and final angular velocities are zero. The initial conditions for angular velocity and MRPs are given as,

$$\boldsymbol{\sigma}_{in} = [-0.1\ 0.5\ 0.8\ ]^T,\ \ \boldsymbol{\omega}_{in} = [0\ 0\ 0]^T \text{ rad/s} \tag{4.48}$$

The reference control ($\mathbf{u}_m$) is generated by using a linear quadratic regulator (LQR). The built-in MATLAB function is used for generating the reference control where the state and control weighting matrices are $\mathbf{Q} = 0.1\mathbf{I}_{6\times6}$ and $\mathbf{R} = 0.1\mathbf{I}_{3\times3}$. The adaptive control tuning parameters are given as using $\mathbf{\Gamma}_e = 1e5\mathbf{I}_{3x3},\ \mathbf{\Gamma}_r = 1e3\mathbf{I}_{3x3},\ \mathbf{\Gamma}_u = 1e3\mathbf{I}_{3x3}$. The adaptive control gains are initialized with zero.

The MRPs and angular velocities are shown in Figure 4.3. It can be seen that the MRPs are successfully regulated with adaptive control. The spacecraft's final orientation is such that the acceleration due to the SRP is maximum, thus resulting in maximum torque. The control torque can be seen in Figure 4.3 (c). Note that a non-zero control is required to counter the SRP and gravity gradient torque in the final orientation. The torque due to SRP and gravity gradient can be seen in Figure 4.3 (d) and (e). The MRP tracking error can found in Figure 4.3 (f).

### 4.7.2. Body-Frame Hovering Trajectory Tracking

The reference trajectory for hovering is designed in the asteroid fixed body frame. The spacecraft is required to track a time-varying trajectory from the initial position to the final hovering position.

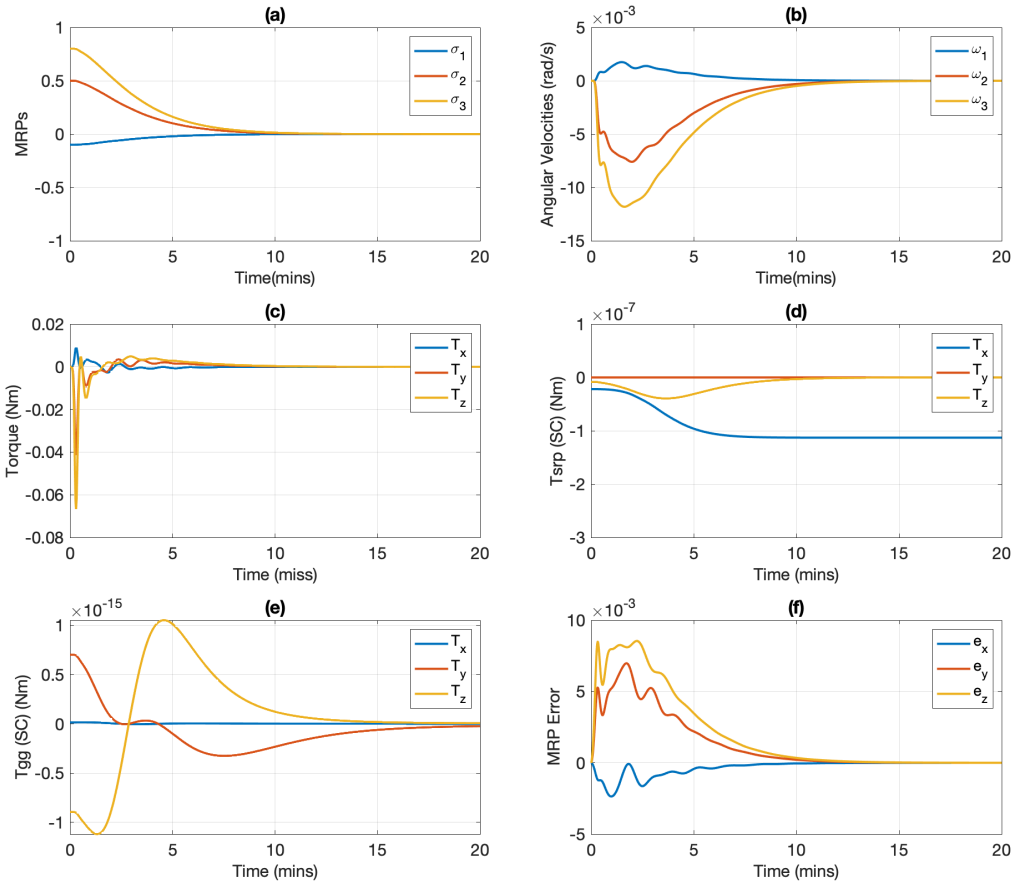


*Figure 4.3* Attitude plots for asteroid Kleopatra(a) MRPs vs. time, (b) angular velocity vs. time (c) control torque history in SC frame, (d) Torque due to SRP in SC frame, (e) gravity gradient torque in SC frame vs. time (f) MRP error vs. time.

The reference trajectory $\mathbf{x}_m(t) = [\mathbf{r}_m,\ \dot{\mathbf{r}}_m]^T$ is given similar to the orbital model as,

$$\mathbf{x}_m(t) = \mathbf{x}_{in}e^{\alpha t^3} + \mathbf{x}_f(1 - e^{\alpha t^3}) \tag{4.49}$$

$$\mathbf{y}_m(t) = \mathbf{C}\mathbf{x}_m(t) \tag{4.50}$$

where $\mathbf{y}_m \in R^3$ is the time-varying output for the spacecraft to track. The tuning parameter $\alpha = -1 \times e^{-9}$ corresponds to the rate of change of position, which can be tuned depending on the dynamical constraints. $\mathbf{x}_{in} = [\mathbf{r}_{in}\ \ \dot{\mathbf{r}}_{in}]$ is the initial position and velocity of the spacecraft, and $\mathbf{x}_f = [\mathbf{r}_f\ \ \dot{\mathbf{r}}_f]$ is the final spacecraft hovering position and

velocity in the asteroid fixed body frame. The reference trajectory from Equation (4.49) generates a time-varying smooth trajectory for the adaptive controller for tracking.

A rest-to-rest hovering maneuver is designed and the initial and the final positions are randomly chosen for the reference model as:

$$\begin{aligned} \mathbf{r}_{in} &= [20\ 45\ 6\ ]^T \text{ km}, \quad \dot{\mathbf{r}}_{in} = [0\ 0\ 0]^T \text{ km/s} \\ \mathbf{r}_f &= [25\ 120\ 6\ ]^T \text{ km}, \quad \dot{\mathbf{r}}_f = [0\ 0\ 0\ ]^T \text{ km/s} \end{aligned} \tag{4.51}$$

The adaptive gains are initialized with zero initial conditions. The adaptive tuning parameters are chosen as $\mathbf{\Gamma}_e = \bar{\mathbf{\Gamma}}_e = 10^6 I_{3\times3}$ and $\mathbf{\Gamma}_r = \bar{\mathbf{\Gamma}}_r = 0.001 I_{3\times3}$.

The spacecraft trajectory, as seen from the inertial frame, is shown in Figure 4.4. The relative magnitude of the external forces on the spacecraft is of the $10^-5 km/s^2$.It can be seen from Figure 4.4 that the spacecraft successfully translated from the initial position to the desired final hovering position. Figure 4.5 shows the spacecraft position in the asteroid fixed body frame. The adaptive controller is able to successfully hover at the desired position with respect to the asteroid.

In the body fixed hovering scenario, the accelerations due to gravity from the asteroid are time-invariant. This is due to the fact that the position of the spacecraft is fixed with respect to the asteroid. Figure 4.6(d) shows the total acceleration acting on the spacecraft due to the asteroid gravity field. It can be noted that non-zero control effort is required for station keeping at the desired location. Figure 4.6(a) shows the time-varying trajectory of the spacecraft in the asteroid fixed body-frame.

The control effort from the direct adaptive controller can be seen in Figure 4.6(b). At the final hovering position, the control effort converges to the summation of acceleration due to gravity, solar radiation pressure, and centrifugal acceleration from rotation of the

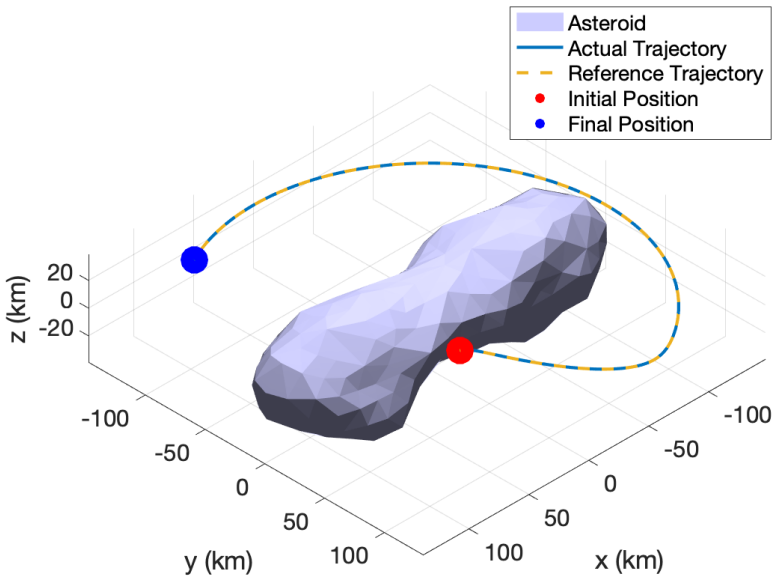


*Figure 4.4* Spacecraft trajectory for asteroid Kleopatra for hovering maneuver in an inertial frame.

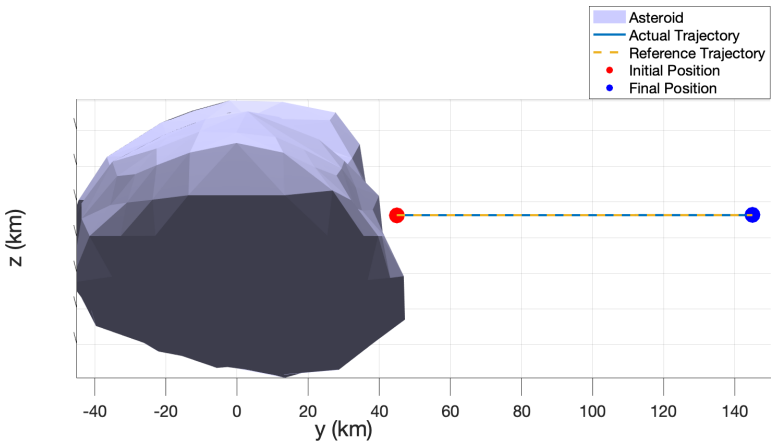


*Figure 4.5* Spacecraft trajectory for asteroid Kleopatra during hovering in asteroid body frame.

asteroid. The control effort resulting from this problem can be further reduced depending on the trajectory and tuning $\alpha$ in Equation (4.49). It can be noted that, since the $y$ coordinate of the spacecraft has the largest change in position, the control effort $\mathbf{u}_y$ is also the highest. Further command shaping can reduce this control effort. Also, the control

efforts are within the acceptable range of currently available chemical thrusters. The final hovering is approximately reached in 1696 seconds ($\sim$ 30 minutes). The maximum magnitude of the control effort is $\mathbf{u}_{max} = 1.9257 \times 10^{-4}$ km/s$^2$.

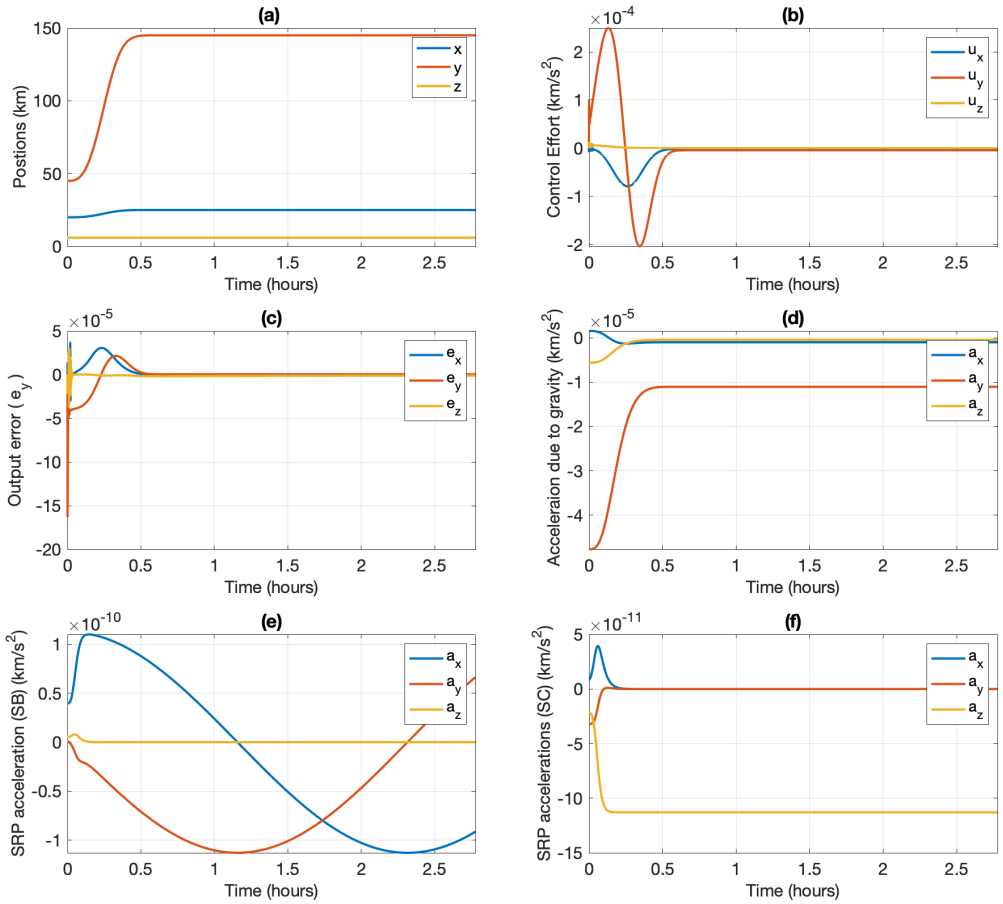


*Figure 4.6* Spacecraft trajectory tracking near Bemnu for hovering case(a) Position w.r.t time in SB frame, (b) control effort vs time in SB frame, (c) output error, (d) acceleration due to gravity, (e) SRP accelerations in SB frame, (f) SRP accelerations in SC frame.

### 4.7.3. Off-Nominal and Robustness Evaluation

Here we present numerical simulations to show the robustness of the adaptive control with $e$ modification. The evaluation is categorized as follows:

1. Numerical simulation of the control system using a different asteroid without

changing the control parameters.

2. Adding Gaussian noise to the system model and high-frequency sinusoidal noise to the measurement model.
3. Showing the advantages of the $e$ modification term in adaptive control for an ideal tracking scenario.

It can be noted that robustness evaluation is performed on asteroid Kleopatra for parts (2) and (3).

#### 4.7.3.1. Numerical Simulation for Asteroid Bennu

To show the robustness of the adaptive control to change in dynamical scenarios, we also show the numerical simulations for asteroid Bennu without changing the adaptive control tuning gains ($\mathbf{\Gamma}, \bar{\mathbf{\Gamma}}$). Asteroid Bennu is chosen since it vastly differs from the asteroid Kleopatra in terms of physical characteristics. The properties of asteroid Bennu are given in Table 4.3. Orbital tracking scenario from Equation (4.42) is considered. The tuning parameter $\alpha$ is changed to $\alpha = -1 \times e^{-12}$ to further change the tracking scenario.

Table 4.3

Asteroid Bennu Parameters

| | |
|---|---|
| Body mass m | $7.329 \times 10^{10}\ kg$ |
| $\omega$ | $4.0626 \times 10^{-4}\ rad/s$ |
| Brillouin Radius | $282.5\ m$ |

The initial condition for the reference model with $R_d = 0.7$ km is given as,

$$\mathbf{r}_{in} = [1\ 1\ 1\ ]^T \text{ km}, \quad \dot{\mathbf{r}}_{in} = [0\ 0\ 0]^T \times 10^{-3}\text{km/s} \tag{4.52}$$

Figure 4.7 shows the actual and reference trajectory of the spacecraft in asteroid body frame. Figure 4.8 shows successful results for trajectory tracking near asteroid Bennu without changing the control parameters.

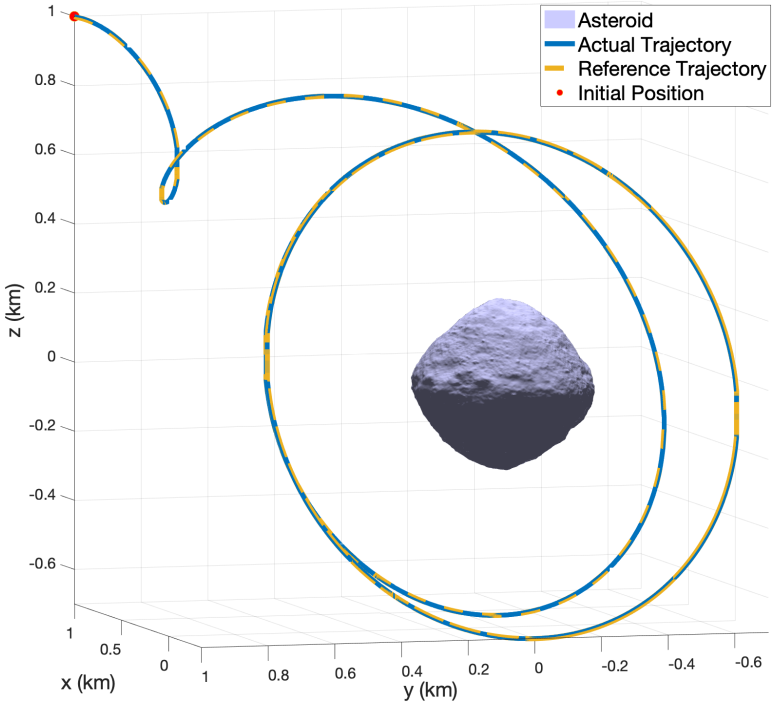


*Figure 4.7* Spacecraft trajectory in asteroid body-frame for asteroid Bennu.

#### 4.7.3.2. Effects of Unknown Noise

To further show the robustness of the adaptive control law in off-nominal conditions, we have shown the effects of random Gaussian noise on the system. A random Gaussian of the order of the gravitational field of asteroid Kleopatra in the reference trajectory is considered $(1 \times 10^{-5}\mathcal{N}(0,\ I_{3\times3})$. It can be seen from Figure 4.9 that the adaptive control is able to successfully handle the disturbances while keeping the order of tracking error low. It can be noted that the adaptive tuning parameters have not been changed for this analysis.

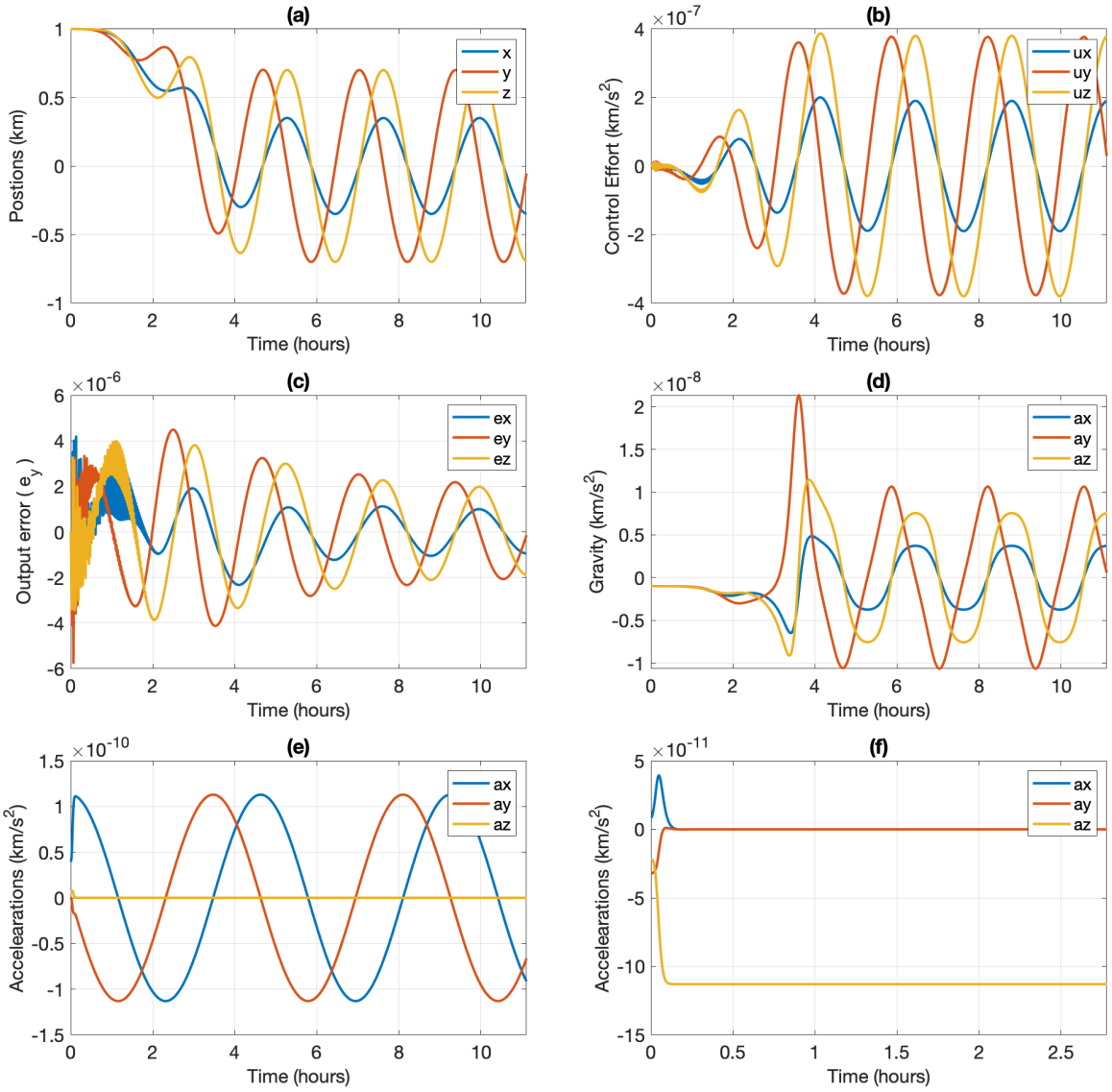


*Figure 4.8* Spacecraft trajecotry tracking plots for asteroid Bennu(a) position vs. time, (b) control effort vs. time, (c) output error vs. time, (d) acceleration due to gravity, (e) SRP vs. time in Sb frame, (f) SRP vs. time in SC frame.

To test the effect of measurement noise on the adaptive control, a high-frequency sinusoidal disturbance is added to the measurements (y). The disturbance is given as,

$$\boldsymbol{\nu} = 0.001 \times [(1 + \sin 0.1t),\ \ (1 + \sin 0.1t),\ \ (1 + \sin 0.1t)]^T \tag{4.53}$$

The results from Figure 4.10 show that the controller is able to successfully account for the measurement disturbance without the need to re-tune.

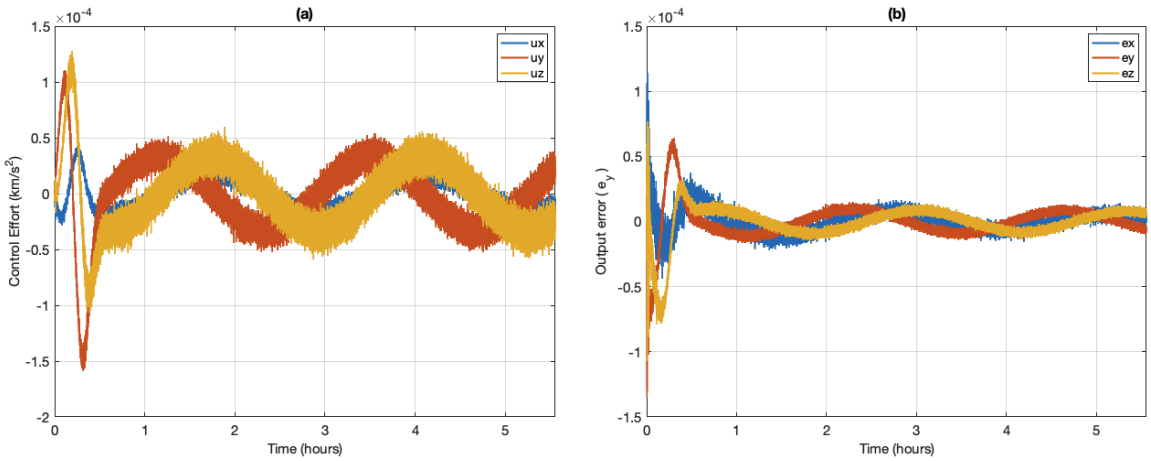


*Figure 4.9* (a) Control effort with Gaussian Noise, (b) Output error vs. time.

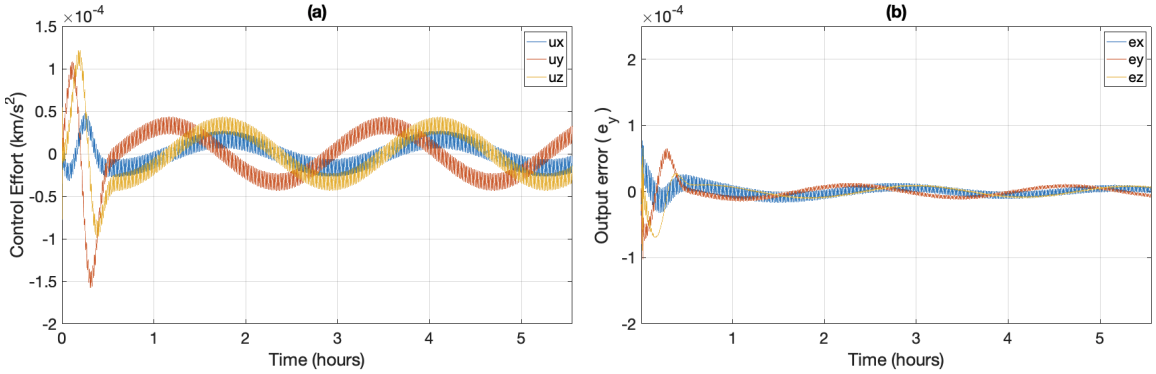


*Figure 4.10* (a) Control effort with sinusoidal noise, (b) Output error vs. time.

#### 4.7.3.3. e Modification Analysis

In this section, we present the comparison between SAC with sigma modification and SAC with e-modification for ideal tracking (without system and measurement noise). For sigma modification the sigma value of $\sigma = 0.1$ is considered, see Equation (4.14). In case of of $e$ modification, a $\mu$ of $\mu = 0.1$ is considered. Results from Figure 4.11 show that a significant improvement in control effort and output error when applying the $e$ modification for the ideal tracking case. Therefore, it is recommended to use $e$

modification for the cases where sigma modification fails to achieve ideal control effort. The results are explained by the fact that during ideal tracking, the $e$ modification term from the adaptive control law from Equation (4.15) tends to zero. It can be noted that lowering the sigma value reduces these effects. However, it does not eliminate the issue and decreases the robustness of the control system.

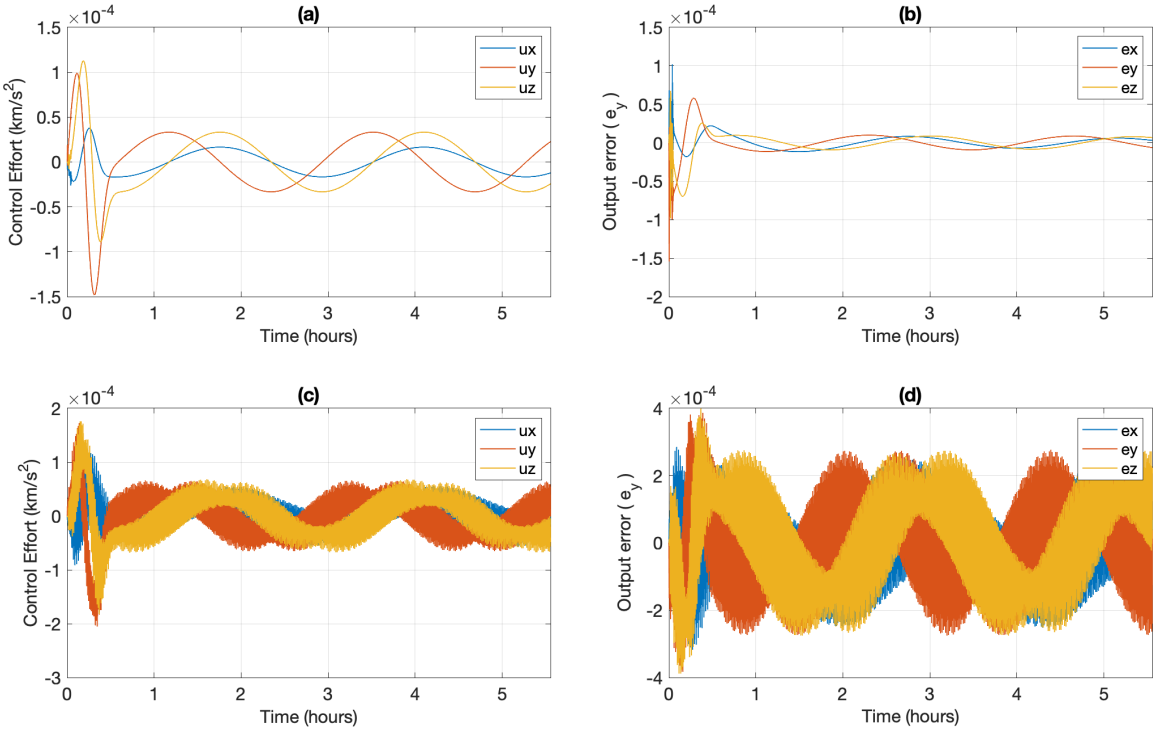


*Figure 4.11* (a) Control effort $e$ with modification (b) Output error vs. time for $e$ modification (c) Control effort with $\sigma$ modification and (d) Output error vs. time for $\sigma$ modification.

# 5. Nonlinear Model Predictive Control

Discrete nonlinear model predictive control (NMPC) is implemented in this work. NMPC is a sub-optimal finite horizon control scheme that minimizes the user defined cost function and outputs the control. Unlike MPC, NMPC is a non-convex optimal problem and the model dynamics are nonlinear in nature. Non-convexity can arise from the model or the constraints. NMPC is solved numerically using direct single shooting, direct multiple shooting or direct collocation methods. The schemes are discussed in (Andersson et al., 2019).

In this work, the optimal control problem is solved using direct multiple shooting. The states of the system model are propagated using fourth order Runge-Kutta scheme. Initially, NMPC is used to generate reference trajectories to be fed into the adaptive controller block. Thus reducing the dependency on manual trajectory generation. The trajectories can be generated using the model and constraints.

Two scenarios for reference trajectories are discussed in this chapter: (1) MPC tracking for a user given trajectory, and (2) MPC trajectory generation and tracking given initial and final conditions. A schematic that gives an overview of the process is shown in Figure 5.1. In case of NMPC, a simplified model for the orbital dynamics is used as the higher order gravity terms are assumed to be unknown. A schematic for the the NMPC reference block is shown in Figure 5.2.

## 5.1. MPC Process

Generally, MPC has three steps,

1. Prediction: Given a set of control inputs the future states are predicted for a given system model.

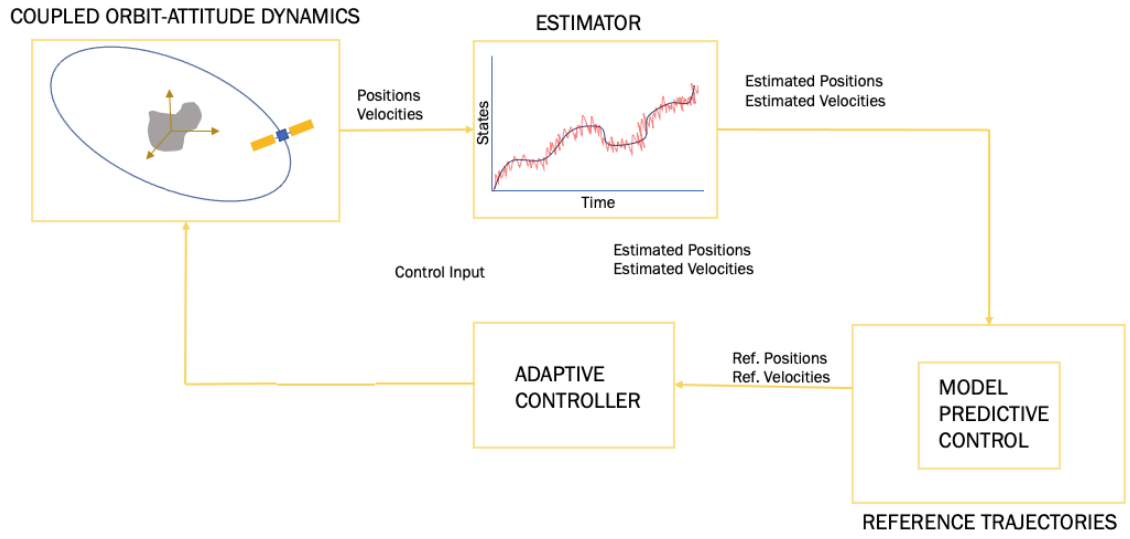


*Figure 5.1* MPC Schematic

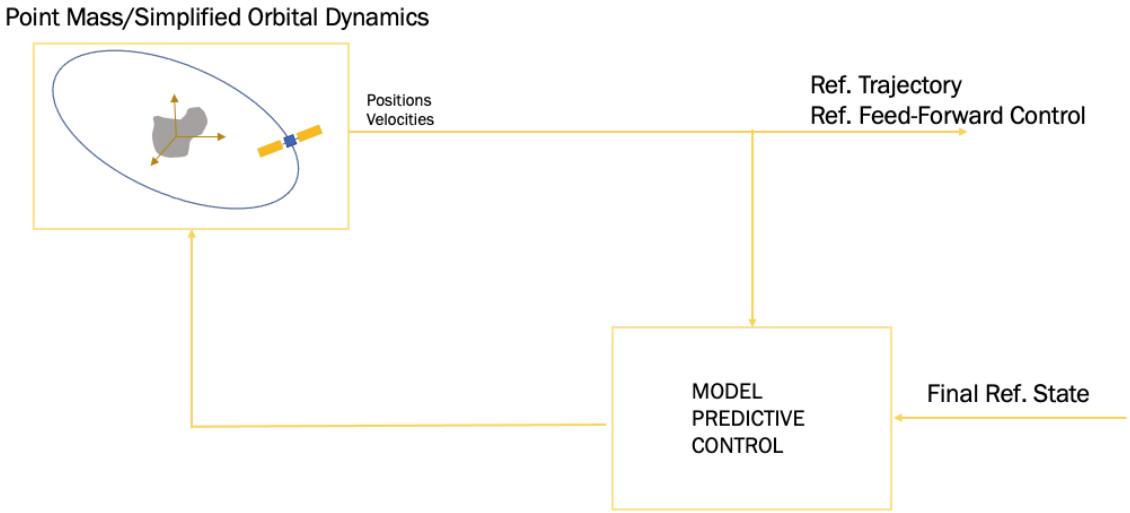


*Figure 5.2* MPC Reference Block Schematic

Let a discrete nonlinear system model be defined as,

$$\mathbf{x}_{k+1} = \mathbf{f}(\mathbf{x}_k, \mathbf{u}_k) \tag{5.1}$$

where $\mathbf{x}_k$ is the system state, $k$ is the prediction step, $\mathbf{f}$ is a nonlinear function that captures the system dynamics, and $\mathbf{u}$ is the control input.

Given the control sequence $\mathbf{u} = [\mathbf{u}_k, \mathbf{u}_{k+1}, ..., \mathbf{u}_{k+N-1}]$, the prediction step outputs the predicted future states of the system $\mathbf{x} = [\mathbf{x}_k, \mathbf{x}_{k+1}, ..., \mathbf{x}_{K+N}]$. Here $N$ is the length of the prediction horizon.

2. Optimization: In this step, an optimal control problem is solved online for a given cost function. The optimal control problem (OCP) is given as,

$$\min_{\mathbf{u},\mathbf{x}} \quad J(\mathbf{x}_0, \mathbf{u}) = F(\mathbf{x}_N) + \sum_{k=0}^{N-1} l(\mathbf{x}_k, \mathbf{u}_k) \tag{5.2}$$

$$\text{subject to} \quad \boldsymbol{x}_{k+1} = \mathbf{f}(\mathbf{x}_k, \mathbf{u}_k) \tag{5.3}$$

$$\mathbf{x}_k \in X \tag{5.4}$$

$$\mathbf{u}_k \in U \tag{5.5}$$

The OCP is required to solve for the control effort $\mathbf{u}$ such that the cost function $J(\mathbf{x}_0, \mathbf{u})$ is minimized. The OCP is subjected to dynamical, state and control constraint given from Equation (5.3), (5.4) and (5.5) respectively.

The cost function $J(\mathbf{x}_0, \mathbf{u})$ is defined as the summation of terminal cost $F(\mathbf{x}_N)$ and the running cost $l(\mathbf{x}, \mathbf{u})$. The terminal cost is defined as deviation of the state at the final step from the desired state. The terminal cost is given as,

$$F(\mathbf{x}_N) = [\mathbf{x}_N - \mathbf{r}_N]^T \mathbf{P} [\mathbf{x}_N - \mathbf{r}_N] \quad \mathbf{x}_N, \mathbf{r}_N \in R^6, \quad \mathbf{P} \in R^{6\times 6} \tag{5.6}$$

Here $\mathbf{P}$ is a tunable positive-definite weighting matrix that penalizes difference between the final state and the desired state. The running cost $l(\mathbf{x}, \mathbf{u})$ is given as,

$$l(\mathbf{x}, \mathbf{u}) = \sum_{k=0}^{N-1} [\mathbf{x}_k - \mathbf{r}_k]^T \mathbf{Q} [\mathbf{x}_k - \mathbf{r}_k] + \mathbf{u}_k^T \mathbf{R} \mathbf{u}_k \tag{5.7}$$

Here $\mathbf{Q}$ and $\mathbf{R}$ are the positive-definite weighting matrices that are manually tuned to penalize the difference between current and desired state and control effort.

Running cost $l(\mathbf{x}, \mathbf{u})$ is calculated as a sum of deviation of the current state $\mathbf{x}_k$ from the desired state $\mathbf{r}_k$ and the deviation of the control $\mathbf{u}_k$ from the reference control. The reference control is considered to be zero in this case.

3. Implementation: OCP outputs a sequence of control inputs $\mathbf{u}^* = [\mathbf{u}_k^*, \mathbf{u}_{k+1}^*, ..., \mathbf{u}_{k+N-1}^*]$. In this step, the first control input $\mathbf{u}_k^*$ is applied drive the system. The process is repeated for new initial state until the desired reference state is achieved. An example of the MPC algorithm is give in Algorithm 1.

---

**Algorithm 1:** MPC algorithm

---

Set $\mathbf{x}_0$

**for** *k = 1,2,3,...,N* **do**

  solve $J(\mathbf{x}_0, \mathbf{u})$

  subject to the constraints

  find the the sequence $\mathbf{u}^* = [\mathbf{u}_k^*, \mathbf{u}_{k+1}^*, ..., \mathbf{u}_{k+N-1}^*]$

  apply the control input $\mathbf{u}_k^*$

**end**

get new $\mathbf{x}_0$

repeat until $[\mathbf{x}_k - \mathbf{r}_k] < tolerance(1 \times 10^{-}4km)$

---

### 5.2. NMPC for Orbital Control

In this section, we discuss the formulation of NMPC for spacecraft control and tracking in the asteroid's vicinity. Model predictive control requires a system model in order to solve of the optimal control problem. However, in the case of asteroids, a

precise model is usually unavailable until several months after the spacecraft's arrival to the asteroid. Therefore, a simple model based on two-body problem is considered in this case. Usually, the mass of the asteroid can be estimated using ground based methods such as light curve analysis prior to the launch (Scheeres & Schweickart, 2004).

### 5.2.1. System Model For NMPC

The system model of NMPC is given as using a two-body problem. The mass and the rotation of the asteroid is assumed to be known. Note that the mass and rotation can be estimated and updated online as well using filtering techniques. The dynamics of the spacecraft around the asteroid is written in asteroid fixed body frame ($x^{SB}, y^{SB}, z^{SB}$) centered at the center of mass of the asteroid as shown in Figure 5.3. The frame is aligned with the principle axis of the asteroid and the z-axis is aligned with the angular velocity vector ($\mathbf{\Omega} \in R^3$) of the asteroid. The asteroid fixed body ($SB$) frame is also known an a rotating Hill frame which is orbiting around the sun as shown in Figure 5.3.

The dynamics of the spacecraft are given in Equation 5.8.

$$\ddot{\mathbf{r}} + 2\mathbf{\Omega} \times \dot{\mathbf{r}} + \mathbf{\Omega} \times (\mathbf{\Omega} \times \mathbf{r}) = -\frac{\mu}{r^3}\mathbf{r} + \mathbf{u} \tag{5.8}$$

where $\mathbf{r} = [x(t), y(t), z(t)]^T$ and $\dot{\mathbf{r}} = [\dot{x}(t), \dot{y}(t), \dot{z}(t)]^T$ are the position and velocity vector of the spacecraft in Cartesian coordinates respectively. $\mathbf{u} = [u_x(t), u_y(t), u_z(t)]^T$ is the thrust control vector. It assumed that a six-thruster configuration is available for controlling the spacecraft in the configuration space.

The state-space formulation of a the two-body problem for a rotating asteroid for nonlinear model predictive control formulation is given as,

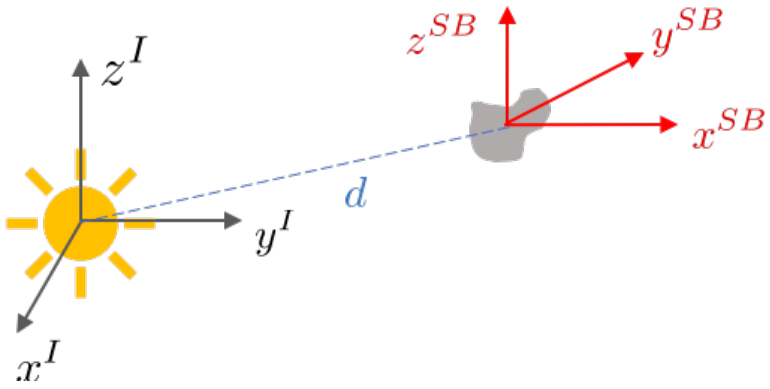


*Figure 5.3* Asteroid Frame

$$\begin{aligned} \dot{\mathbf{x}} &= \mathbf{A}\mathbf{x} + \mathbf{B}\mathbf{u} \\ \mathbf{y} &= \mathbf{C}\mathbf{x} \end{aligned} \tag{5.9}$$

where $\mathbf{A}$, $\mathbf{B}$ and $\mathbf{C}$ are given as,

$$\mathbf{A} = \begin{bmatrix} \dot{x} \\ \dot{y} \\ \dot{z} \\ -\frac{\mu}{\sqrt{x^2+y^2+z^2}^3}x + 2\omega\dot{y} + \omega^2 x \\ -\frac{\mu}{\sqrt{x^2+y^2+z^2}^3}y - 2\omega\dot{x} + \omega^2 y \\ -\frac{\mu}{\sqrt{x^2+y^2+z^2}^3}z \end{bmatrix}, \mathbf{B} = \begin{bmatrix} \mathbf{0}_{3\times3} \\ \mathbf{I}_{3\times3} \end{bmatrix}, \mathbf{C} = [\mathbf{I}_{3\times3} \;\; \mathbf{I}_{3\times3}] \tag{5.10}$$

### 5.2.2. Safety Ellipsoid

During the path planning and execution phase, a safety ellipsoid is considered as a constraint to the NMPC. This helps ensure a safe distance of the spacecraft from the asteroid during the circumnavigation phase of the mission. This is common constraint that is used during the circumnavigation phase. For a landing scenario, cone constraint can be implemented for an irregular asteroid. An example of the safety ellipsoid for asteroid Eros

can be seen in Figure 5.4. The safety ellipsoid constraint is given as follows,

$$1 - \left[ \left( \frac{x_k}{a} \right)^2 + \left( \frac{y_k}{b} \right)^2 + \left( \frac{z_k}{c} \right)^2 \right] \leq 0 \tag{5.11}$$

Here $k$ is the time step, $[x, y, z]$ are the position coordinates of the spacecraft, and $[a, b, c]$ are the half-length of the principle axes of the ellipsoid.

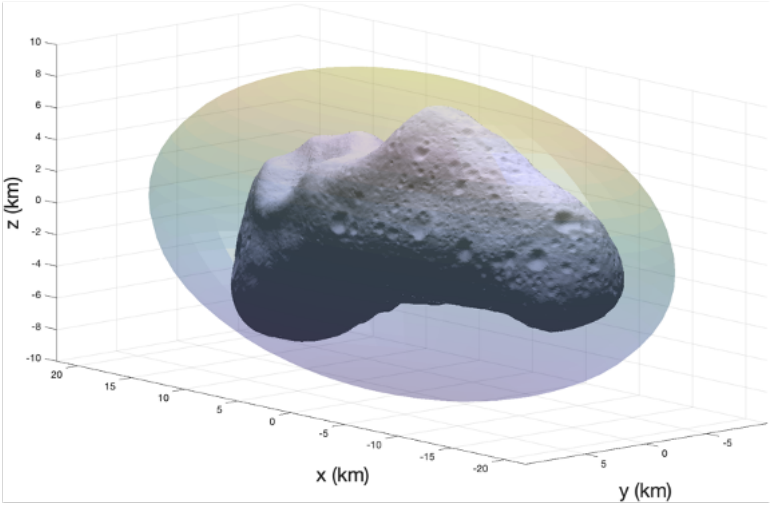


*Figure 5.4* Safety Ellipsoid

### 5.3. NMPC Design

In this section, we formulate the discrete NMPC for spacecraft trajectory planning and tracking. Figure 5.1 shows the schematic of the NMPC controller. It can be noted that the NMPC controller is implemented on the "actual" system model as given in Equation 3.1.

A discrete time NMPC with piece-wise continuous control effort is formulated in this paper. The prediction model is discretized using the fourth order Runge-Kutta integration scheme.

$$\mathbf{x}_{k+1} = \mathbf{f}(\mathbf{x}_k, \mathbf{u}_k),\ \mathbf{x} \in R^6,\ \mathbf{u} \in R^3 \tag{5.12}$$

The Runge-Kutta scheme for the state-space system defined in Equation 5.9 is given in Algorithm 2. It can be noted that the dynamics are discretized in RK-4, but the controller are assumed to be piece-wise continuous.

**Algorithm 2:** Runge-Kutta Algorithm

Set $\mathbf{x}_1 = \mathbf{x}_0$
Set $T = \Delta T$ (Time step)
**for** *k = 1,2,3,...,N* **do**
  $\mathbf{k}_1 = \mathbf{f}(\mathbf{x_k}, \mathbf{u_k})$
  $\mathbf{k}_2 = \mathbf{f}(\mathbf{x}_k + 0.5T\mathbf{k}_1, \mathbf{u}_k)$
  $\mathbf{k}_3 = \mathbf{f}(\mathbf{x}_k + 0.5T\mathbf{k}_2, \mathbf{u}_k)$
  $\mathbf{k}_4 = \mathbf{f}(\mathbf{x}_k + T\mathbf{k}_3, \mathbf{u}_k)$
  $\mathbf{x}_{k+1} = \mathbf{x}_k + T/6(\mathbf{k}_1 + 2\mathbf{k}_2 + 2\mathbf{k}_3 + \mathbf{k}_4)$
**end**

### 5.3.1. Nonlinear Program

A direct multiple shooting method is implemented to solve the optimal control problem. In direct multiple shooting, the problem is lifted to higher dimension by including state variables optimization variables. Even though this increases the number of variables, this process reduces the non linearity of the OCP and improves the computational efficiency.

Equation 5.13 defines the cost function to be minimized. The dynamical constraints are given in Equation 5.14 and control constraints are given in Equation 5.15 where $\mathbf{u}_{min}$ and $\mathbf{u}_{max}$ are the lower and upper-bound of the control effort. The safety ellipsoid constraint is given in Equation 5.16.

The nonlinear program a nonlinear model predictive control is given as follows:

$$\min_{\mathbf{u}_k,..,\mathbf{u}_{k+N-1},\mathbf{x}_k,..,\mathbf{x}_{k+N-1}} \quad F(\mathbf{x}_N) + \sum_{k=0}^{N-1} [\mathbf{x}(k) - \mathbf{x}_\mathbf{r}(k)]^T \mathbf{Q} [\mathbf{x}(k) - \mathbf{x}_\mathbf{r}(k)] + \mathbf{u}(k)^T \mathbf{R} \mathbf{u}(k) \tag{5.13}$$

subjected to:

$$\mathbf{x}_{k+1} = \mathbf{f}(\mathbf{x}_k, \mathbf{u}_k),\ \mathbf{x} \in R^6,\ k = 0, ..., N \tag{5.14}$$

$$\mathbf{u}_{min}(k) \leq \mathbf{u}(k) \leq \mathbf{u}_{max}(k),\ k = 0, ..., N-1 \tag{5.15}$$

$$1 - \left[ \left( \frac{x_k}{a} \right)^2 + \left( \frac{y_k}{b} \right)^2 + \left( \frac{z_k}{c} \right)^2 \right] \leq 0 \tag{5.16}$$

The term $F(\mathbf{x}_N)$ is the cost on the final state and is defined as,

$$F(\mathbf{x}_N) = [\mathbf{x}_N - \mathbf{r}_N]^T \mathbf{P} [\mathbf{x}_N - \mathbf{r}_N] \quad \mathbf{x}_N, \mathbf{r}_N \in R^6, \quad \mathbf{P} \in R^{6 \times 6} \tag{5.17}$$

### 5.4. Comments on Stability of NMPC

The stability of NMPC has been studied extensively. Generally, the stability of the system with a nonlinear model predictive control for a non convex system cannot be guaranteed (Mehrez Said, 2018). However, there are several types of approaches that are discussed in this section.

Mehrez (2018) presents various NMPC stability analysis for a nonlinear dynamical system. Regulation and tracking problem using NMPC is discussed based on Lyapunov stability analysis for multiple shooting problem. The proofs are accompanied with several non-holonomic examples. Worthmann (2011) presents Lyapunov based stability proof for unconstrained receding horizon control systems.

Grune (2010) presents an analysis of unconstrained nonlinear MPC schemes for discrete dynamic systems satisfying an finite time controllability assumption. Asymptotic stability is proved these systems. Tuna (2006) presented work on shorter horizons for

model predictive control (similar to ones used in our work). Asymptotic stability is proved using Lyapunov analysis and example.

The stability of nonlinear model predictive control is difficult to guarantee even after proving mathematically because its also dependent of solvers implemented. Therefore, its important to present examples via simulations or experiments to further test the stability of NMPC.

### 5.5. Simulations and Results

In this section, we present the simulation and results for orbital trajectory tracking for three different asteroids. As previously mentioned, two types of scenarios are discussed for orbital trajectory tracking: (1) trajectory tracking for a user given trajectory, (2) trajectory generation and tracking for a given initial and final condition. The second is more relevant to a realistic scenario where only the initial and a desired final condition of the spacecraft is known and the NMPC is required to generate the trajectory and track it. The simulation is shown for asteroid Eros, Kleopatra and Bennu.

#### 5.5.1. Reference Trajectory Model

The reference model for the user given trajectory case is similar to shown in Chapter 4. For completeness, the trajectory is given as follows.

In this case a closed orbit trajectory $\mathbf{x}_m(t) = [\mathbf{r}_m,\ \dot{\mathbf{r}}_m]^T$ is given as,

$$\mathbf{x}_m(t) = \mathbf{x}_{in}e^{\alpha t^3} + \mathbf{x}_f(1 - e^{\alpha t^3}) \tag{5.18}$$

$$\mathbf{y}_m(t) = \mathbf{C}\mathbf{x}_m \tag{5.19}$$

where $\mathbf{x}_{in} = [\mathbf{r}_{in},\ \dot{\mathbf{r}}_{in}]^T$ is the initial condition of the the reference trajectory, and $\mathbf{x}_f = [\mathbf{r}_f(t),\ \dot{\mathbf{r}}_f(t)]^T$ is the final time-varying orbital reference trajectory. The tuning

parameter $\alpha$ corresponds to the response characteristics and can be tuned depending on the dynamics of the system. The blended output $\mathbf{y}_m$ is the combination of reference position ($\mathbf{r}_m$) and velocity ($\dot{\mathbf{r}}_m$). The time-varying final orbital trajectory ($\mathbf{x}_f = [\mathbf{r}_f(t),\ \dot{\mathbf{r}}_f(t)]^T$) is given as,

$$\mathbf{r}_f(t) = \begin{bmatrix} 0.5R_d \sin(\omega_e t) \\ R_d \cos(\omega_e t) \\ R_d \sin(\omega_e t) \end{bmatrix}, \quad \dot{\mathbf{r}}_f(t) = \begin{bmatrix} 0.5R_d\omega_e \cos(\omega_e t) \\ -R_d\omega_e \sin(\omega_e t) \\ Rd\omega_e \cos(\omega_e t) \end{bmatrix} \tag{5.20}$$

where $R_d$ is the desired final orbit radius. It can be noted that the trajectory is designed such that, as time grows, the initial reference state ($\mathbf{x}_{in}$) converges to the final reference orbit ($\mathbf{x}_f$). For the second case, simply an initial and final states are given along with ellipsoidal constraints.

### 5.5.2. Asteroid 433 Eros

In this section we present the simulation results for Asteroid Eros. The parameters for asteroid is given in Table 5.1. Asteroid Eros has in studied in several studies due to its unique shape and composition. The asteroid has varying composition and the shape is irregular with high a relatively high angular velocity compared to several asteroids in the asteroid belt. User given and point-to-point cases are studied in the following sub-sections.

Table 5.1

Asteroid Eros Parameters

| | |
|---|---|
| Body mass m | $6.69 \times 10^{15}\ kg$ |
| $\omega$ | $5.27\ hours$ |

#### 5.5.2.1. Case 1: User Given Reference Trajectory

The NMPC parameters and required parameters for this case is given in Table 5.2. The initial condition for the reference model with $R_d = 20$ km is given as,

$$\mathbf{r}_{in} = [5\ 22\ 6\ ]^T \text{ km}, \quad \dot{\mathbf{r}}_{in} = [0\ 0\ 0]^T \times 10^{-3}\text{km/s} \tag{5.21}$$

Table 5.2

NMPC Parameters for Case 1

| | |
|---|---|
| N | 20 |
| **Q** | $\begin{bmatrix} \mathbf{I}_{3\times3} & \mathbf{0}_{3\times3} \\ \mathbf{0}_{3\times3} & \mathbf{I}_{3\times3} \end{bmatrix}$ |
| **R** | $100\mathbf{I}_{3\times3}$ |
| $\Delta T$ | 0.2 |
| $\alpha$ | $-1 \times 10^{-8}$ |

It can be seen from Figure 5.5 that the spacecraft is able to successfully track the desired trajectory around the asteroid Eros. It was found that the tracking performance is less ideal compared to the case of adaptive control since in the MPC formulation the tracking is considered as a part of cost and not constraint. This effect can be in seen in Figure 5.6 (d). The gap can be closed by further tuning $\mathbf{Q}$.

Figure 5.6 (a) shows the position versus time plot for the spacecraft and Figure 5.6 (b) shows the velocity of the the spacecraft. It can be seen from the Figure 5.6 (c) that the control efforts remains realistic compared to current thruster availability. The control effort never reaches a steady state value as the the desired trajectory is time-dependent.

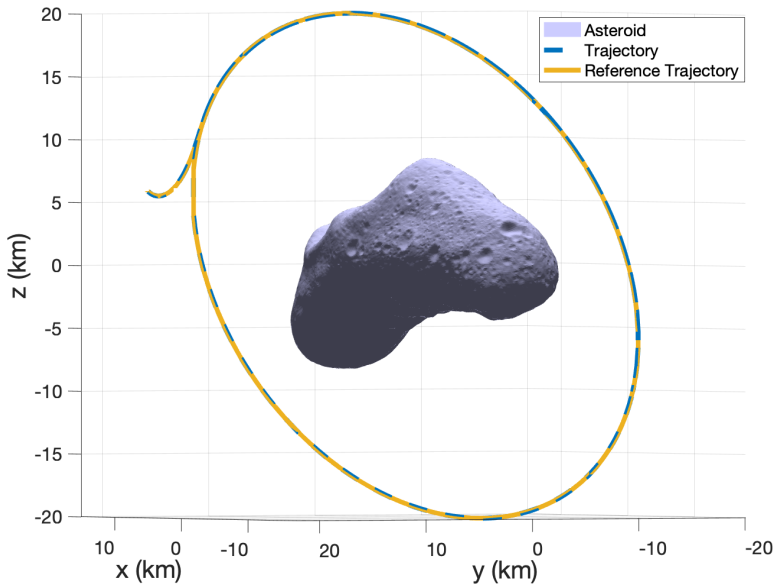


*Figure 5.5* Trajectory of spacecraft around asteroid Eros in asteroid fixed body-frame.

#### 5.5.2.2. Case 2: Point-to-Point Tracker

In case of point-to-point tracker. An initial and final state of the spacecraft is given and the NMPC is used to solve for a sub-optimal trajectory and control while avoiding the asteroid. The NMPC parameters for this case is given in Table 5.3. It can be noted tha the velocities are independently constrained in each axis. The initial and final conditions are given as follows:

$$\begin{aligned} \mathbf{r}_{in} &= [0 \ -8 \ 8 \ ]^T \text{ km}, \quad \dot{\mathbf{r}}_{in} = [0 \ 0 \ 0]^T \text{ km/s} \\ \mathbf{r}_f &= [0 \ 10 \ 5 \ ]^T \text{ km}, \quad \dot{\mathbf{r}}_f = [0 \ 0 \ 0 \ ]^T \text{ km/s} \end{aligned} \tag{5.22}$$

It was found that a large control horizon of $N = 100$ is implemented in this case. Control horizon significantly affects the performance and efficiency of the NMPC formulation. Increasing the the horizon increases the performance and results in a more optimal trajectory while meeting all the constraints.

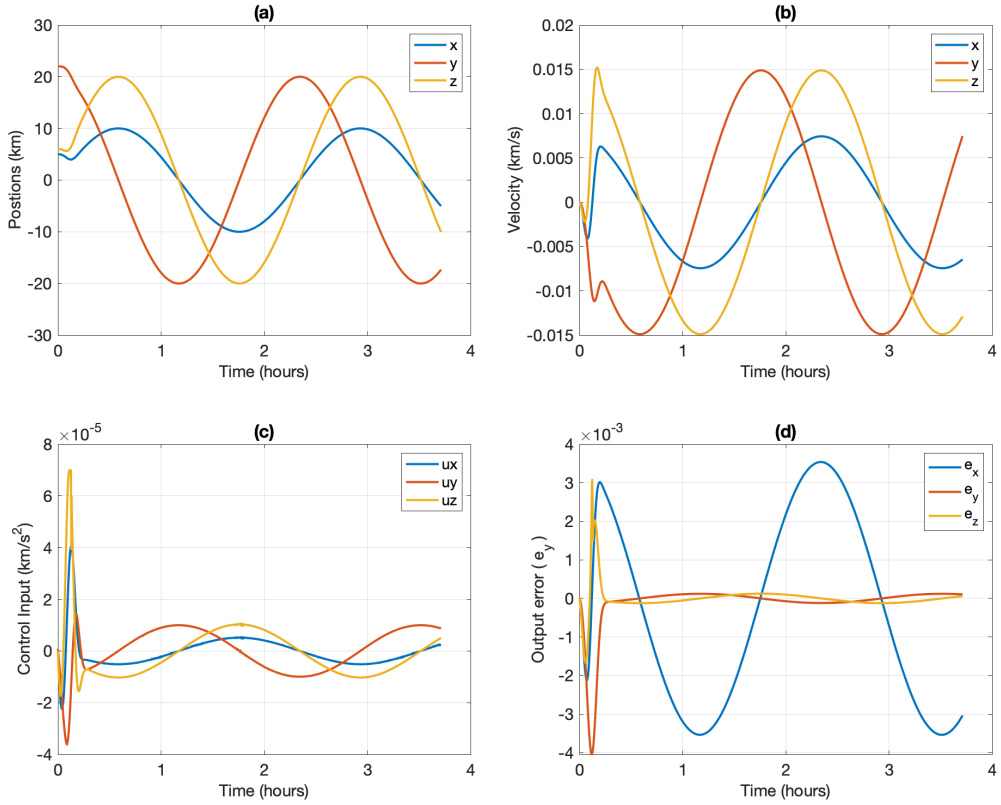


*Figure 5.6* Plots for trajectory of spacecraft around asteroid Eros (a) position vs. time, (b) velocity vs. time, (c) control effort vs. time, (d) output error vs. time.

However, this significantly increases the computational load and increases the time to compute. The NMPC is also highly dependent on the weighting matrices $\mathbf{Q}$ and $\mathbf{R}$. Tuning these matrices was found to be a challenging task. Therefore, this formulation suffers from lack of computational efficiency and might not be suitable for on-board and online implementation.

Spacecraft trajectory with the ellipsoid can be seen in Figure 5.7. It can be seen that the trajectory remains above the ellipsoid and the NMPC formulation is able to successfully avoid the asteroid. Figure 5.8 shows the trajectory without the ellipsoid and shows the successful trajectory generation using the NMPC.

Table 5.3

NMPC Parameters for Case 2

| | |
|---|---|
| N | 100 |
| **Q** | $1 \times 10^{-5} \begin{bmatrix} \mathbf{I}_{3\times3} & \mathbf{0}_{3\times3} \\ \mathbf{0}_{3\times3} & \mathbf{I}_{3\times3} \end{bmatrix}$ |
| **R** | $0.5\mathbf{I}_{3\times3}$ |
| $\Delta T$ | 0.2 |
| Control Constraint | $-0.0007 \leq \mathbf{u} \leq 0.0007\ km/s^2$ |
| Velocity Constraint | $-0.05 \leq \mathbf{u} \leq 0.05\ km/s$ |
| a | 22 km |
| b | 10 km |
| c | 10 km |

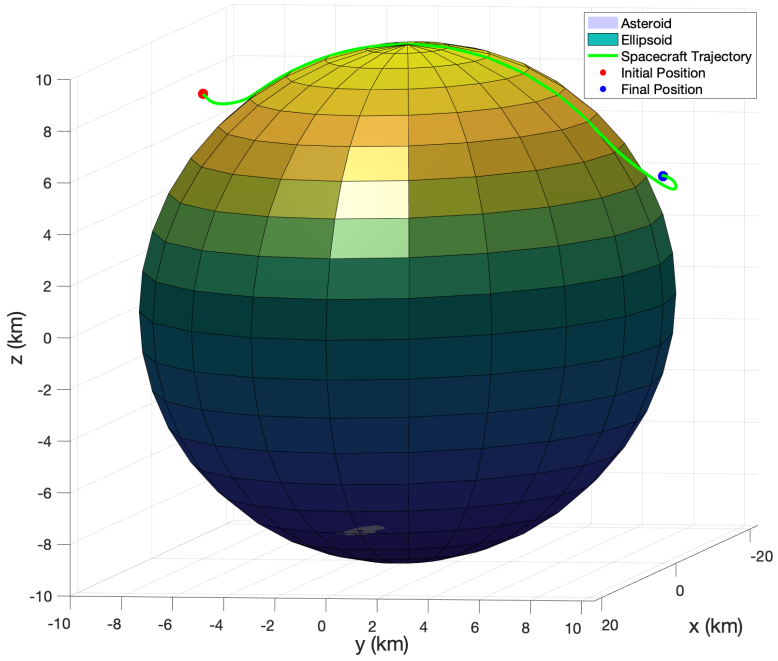


*Figure 5.7* Trajectory of spacecraft around asteroid Eros for point-to-point case with ellipsoidal constraint.

Figure 5.9 shows the position, velocity and control plots for this case. The position plots shows a successful convergence to the desired location. The velocities are shown

in Figure 5.9 (b). It can be noted that the velocities are also constrained in this case. This is done in order to limit the spacecraft speeds such that the spacecraft is still controllable given the control constraints.

It was found that if the velocities are not constrained the spacecraft cannot maneuver in the case of obstacle avoidance situations due the constraints on the control effort. The control effort plot is shown in Figure 5.9 (c). It can be seen that the control effort stays withing the defined control constraints.

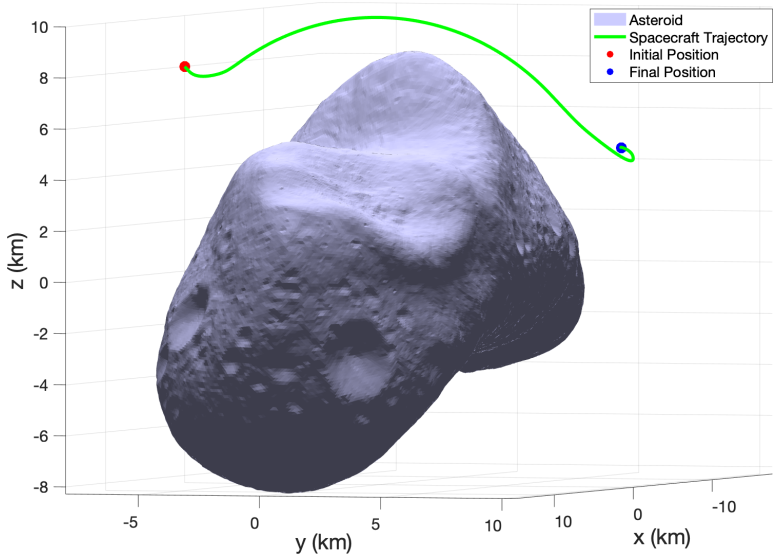


*Figure 5.8* Trajectory of spacecraft around asteroid Eros for point-to-point case without ellipsoidal constraint.

### 5.5.3. Asteroid Bennu

In this section we present the simulation results for Asteroid Bennu. Asteroid Bennu has been recently visited by NASA by OSIRIS-Rex. Asteroid Bennu is almost spherical in shape and the gravitational field is very close to a spherical. This effect will be demonstrated in the later chapter.

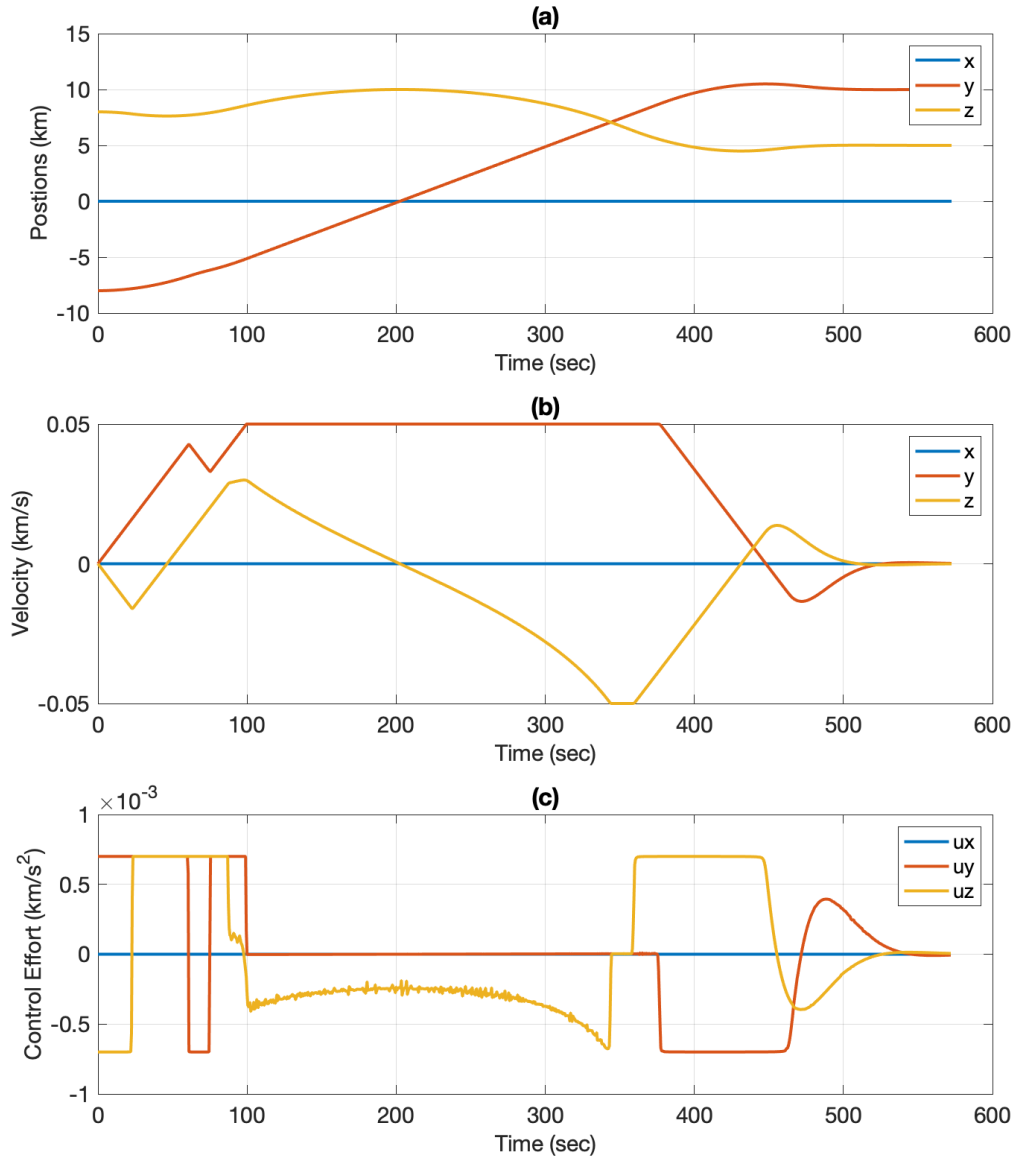


*Figure 5.9* Plots for point-to-point case for spacecraft around asteroid Eros (a) position vs. time, (b) velocity vs. time, (c) control effort vs. time.

#### 5.5.3.1. Case 1: User Given Reference Trajectory

The NMPC parameters and required parameters for this case is given in 5.4. The initial condition for the reference model with $R_d = 0.7$ km is given as,

$$\mathbf{r}_{in} = [1\ 1\ 1\ ]^T \text{ km}, \quad \dot{\mathbf{r}}_{in} = [0\ 0\ 0]^T \times 10^{-3}\text{km/s} \tag{5.23}$$

Table 5.4

NMPC Parameters for Case 1

| | |
|---|---|
| N | 100 |
| $\mathbf{Q}$ | $\begin{bmatrix} \mathbf{I}_{3\times3} & \mathbf{0}_{3\times3} \\ \mathbf{0}_{3\times3} & \mathbf{I}_{3\times3} \end{bmatrix}$ |
| $\mathbf{R}$ | $100\mathbf{I}_{3\times3}$ |
| $\Delta T$ | 0.2 |
| $\alpha$ | $-1 \times 10^{-8}$ |

The trajectory of the spacecraft around the asteroid Bennnu can be seen in Figure 5.11. It can be seen from that figure that the spacecraft is able to successfully track the desired path. Due to the extremely low gravitational force of Bennu the control requirements were found to be low as well. Resulting mainly due the tracking requirements. The positions and velocities for this case can be seen in Figure 5.10 (a) and Figure 5.10 (b).The output tracking error is given in Figure 5.10 (d). It can be seen that the tracking error is low in this case. The control effort plot is given in Figure 5.10 (b). It can be noted that the NMPC solver was found to be more time efficient in this due the high thruster force availability i.e. higher upper and lower limit on thrust constraints compared to the gravitational force of the asteroid.

#### 5.5.3.2. Case 2: Point-to-Point Tracker

In case of point-to-point tracker. An initial and final state of the spacecraft is given and the NMPC is used to solve for a sub-optimal trajectory and control while avoiding the asteroid. The NMPC parameters for this case is given in Table 5.5. The initial and final

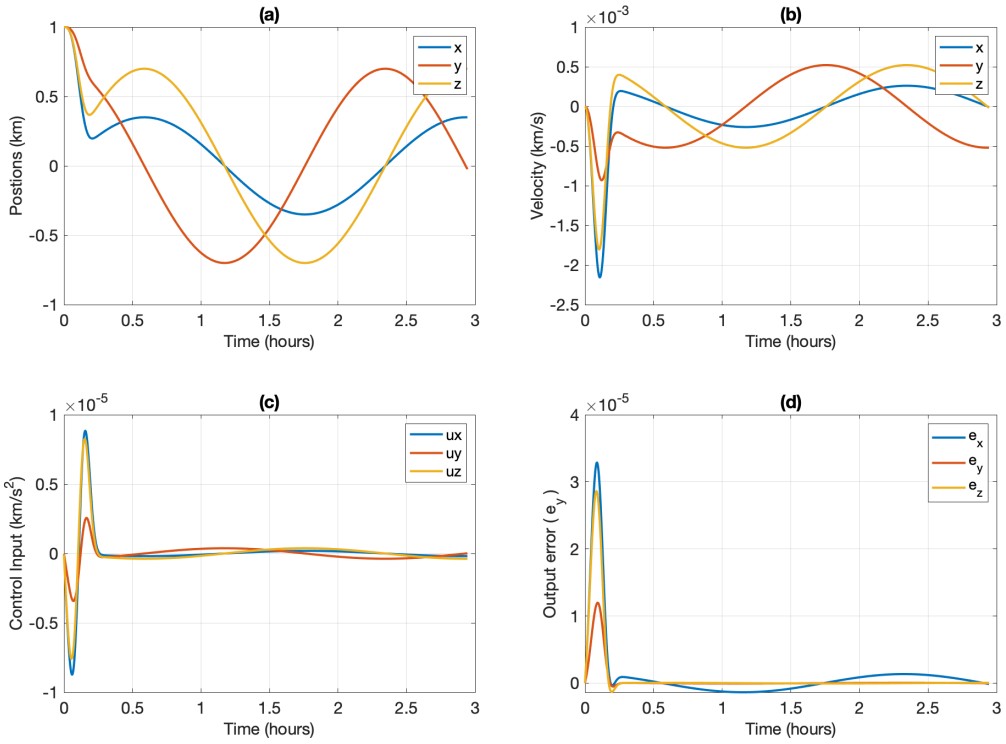


*Figure 5.10* Plots for trajectory tracking case for spacecraft around asteroid Bennu (a) position vs. time, (b) velocity vs. time, (c) control effort vs. time, (d) output error vs. time.

conditions are given as follows,

$$\mathbf{r}_{in} = [0 \ -0.35 \ 0.1 \ ]^T \text{ km}, \quad \dot{\mathbf{r}}_{in} = [0 \ 0 \ 0]^T \text{ km/s}$$
$$\mathbf{r}_f = [0.1 \ 0.4 \ 0.2 \ ]^T \text{ km}, \quad \dot{\mathbf{r}}_f = [0 \ 0 \ 0 \ ]^T \text{ km/s} \tag{5.24}$$

In case of the asteroid Bennu, an ellipsoidal constraint is used for generating an obstacle avoidance trajectory. The velocity constraint is also reduced since the the control requirement is reduced relative to asteroid Eros. Figure 5.11 shows the trajectory of the spacecraft with spherical constraint. It can be seen that the NMPC formulation is able to successfully generate and converge to the desired final position. Figure 5.13 shows the same trajectory without the spherical constraint.

The position and velocities plot can be seen in Figure 5.14 (a) and (b). It can be seen

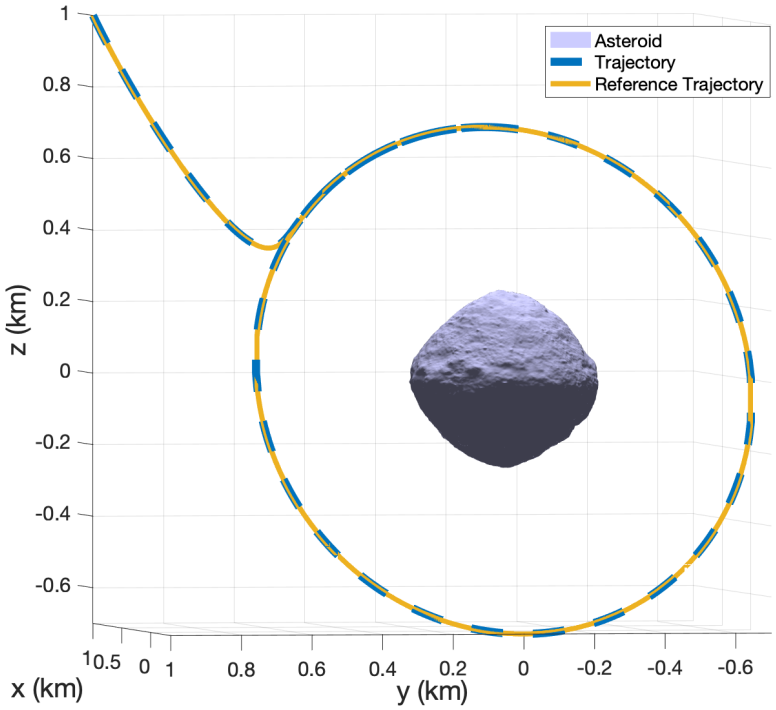


*Figure 5.11* Trajectory of spacecraft around asteroid Bennu.

Table 5.5

NMPC Parameters for Case 2 for asteroid Bennu

| | |
|---|---|
| N | 100 |
| **Q** | $1 \times 10^{-5} \begin{bmatrix} \mathbf{I}_{3\times3} & \mathbf{0}_{3\times3} \\ \mathbf{0}_{3\times3} & \mathbf{I}_{3\times3} \end{bmatrix}$ |
| **R** | $0.5\mathbf{I}_{3\times3}$ |
| $\Delta T$ | 0.1 |
| Control Constraint | $-0.0025 \leq \mathbf{u} \leq 0.0025\ km/s^2$ |
| Velocity Constraint | $-0.005 \leq \mathbf{u} \leq 0.005\ km/s$ |
| a | 0.3 km |
| b | 0.3 km |
| c | 0.3 km |

that the positions converge to the desired final position and the velocities converge to zero. As in the previous case, the velocities are constrained and reach the maximum value

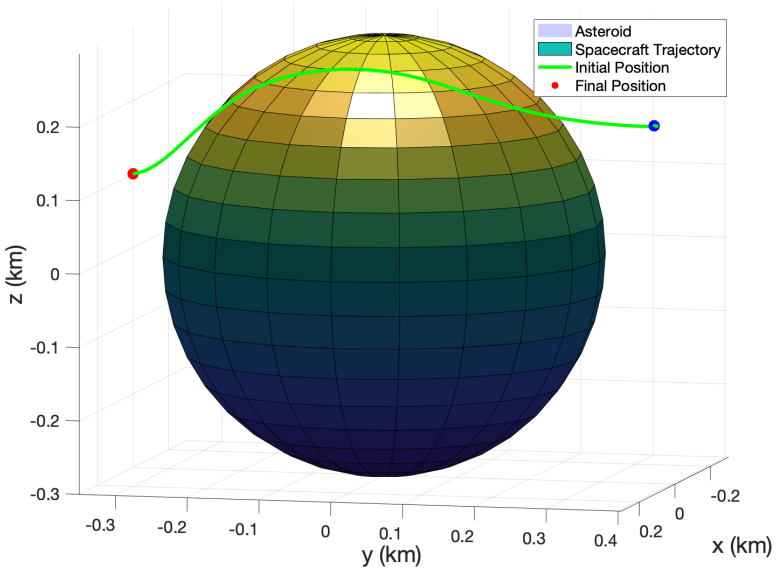


*Figure 5.12* Spacecraft Trajectory for point-to-point case for asteroid Bennu with the ellipsoidal constraint.

initially. The control effort can be in Figure 5.14 (c) and (d). The last figure shows the zoomed-in control plot and it shows the steady state control effort for the hovering case.

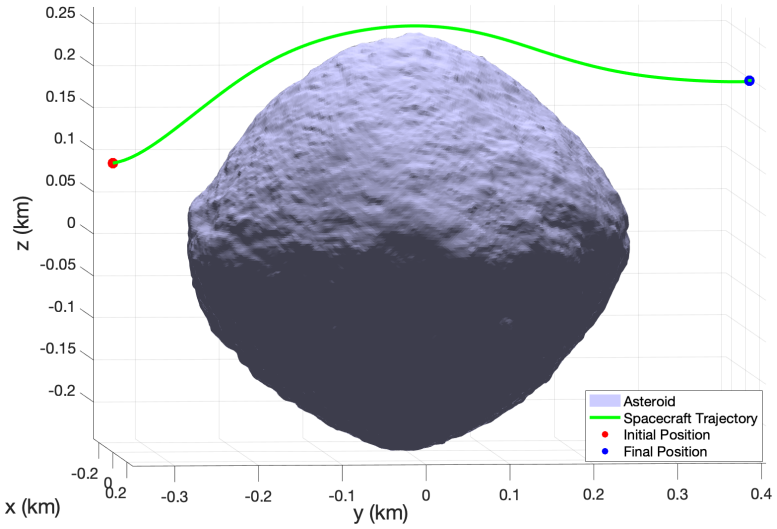


*Figure 5.13* Spacecraft Trajectory for point-to-point case for asteroid Bennu without the ellipsoidal constraint.

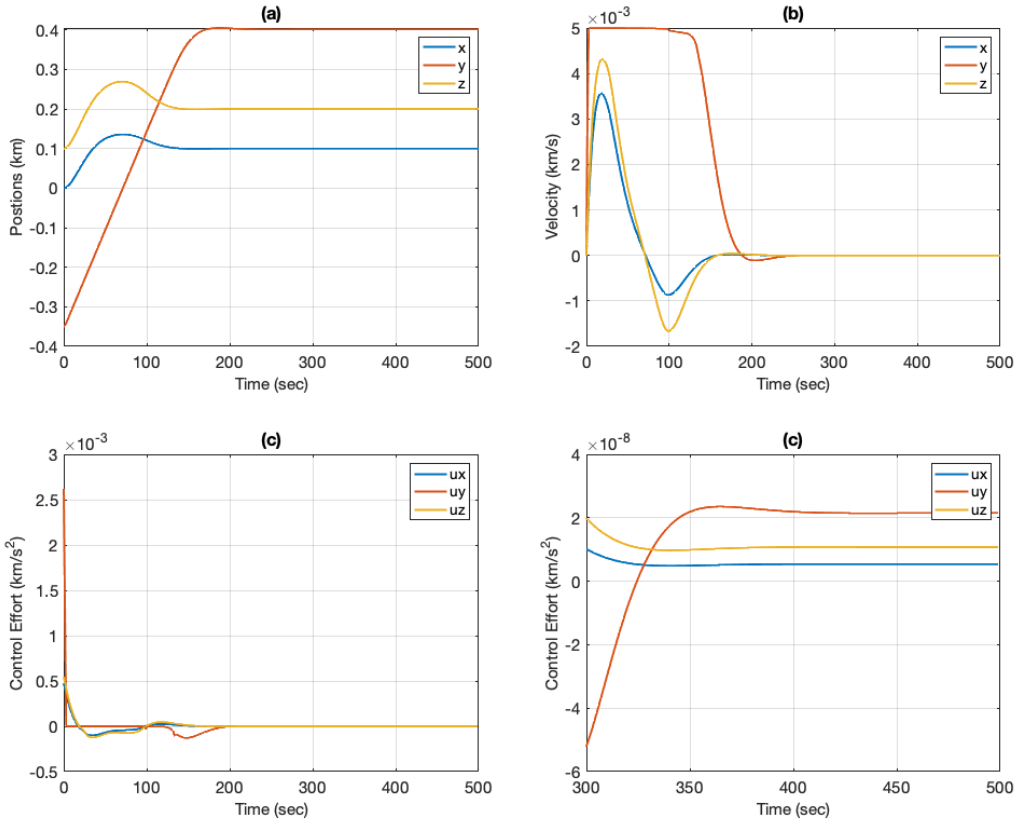


*Figure 5.14* Plots for trajectory of spacecraft around asteroid Bennu (a) position vs. time, (b) velocity vs. time, (c) control effort vs. time, (d) output error vs. time.

### 5.5.4. Asteroid Kleopatra

In this section we present the simulation results for Asteroid Kleopatra.

#### 5.5.4.1. Case 1: User Given Reference Trajectory

he NMPC parameters and required parameters for this case is given in Table 5.6. The initial condition for the reference model with $R_d = 60$ km is given as,

$$\mathbf{r}_{in} = [20\ 45\ 6\ ]^T \text{ km}, \quad \dot{\mathbf{r}}_{in} = [0\ 0\ 0]^T \text{km/s} \tag{5.25}$$

It can be seen from Figure 5.16 that the spacecraft is able to successfully track the desired trajectory around the asteroid Kleopatra. Due to a stronger gravitational pull from the asteroid the the tuning matrices $\mathbf{Q}$ and $\mathbf{R}$ are updated as compared to the previous

Table 5.6

NMPC Parameters for Case 1 for asteroid Kleopatra

| | |
|---|---|
| N | 20 |
| **Q** | $\begin{bmatrix} \mathbf{I}_{3\times3} & \mathbf{0}_{3\times3} \\ \mathbf{0}_{3\times3} & \mathbf{I}_{3\times3} \end{bmatrix}$ |
| **R** | $\mathbf{I}_{3\times3}$ |
| $\Delta T$ | 0.2 |
| $\alpha$ | $-1 \times 10^{-8}$ |

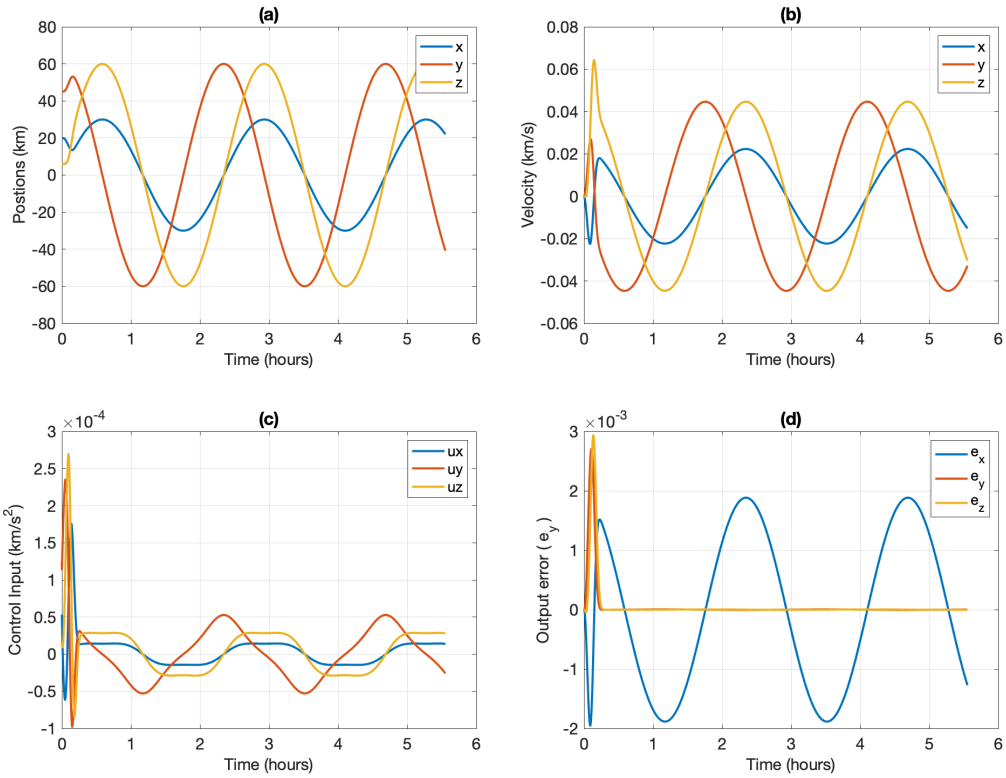


*Figure 5.15* Plots for trajectory of spacecraft around asteroid Kleopatra (a) position vs. time, (b) velocity vs. time, (c) control effort vs. time, (d) output error vs. time.

case to the values as shown in Table 5.6.

The positions and velocities are shown in Figure 5.15 (a) and (b). The control effort

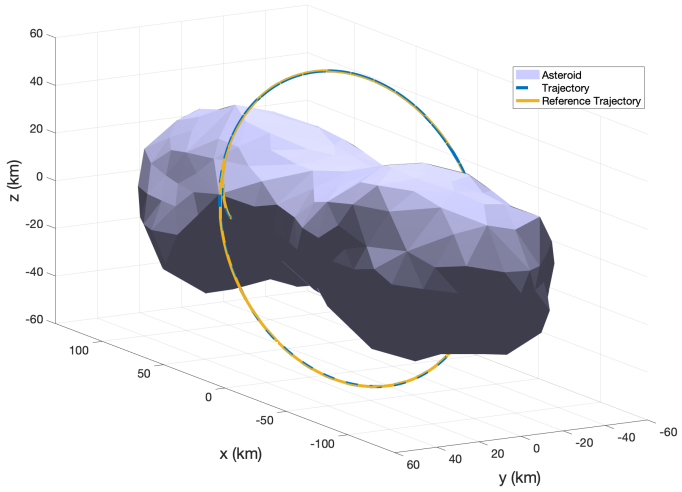


*Figure 5.16* Trajectory of spacecraft around asteroid Kleopatra in asteroid fixed body-frame.

is given in Figure 5.15 (c). It can be noted that the control effort is higher than previous cases due the stronger effect of gravitational force of asteroid Kleopatra.

#### 5.5.4.2. Case 2: Point-to-Point Tracker

In case of point-to-point tracker. An initial and final state of the spacecraft is given and the NMPC is used to solve for a sub-optimal trajectory and control while avoiding the asteroid. The NMPC parameters for this case is given in Table 6.3. The initial and final conditions are given as follows,

$$\begin{aligned} \mathbf{r}_{in} &= [10 \ -100 \ 0 \ ]^T \text{ km}, \quad \dot{\mathbf{r}}_{in} = [0 \ 0 \ 0]^T \text{ km/s} \\ \mathbf{r}_f &= [50 \ 60 \ 25 \ ]^T \text{ km}, \quad \dot{\mathbf{r}}_f = [0 \ 0 \ 0 \ ]^T \text{ km/s} \end{aligned} \tag{5.26}$$

In case of the asteroid Kleopatra, an ellipsoidal constraint is used for generating an obstacle avoidance trajectory. The velocity constraint is also increased since the the control requirement can be higher relative to asteroid Eros and Bennu. Figure 5.16 shows the trajectory of the spacecraft with spherical constraint. It can be seen that the NMPC formulation is able to successfully generate and converge to the desired final position.

Table 5.7

NMPC Parameters for Case 2 for asteroid Kleopatra

| | |
|---|---|
| N | 100 |
| **Q** | $1 \times 10^{-5} \begin{bmatrix} \mathbf{I}_{3\times3} & \mathbf{0}_{3\times3} \\ \mathbf{0}_{3\times3} & \mathbf{I}_{3\times3} \end{bmatrix}$ |
| **R** | $0.5\mathbf{I}_{3\times3}$ |
| $\Delta T$ | 0.2 |
| Control Constraint | $-0.007 \leq \mathbf{u} \leq 0.007\ km/s^2$ |
| Velocity Constraint | $-0.1 \leq \mathbf{u} \leq 0.1\ km/s$ |
| a | 150 km |
| b | 70 km |
| c | 50 km |

Figure 5.17 shows the same trajectory without the spherical constraint.

The position and velocities plot can be seen in Figure 5.18 (a) and (b). It can be seen that the positions converge to the desired final position and the velocities converge to zero. As in the previous case, the velocities are constrained and reach the maximum value initially. The control effort can be in Figure 5.18 (c) and (d).

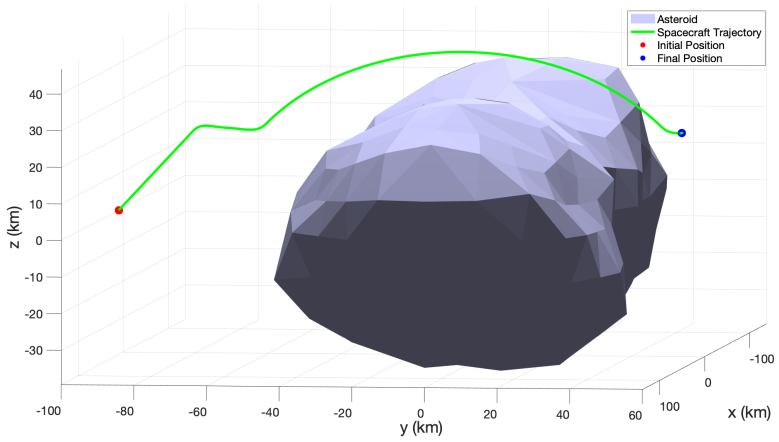


*Figure 5.17* Trajectory of spacecraft for point-to-point case around asteroid Kleopatra without ellipsoidal constraint.

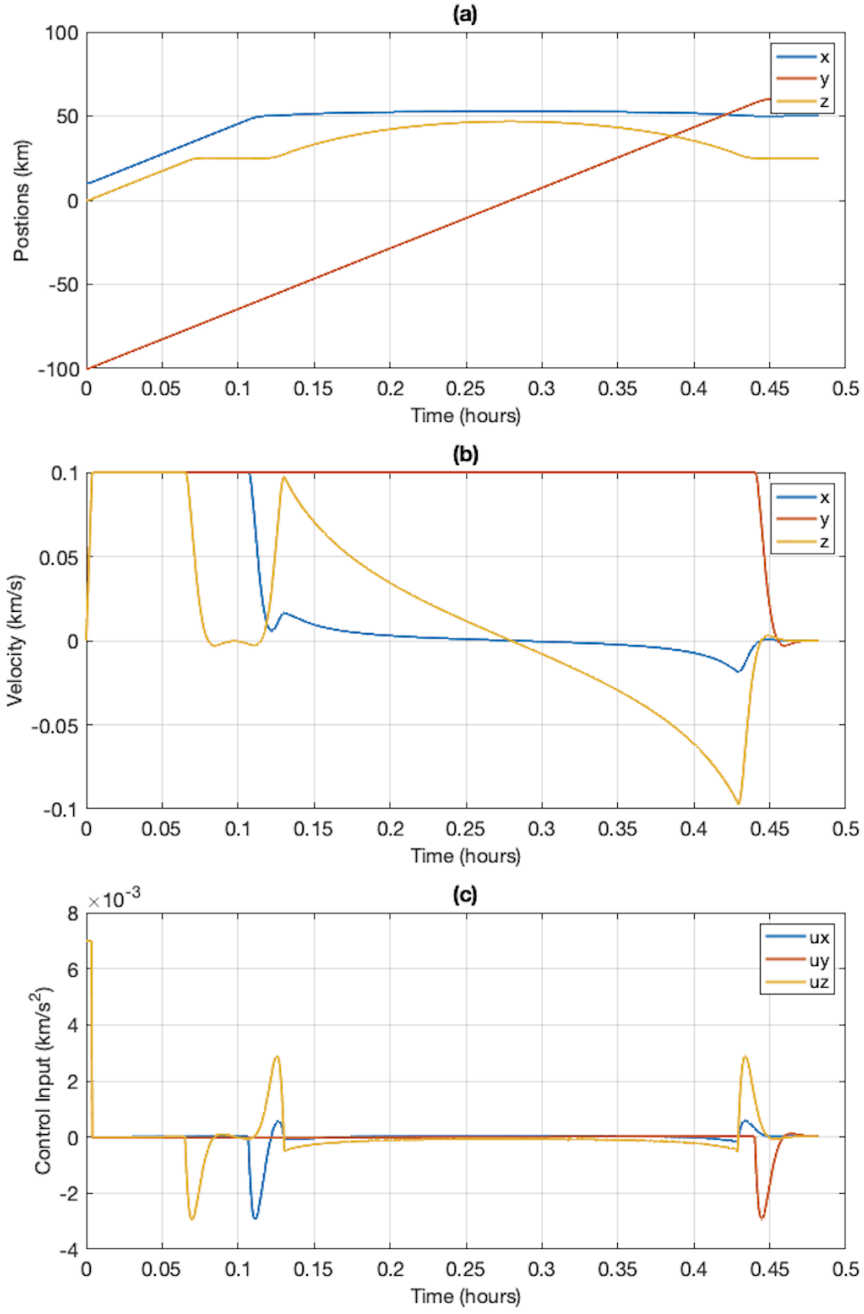


*Figure 5.18* Plots for point-to-point case for spacecraft around asteroid Kleopatra (a) position vs. time, (b) velocity vs. time, (c) control effort vs. time.

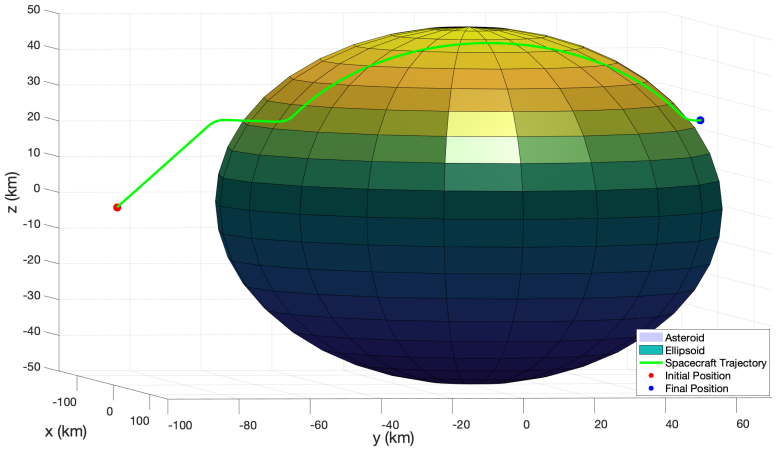


*Figure 5.19* Trajectory of spacecraft for point-to-point case around asteroid Kleopatra with ellipsoidal constraint.

# 6. Direct Adaptive-Model Predictive Control

A novel control approach combining the benefits of a direct model reference adaptive control and a model predictive control is proposed in this chapter. A schematic of this control is scheme is shown in Figure 6.1.

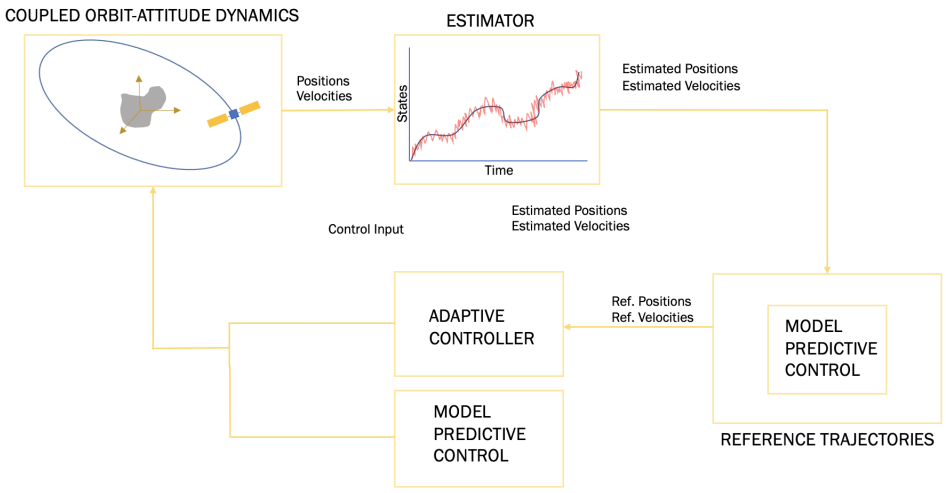


*Figure 6.1* Schematic for direct-adaptive model predictive control.

Here the reference trajectories are generated using a nonlinear model predictive controller for the adaptive controller to track. The reference control generated from the model predictive control is added to the adaptive control law as a feedforward control input.

As mentioned before, the direct adaptive-model predictive control (DAMPC) has two major advantages:

- The adaptive control component adds robustness to the MPC since the system model for the MPC is a low-fidelity simplified version of the gravitational field and the unmodeled forces are missing.
- The MPC adds optimality to the control system via the feedforward control inputs

and generates sub-optimal trajectories to for the adaptive control to track.

This approach balances the effects of both adaptive and MPC control. Even though the NMPC is inherently adaptive it cannot guarantee stabilizing input for unknown model and system parameters (Grimm et al., 2004).Therefore, the adaptive control increases the robustness of the MPC. Also, as it will be shown later in the section, adding MPC control inputs as feedforward is more computationally efficient since the adaptive control converges several times faster than MPC.

### 6.1. DAMPC Formulation

DAMPC is built on the direct model reference adaptive control and model predictive control methodology. The control law comprises of an integral control law with $e$ modification for robustness with a feedforward nonlinear/linear MPC term. The control law is defined as follows:

$$\mathbf{u}_{DAMPC} = \mathbf{K}_e(t)\mathbf{e}_y + \mathbf{u}_{MPC} \tag{6.1}$$

Here $\mathbf{K}_e(t) \in R^{n\times n}$ is the adaptive control law, $\mathbf{e}_y \in R^n$ is the error term between actual and ideal reference model and $\mathbf{u}_{MPC}$ is the feedforward model predictive control.

The adaptive gain $\mathbf{K}_e(t)$ is a combination of integral and proportional gain given as,

$$\mathbf{K}_e(t) = \mathbf{K}_{Ie}(t) + \mathbf{K}_{Pe}(t) \tag{6.2}$$

The update law for the adaptive gains $\mathbf{K}_{Ie}(t)$ and $\mathbf{K}_{Pe}(t)$ is given as,

$$\dot{\mathbf{K}}_{Ie}(t) = \mathbf{e}_y(t)\mathbf{e}_y^T(t)\mathbf{\Gamma}_e - \mu\|\mathbf{e}_y\|\mathbf{K}_{Ie}(t) \tag{6.3}$$

$$\mathbf{K}_{Pe}(t) = \mathbf{e}_y(t)\mathbf{e}_y^T(t)\bar{\mathbf{\Gamma}}_e \tag{6.4}$$

Here $\mathbf{\Gamma}_e$ and $\bar{\mathbf{\Gamma}}_e$ are the constant weighting matrices. As shown in (Kaufman et al., 1997a), the adaptive control doesn't require feedforward given in 4.11 to guarantee

stability. Therefore, $\mathbf{K}_e(t)$ is sufficient. The feedforward MPC terms adds another advantage to the adaptive control by initializing the control input by a non-zero stabilizing control effort. As shown in previous chapter, the adaptive gains were initialized by a zero initial condition which causes the control signal to overshoot. However, this is avoided by use of MPC feedforward terms as shown in later sections.

### 6.2. Comments on Stability

The stability if DAMPC is dependent on the stability of the adaptive control term and the feed-forward nonlinear model predictive term. The adaptive control terms has been shown to work without the feed-forward term and it has been proven by (Kaufman et al., 1997a) that only the feedback term is necessary to guarantee the stability of the adaptive control.

Therefore, in order to guarantee the stability of the system, only the stability of NMPC needs to be proven, which has been discussed in the previous chapter. A more rigorous analysis will the part of future work. It can noted that since the NMPC control is applied as a feedforward term (which is calculated offline), only the stable solutions are accepted and hence the DAMPC is inherently stable due to this assumption.

### 6.3. Simulation and Results

To showcase the improvements from DAMPC, three following scenarios for a point-to-point tracking case are considered:

1. NMPC feedforward control with application to the actual system: In this case the NMPC control generated from the point-to-point tracker from the previous chapter will be applied to the actual system with polyhedral gravitational model and additional forces as discussed in Chapter 3.

2. Adaptive control application: In this case the adaptive control will be implemented to track the trajectories generated from the NMPC. It will be shown that even though the adaptive control can successfully track the trajectories, the control effort overshoots in some cases.
3. Application of DAMPC: In this case, the full DAMPC formulation will be implemented to track the trajectories from the NMPC on the actual model. It will be shown that the DAMPC is superior in terms of control effort. The DAMPC formulation will be compared to the adaptive control system in the presence of noise.
4. Effect of unknown noise:In this case we will present the results for DAMPC in the presence of unknown system noise. We also compare the performance of DAMPC with adaptive control.

### 6.3.1. Asteroid Eros

In this section we consider asteroid Eros and present the simulation results. Point-to-point tracker case is considered and the conditions are similar to as previously defined.

The initial and final conditions are given as follows:

$$\begin{aligned} \mathbf{r}_{in} &= [0 \ -8 \ 8 \ ]^T \text{ km}, \ \ \dot{\mathbf{r}}_{in} = [0 \ 0 \ 0]^T \text{ km/s} \\ \mathbf{r}_f &= [0 \ 10 \ 5 \ ]^T \text{ km}, \quad \dot{\mathbf{r}}_f = [0 \ 0 \ 0 \ ]^T \text{ km/s} \end{aligned} \tag{6.5}$$

The NMPC conditions are given in Table 6.1. The adaptive control tuning parameter is set to $\alpha = -1 \times e^{-9}$. The adaptive control gains are initialized with zero initial condition and the adaptive tuning parameter is set to $\Gamma_e = \bar{\Gamma}_e = 10^3 I_{3\times 3}$.

Table 6.1

NMPC Parameters for Asteroid Eros

| | |
|---|---|
| N | 100 |
| $\mathbf{Q}$ | $1 \times 10^{-5} \begin{bmatrix} \mathbf{I}_{3\times3} & \mathbf{0}_{3\times3} \\ \mathbf{0}_{3\times3} & \mathbf{I}_{3\times3} \end{bmatrix}$ |
| $\mathbf{R}$ | $0.5\mathbf{I}_{3\times3}$ |
| $\Delta T$ | 0.2 |
| Control Constraint | $-0.0007 \leq \mathbf{u} \leq 0.0007\ km/s^2$ |
| Velocity Constraint | $-0.05 \leq \mathbf{v} \leq 0.05\ km/s$ |
| a | 22 km |
| b | 10 km |
| c | 10 km |

#### 6.3.1.1. Case 1: MPC Feed-forward Only

In this section, we present the results for the first case where we apply the NMPC control found in the previous chapter to asteroid Eros with the "actual" system as presented in Chapter 3. The actual trajectory and desired trajectory is given in Figure 6.2. As expected the trajectories do not completely coincide since the system model differs from the NMPC model. However, it can also be noticed that the actual final position does not differ by much due to the low mass of asteroid Eros. However, for a long term trajectory tracking the difference will grow and the MPC feedforward control will not be able to track the final desired position.

Figure 6.3 (a) shows the actual positions of the spacecraft with NMPC feedforward control law. It can be noted that the position do not converge to the desired final position which is further confirmed by Figure 6.3 (d) where the output error is shown. The output

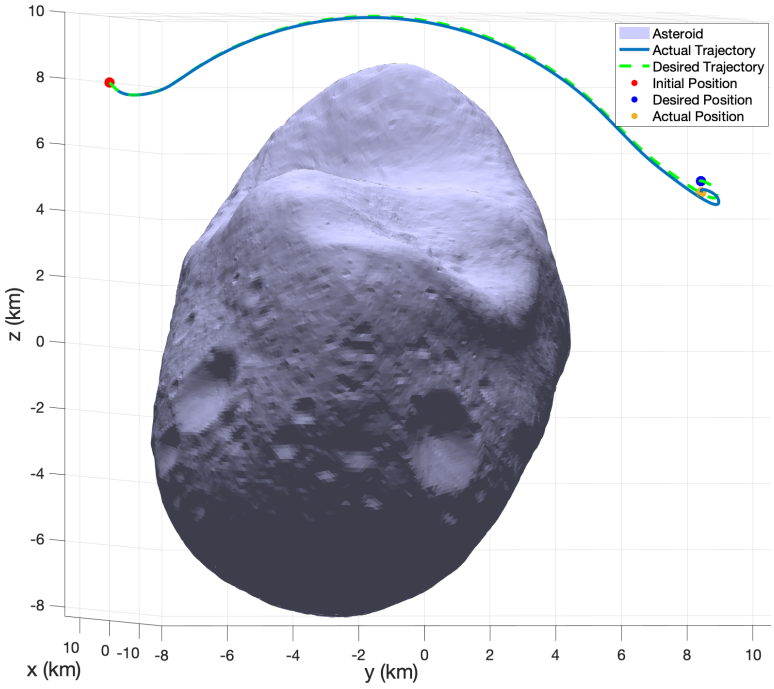


*Figure 6.2* Trajectory of spacecraft around asteroid Eros.

error is the combination of position and velocity. The output clearly shows that the error is diverging as the time grows. The control effort is given in Figure 6.3 (c), the control is solely from the feedforward NMPC control found in previous chapter. Figure 6.3 (b) shows the actual velocity of the spacecraft and it can be noted that the velocity does not converge to zero as the spacecraft approaches the final actual position. It is shown in the following sections that a stronger gravitational field drastically affects the performance of NMPC feedforward control.

#### 6.3.1.2. Case 2: Adaptive Control

In this section, we discuss the simulation and results for the case where the adaptive control is implemented to track the trajectories found using the NMPC methodology from the previous chapter. The adaptive control will be tuned once and the tuning the parameters will be kept constant for other asteroids. This is to show the robustness of

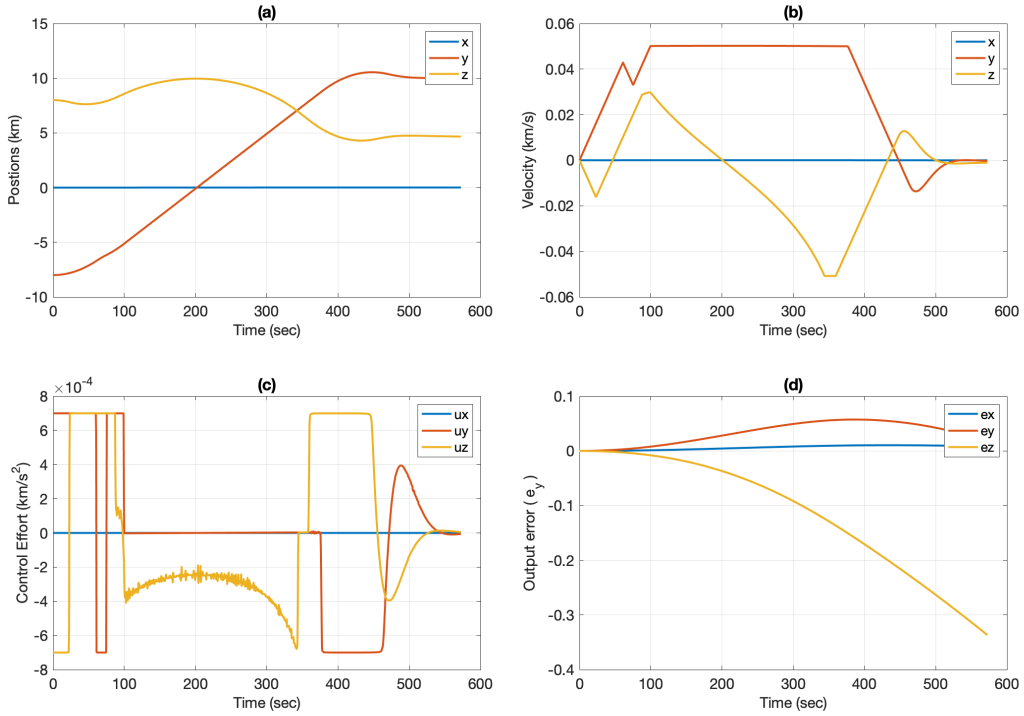


*Figure 6.3* Plots for MPC Failure case for asteroid Eros, (a) position vs. time, (b) velocity vs. time, (c) control effort vs. time, (d) output error vs. time.

adaptive control to different asteroids and dynamical conditions.

Figure 6.4 shows the actual and desired trajectory of the spacecraft with adaptive control. It can be seen that the adaptive control is able to successfully track the trajectories and the final position coincides with the desired position. Therefore, adaptive control is able to reject the disturbances and track the NMPC generated trajectory.

The positions and velocities can be seen in Figure 6.5 (a) and (b). The positions converge to the final desired and locations the velocities converge to zero as desired. The control effort from adaptive control is shown in Figure 6.5 (c). It can be seen that even though control effort remains within the realistic thruster limit, there is significant overshooting resulting from initialization and the inherent issue that the adaptive control does not any a-priori knowledge about the system model. However, the output error

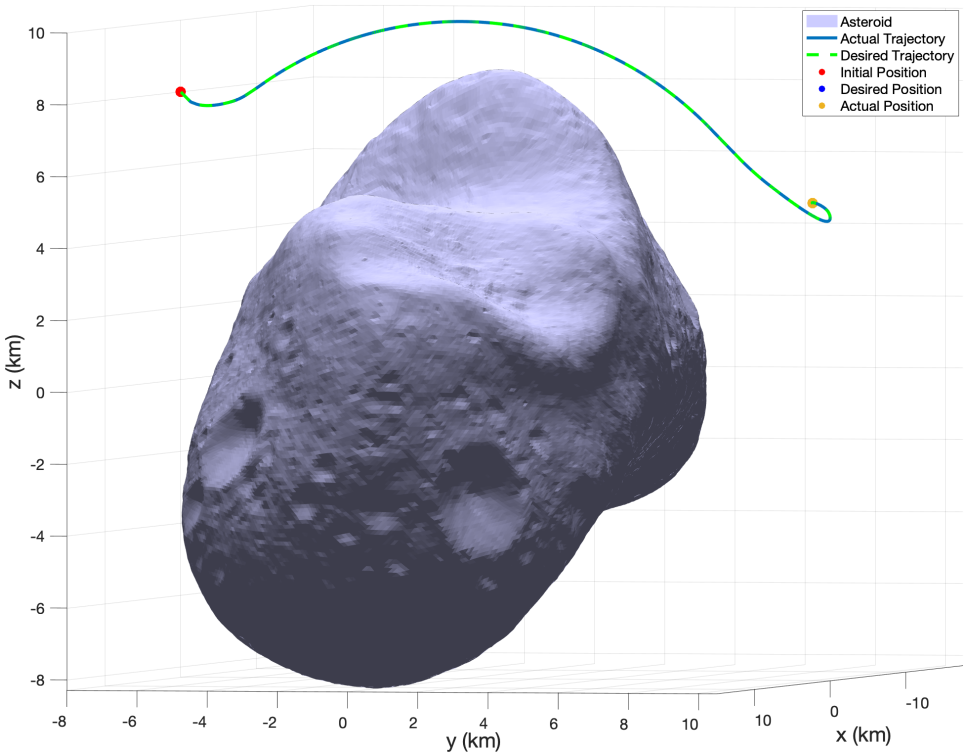


*Figure 6.4* Trajectory of spacecraft around asteroid Eros with adaptive control only.

approaches zero which can be seen from Figure 6.5 (d) which shows that the adaptive control is not only robust to the unknown environment but also improves the tracking performance.

The adaptive control tuning parameters can be further tuned depending upon the mission requirements and robustness. Generally, increasing the gains increases the tracking performance but reduces the robustness of the adaptive control especially in the presences of sensor and system noise. It found that the adaptive control was fairly easy to tune and a wide variety of gains can be implemented.

#### 6.3.1.3. Case 3: DAMPC Implementation

In this section we show the simulation and results for the combined control i.e. direct adaptive model predictive control (DAMPC). As mentioned before, the DAMPC is a

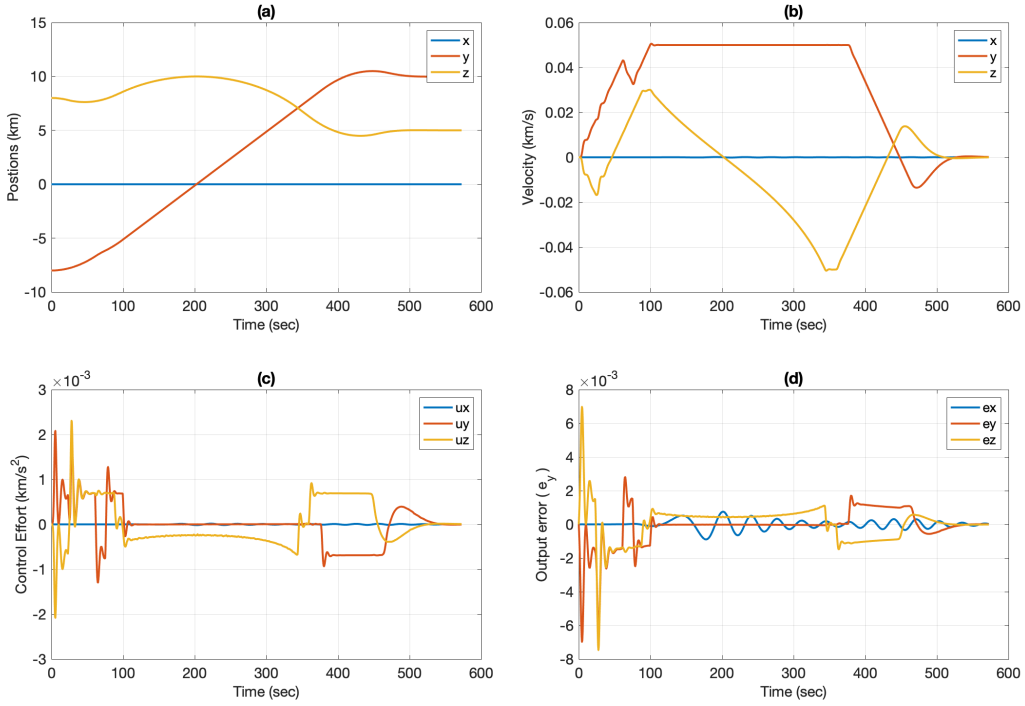


*Figure 6.5* Plots for adaptive control case for asteroid Eros, (a) position vs. time, (b) velocity vs. time, (c) control effort vs. time, (d) output error vs. time.

combination of adaptive control and MPC, where the adaptive control is the feedback control and the NMPC is the feedfoward control. The NMPC feedforward control values are similar to one used in Case 1 and in the previous chapter.

As in the case for adaptive control, DAMPC is able to successfully track the desired trajectories generated from NMPC with actual system model. The desired position and actual position coincides. However, the tracking performance is superior to adaptive control and the output error can be seen in Figure 6.7 (d). The addition of the feedforward control has shown to improve the tracking performance of the adaptive control while adding optimally to trajectory tracking.

The position and velocities can be seen in Figure 6.7 (a) and (b). The control system is able to reach the desired state as the position converges to desired position and the

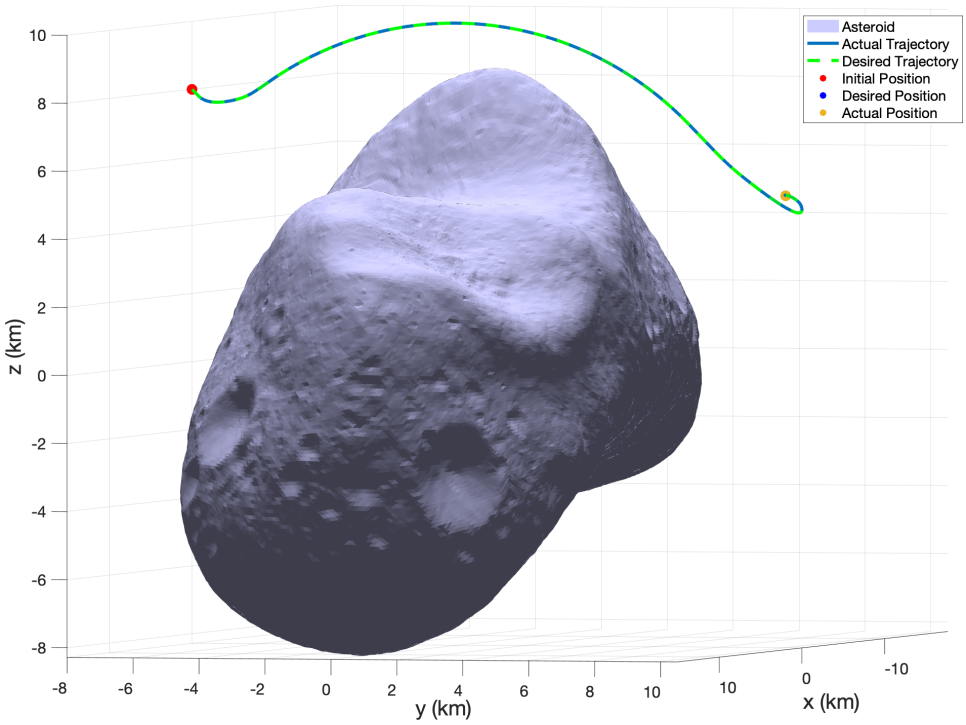


*Figure 6.6* Trajectory of spacecraft around asteroid Eros with DAMPC.

velocities converge to zero. The control effort from DAMPC can be seen in Figure 6.7 (c). It can be seen that the control effort from DAMPC does not overshoot like the case where only adaptive control is applied.

Therefore, DAMPC not only offers superior tracking performance by reducing the output error but also a better control effort in terms of overshooting and chattering. In case of DAMPC, the feedforward term helps to better initialize the control effort which is not possible with the adaptive control since the adaptive control is initialized by zero initial condition.

Also, the adaptive control effort is relatively low as compared to the total control effort applied since the adaptive control acts as a disturbance rejection control for higher order forces and system disturbances. The contribution of adaptive control in DAMPC

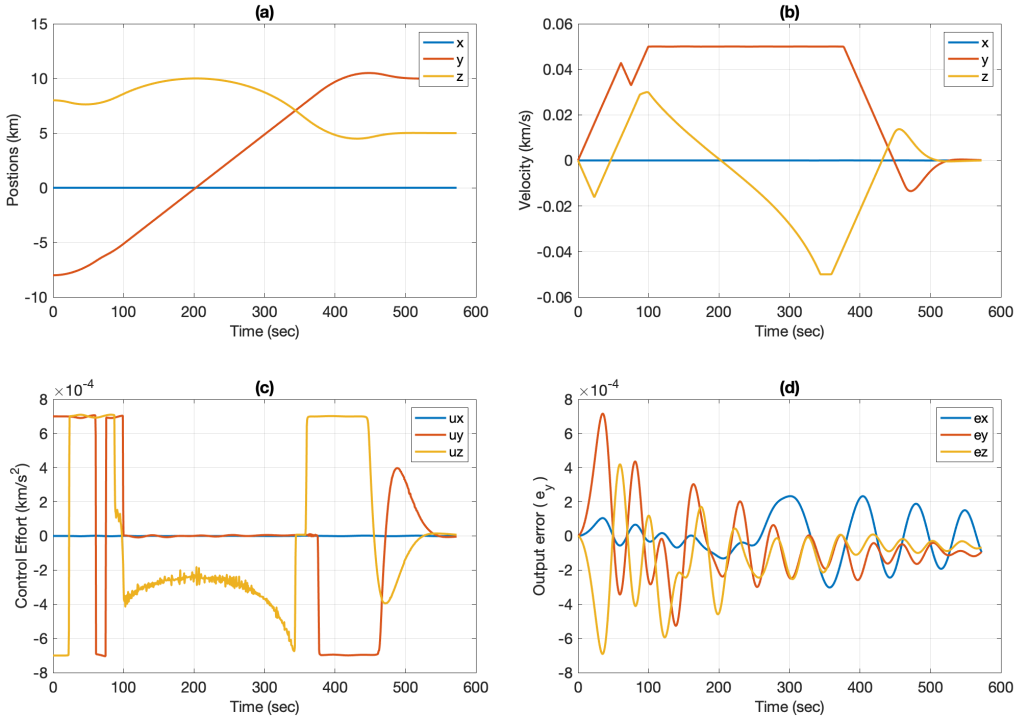


*Figure 6.7* Plots for DAMPC case for asteroid Eros, (a) position vs. time, (b) velocity vs. time, (c) control effort vs. time, (d) output error vs. time.

is shown in Figure 6.8 and it can be noted that the adaptive control is much lower than compared to the total control effort from DAMPC as shown in Figure 6.7 (c).

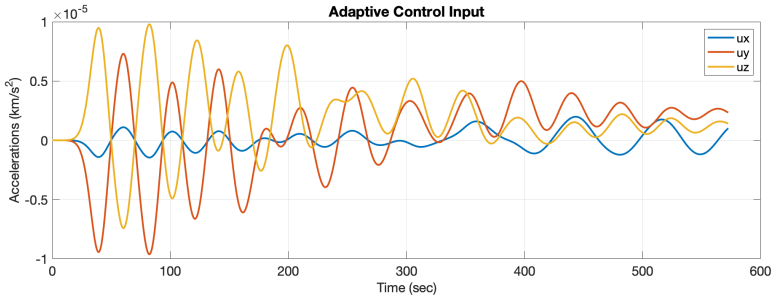


*Figure 6.8* Adaptive control plot for asteroid Eros for DAMPC formulation.

#### 6.3.1.4. Case 4: Effects of Unknown Noise

In this section we discuss the effects of system noise on the DAMPC and compare it with the case adaptive control only. It was found that DAMPC offers a better tracking performance in the presence of noise and a reduced chatter in the control effort as compared to the adaptive control only. A random Gaussian noise of $(1 \times 10^{-4}\mathcal{N}(0,\ I_{3\times 3})$ is added to the system. The magnitude of the error is taken to be higher than the order of the gravity to further test the robustness of the control system to unknown noise.

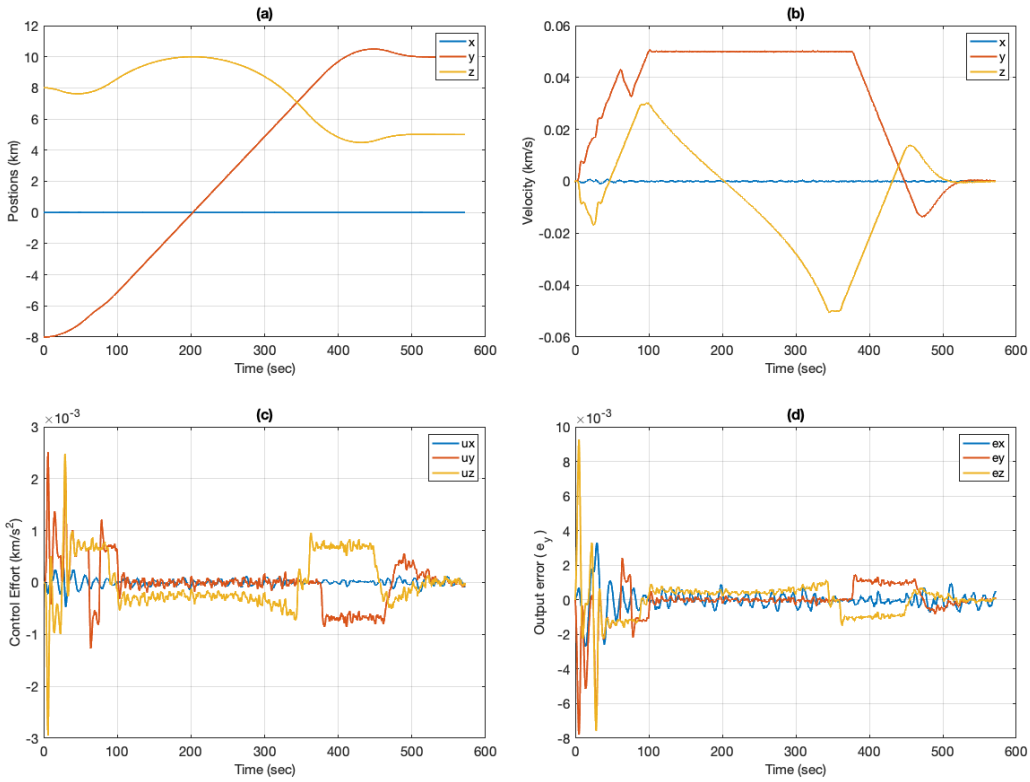


*Figure 6.9* Plots for adaptive control with noise case for asteroid Eros, (a) position vs. time, (b) velocity vs. time, (c) control effort vs. time, (d) output error vs. time.

Figure 6.9 (a) and (b) shows the position and velocities for the case where only adaptive control is implemented. The control effort is given in Figure 6.9 (c). It can be

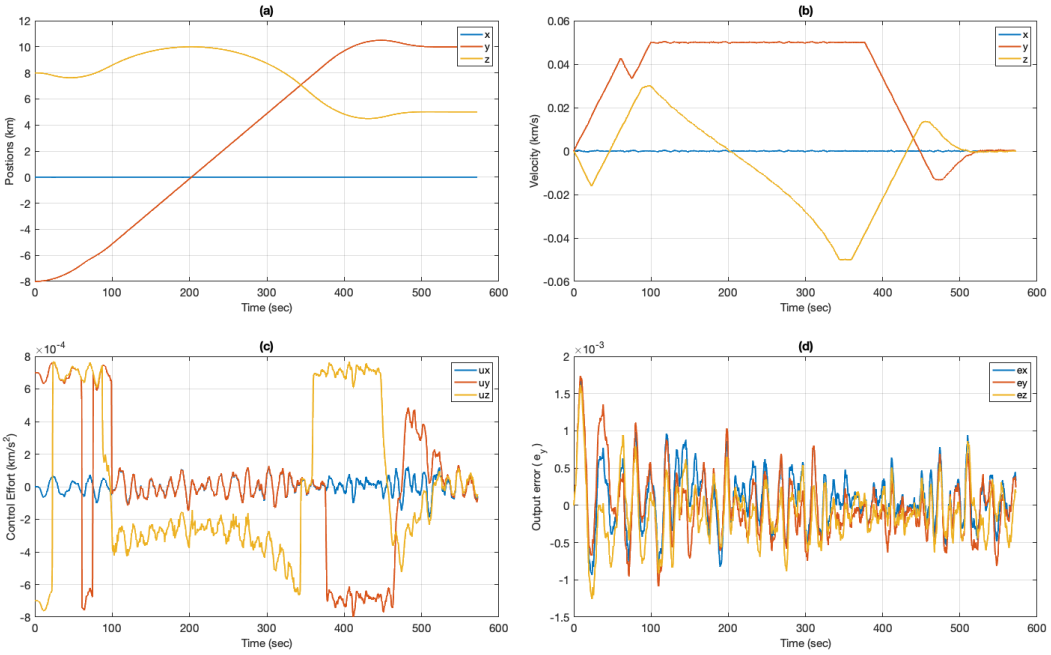


*Figure 6.10* Plots for DAMPC case with noise for asteroid Eros, (a) position vs. time, (b) velocity vs. time, (c) control effort vs. time, (d) output error vs. time.

seen that the control effort is not only higher in this case as compared to DAMPC (shown in Figure 6.10 (c)) but also there is high chatter in the control effort.

The magnitude of the output error is also less in the case where DAMPC is implemented as shown in Figure 6.10 (d) compared to the output error for adaptive control only as given in Figure 6.9 (d). However, both adaptive control with $e$ modification and DAMPC can handle system noise and tracking performance is comparable.

### 6.3.2. Asteroid Bennu

In this section we consider asteroid Bennu and present the simulation results. Point-to-point tracker case is considered and the conditions are similar to as previously defined.

The initial and final conditions are given as follows,

$$\begin{aligned} \mathbf{r}_{in} &= [0 \ -0.35 \ 0.1 \ ]^T \text{ km}, \ \ \dot{\mathbf{r}}_{in} = [0 \ 0 \ 0]^T \text{ km/s} \\ \mathbf{r}_f &= [0.1 \ 0.4 \ 0.2 \ ]^T \text{ km}, \quad \dot{\mathbf{r}}_f = [0 \ 0 \ 0 \ ]^T \text{ km/s} \end{aligned} \tag{6.6}$$

The NMPC conditions are given in Table 6.2. The adaptive control tuning parameter is set to $\alpha = -1 \times e^{-9}$. The adaptive control gains are initialized with zero initial condition and the adaptive tuning parameter is set to $\Gamma_e = \bar{\Gamma}_e = 10^3 I_{3\times3}$.

Table 6.2

NMPC Parameters for Case 2 for asteroid Bennu

| | |
|---|---|
| N | 100 |
| **Q** | $1 \times 10^{-5} \begin{bmatrix} \mathbf{I}_{3\times3} & \mathbf{0}_{3\times3} \\ \mathbf{0}_{3\times3} & \mathbf{I}_{3\times3} \end{bmatrix}$ |
| **R** | $0.5\mathbf{I}_{3\times3}$ |
| $\Delta T$ | 0.1 |
| Control Constraint | $-0.0025 \leq \mathbf{u} \leq 0.0025 \ km/s^2$ |
| Velocity Constraint | $-0.005 \leq \mathbf{u} \leq 0.005 \ km/s$ |
| a | 0.3 km |
| b | 0.3 km |
| c | 0.3 km |

#### 6.3.2.1. Case 1: MPC Feed-forward Only

In this section, we present the results for the first case where we apply the NMPC control found in the previous chapter to asteroid Bennu with the "actual" system as presented in Chapter 3. The spacecraft actual and desired trajectory can be seen in Figure 6.11. It can be seen that the desired and actual position are very close. This is due to the fact that asteroid Bennu is small and almost spherical asteroid with a weak gravitational pull. The gravitational field is dominated by the two-body terms and the off two-body

terms do not play a significant role. However, the divergence between actual and desired trajectory is subject to the duration of the mission. Increasing the mission duration tends to increase the divergence.

The position and velocities are given in Figure 6.11 (a) and (b). Both tends to converge to the desired location. However, it can be seen from the output error plot that the error does tend to zero, but in fact is increasing as the time grows. This is expected since only feed-forward MPC is being implemented. The control effort can be shown in Figure 6.12 (c).

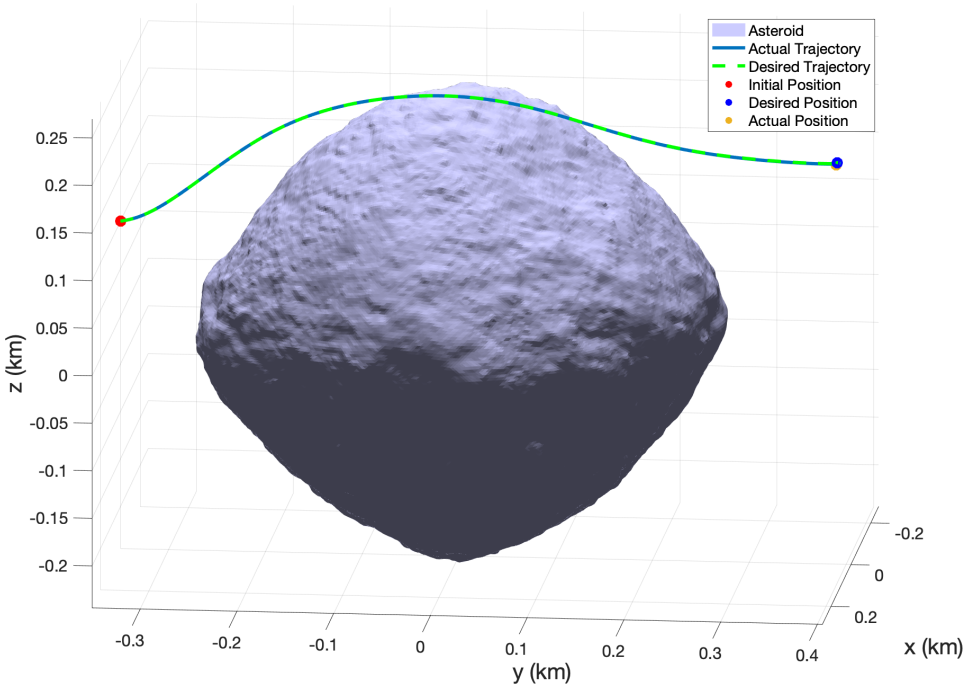


*Figure 6.11* Trajectory of spacecraft around asteroid Bennu for MPC feed-forward case.

#### 6.3.2.2. Case 2: Adaptive Control

In this section we discuss the simulation and results for the case where the adaptive control is implemented to track the trajectories found using the NMPC methodology

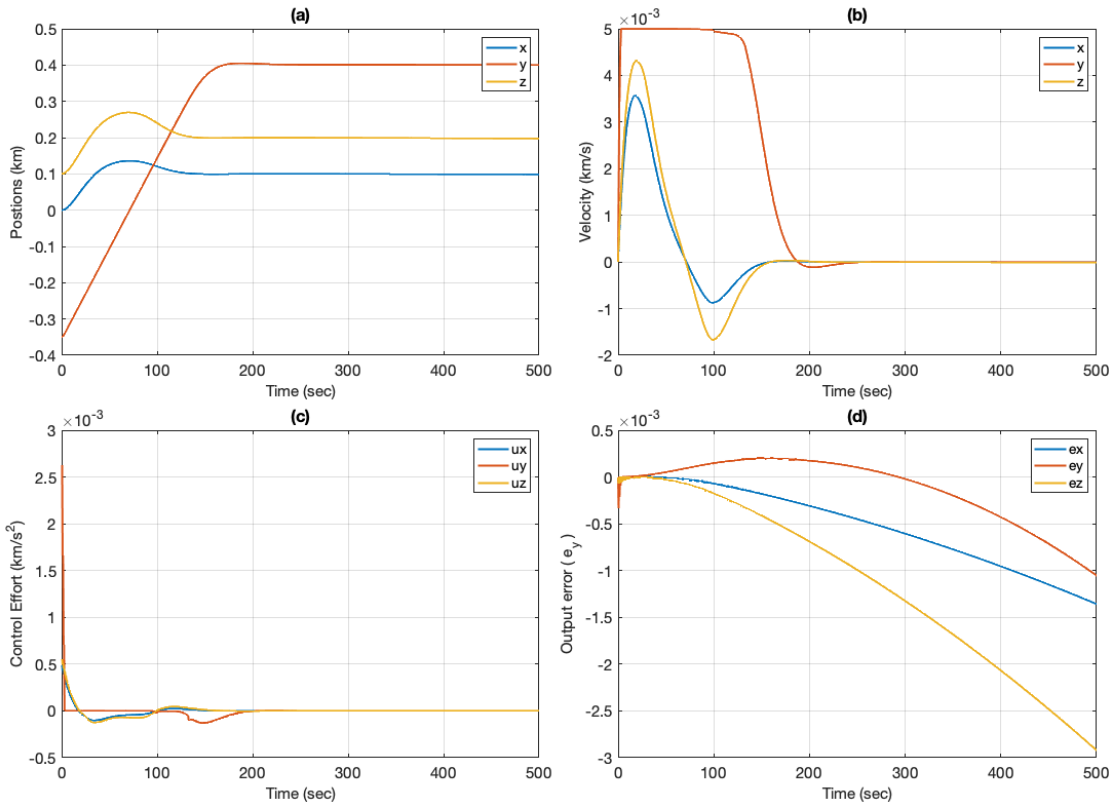


*Figure 6.12* Plots for MPC Failure case for asteroid Bennu, (a) position vs. time, (b) velocity vs. time, (c) control effort vs. time, (d) output error vs. time.

from the previous chapter. The adaptive control will be tuned once and the tuning the parameters will be kept constant for other asteroids. This is to show the robustness of adaptive control to different asteroids and dynamical conditions.

Figure 6.13 shows the actual and desired trajectory of the spacecraft with adaptive control. It can be seen that the adaptive control is able to successfully track the trajectories and the final position coincides with the desired position. Therefore, adaptive control is able to reject the disturbances and track the NMPC generated trajectory.

The positions and velocities can be seen in Figure 6.14 (a) and (b). The positions converge to the final desired and locations the velocities converge to zero as desired.

Unlike the previous case the errors tends to converge to zero which can be seen in Figure 6.14 (d). This shows that a feedback control is still necessary even though the gravitational field of the Bennu is weaker than asteroid Eros.

It can be noted that the forces due to solar radiation pressure in this case could be larger than the gravitational field of the asteroid depending on the size and shape of the spacecraft. The control effort can be seen in Figure 6.14 (c). It can be seen that there is significant overshooting and chatter in the adaptive control which will be further improved using the DAMPC modification. The steady-state adaptive control effort can be seen in the magnified Figure 6.14 (e). It can be seen that a non-zero adaptive control effort is required to keep hovering over asteroid Bennu.

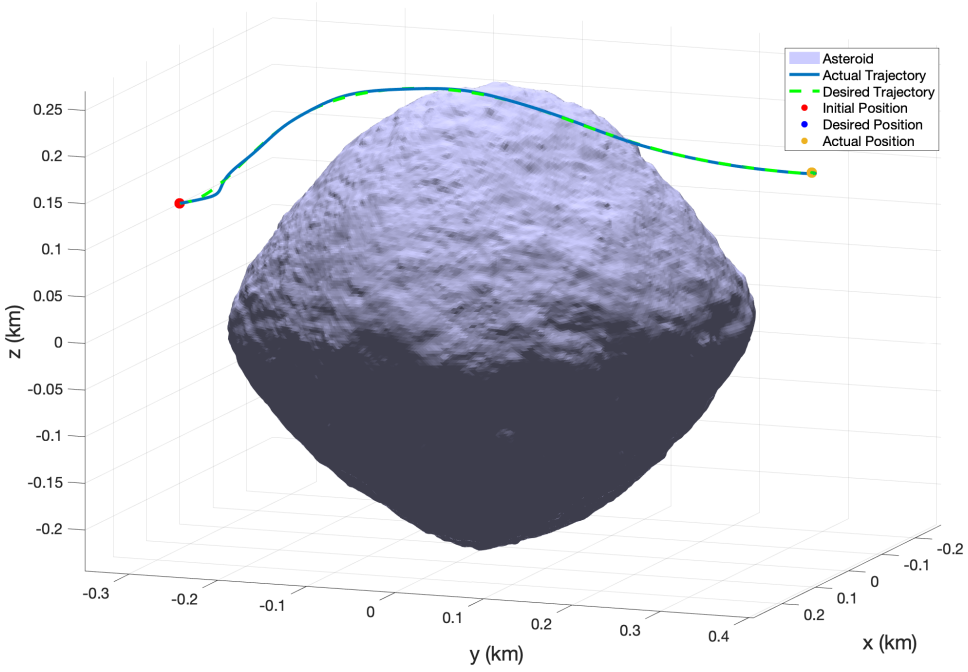


*Figure 6.13* Trajectory of spacecraft around asteroid Bennu with adaptive control.

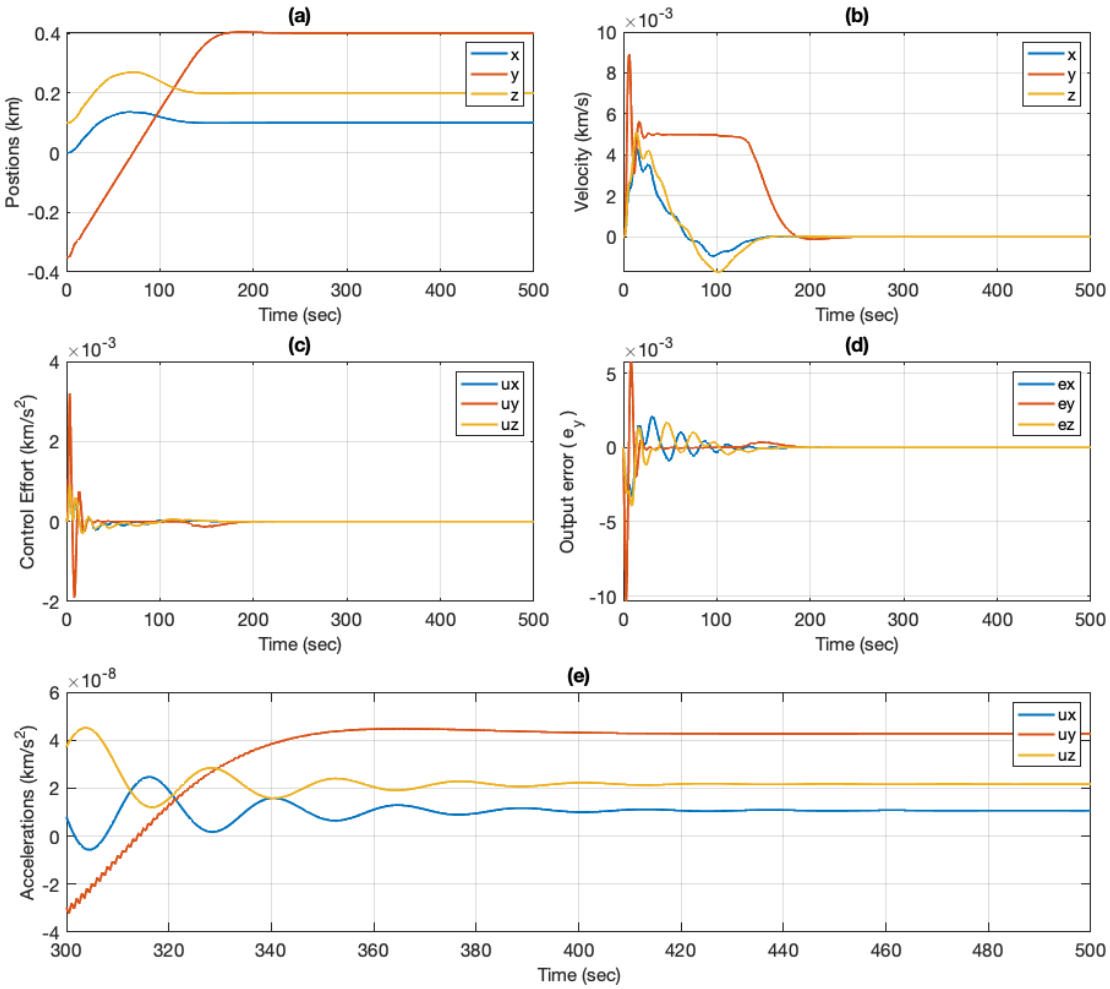


*Figure 6.14* Plots for adaptive control case for asteroid Eros, (a) position vs. time, (b) velocity vs. time, (c) control effort vs. time, (d) output error vs. time, (e) control effort zoomed in.

#### 6.3.2.3. Case 3: DAMPC Implementation

In this section we show the simulation and results for the combined control i.e. direct adaptive model predictive control (DAMPC). As mentioned before, the DAMPC is a combination of adaptive control and MPC, where the adaptive control is the feedback control and the NMPC is the feed-forward control. The NMPC feedforward control values are similar to one used in Case 1 and in the previous chapter.

As in the case for adaptive control, DAMPC is able to successfully track the desired trajectories generated from NMPC with actual system model. The desired position and actual position coincides. However, the tracking performance is superior to adaptive control and the output error can be seen in Figure 6.16 (d).

The addition of the feedforward control has shown to improve the tracking performance of the adaptive control while adding optimally to trajectory tracking. The position and velocities can be seen in Figure 6.16 (a) and (b). The DAMPC control system is able to successfully track the trajectories.

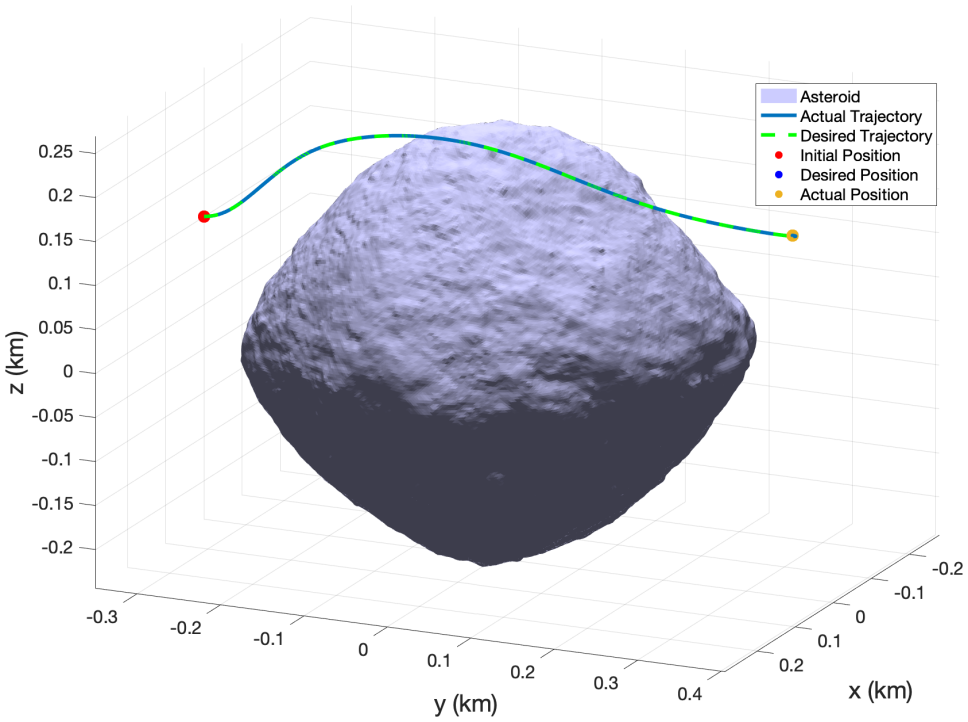


*Figure 6.15* Trajectory of spacecraft around asteroid Bennu for DAMPC.

#### 6.3.2.4. Case 4: Effects of Unknown Noise

In this section we discuss the effects of system noise on the DAMPC and compare it with the case adaptive control only. It was found that DAMPC offers a better tracking

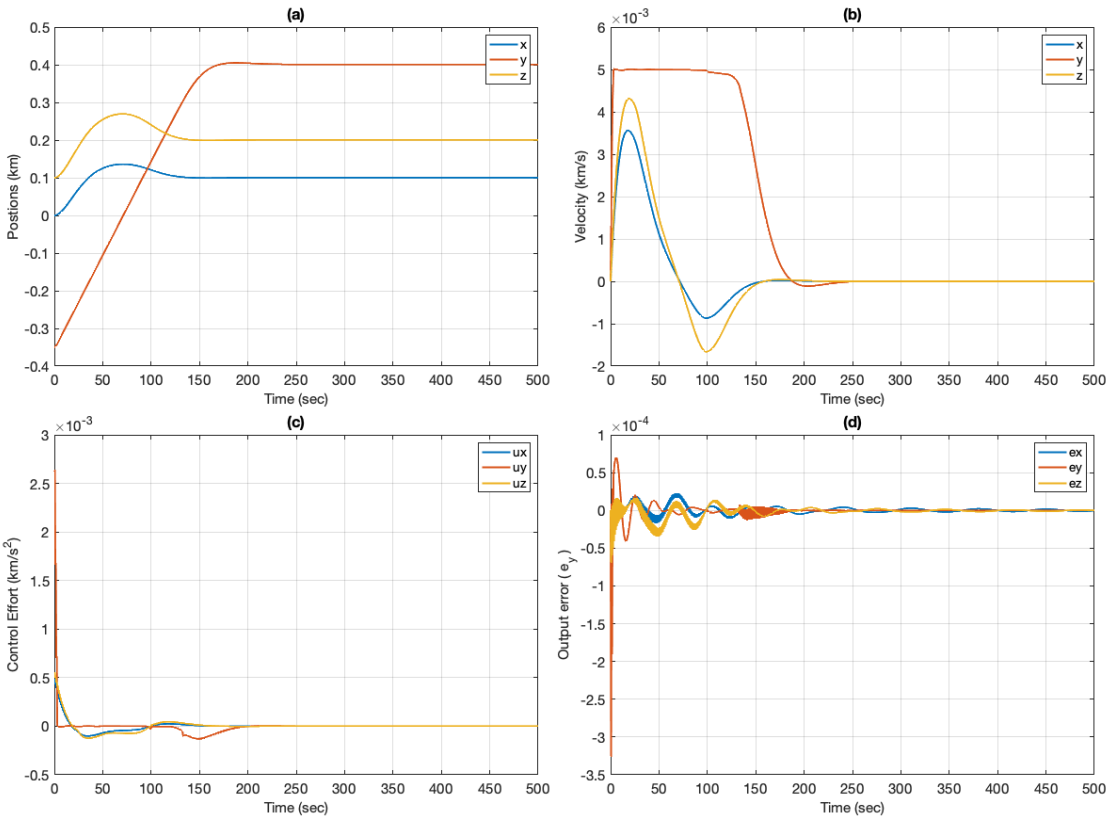


*Figure 6.16* Plots for DAMPC case for asteroid Bennu, (a) position vs. time, (b) velocity vs. time, (c) control effort vs. time, (d) output error vs. time.

performance in the presence of noise and a reduced chatter in the control effort as compared to the adaptive control only. A random Gaussian noise of $(1 \times 10^{-5}\mathcal{N}(0,\, I_{3\times 3})$ is added to the system. The magnitude of the error is taken to be one order higher than the gravity to further test the robustness of the control system to unknown noise.

Figure 6.17 shows the plots for the case where only adaptive controller is implemented with noise and Figure 6.18 shows the plots for where DAMPC is implemented. It can be seen from the figures that the DAMPC is able to handle the noise better than adaptive control in terms of the output error and control effort. Figure 6.17 (e) and Figure 6.18 (e) shows the magnified control efforts and it can be seen that

the DAMPC's control effort less in magnitude and chatter as compared to the adaptive control.

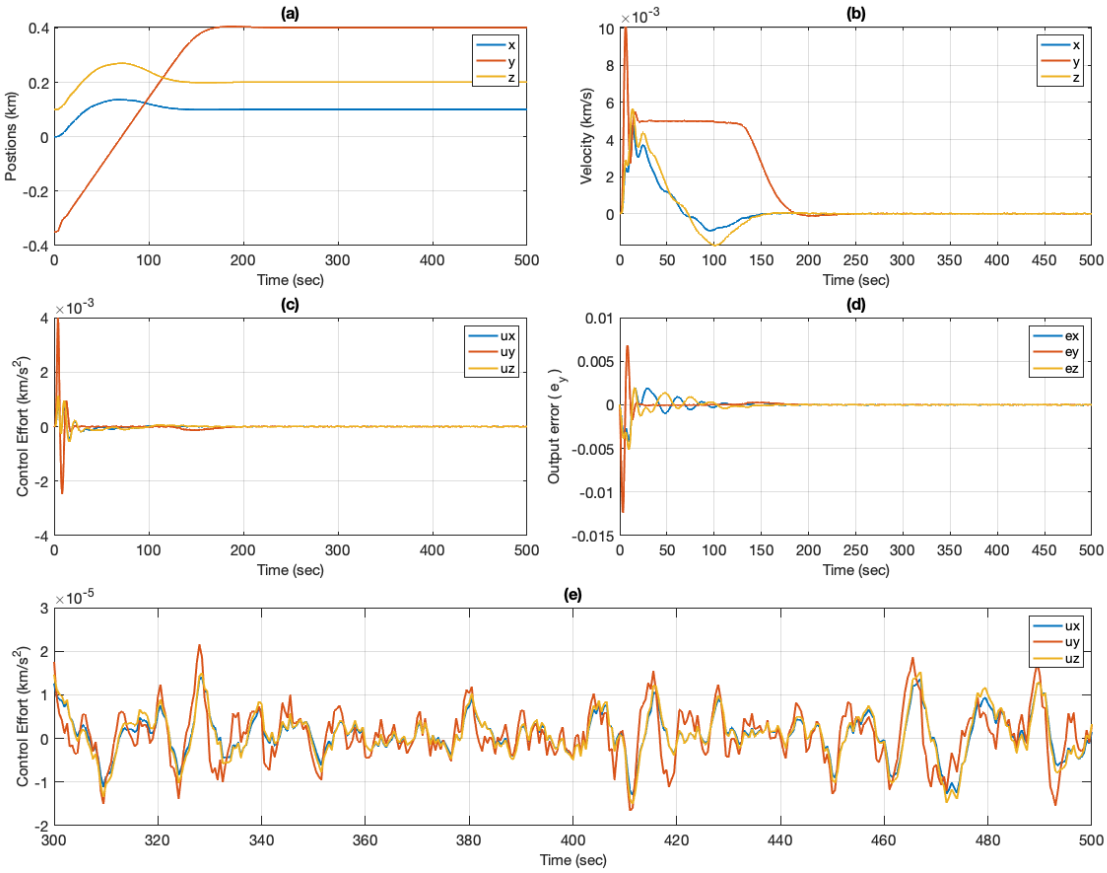


*Figure 6.17* Plots for adaptive case with noise for asteroid Bennu, (a) position vs. time, (b) velocity vs. time, (c) control effort vs. time, (d) output error vs. time, (e) control effort zoomed in.

### 6.3.3. Asteroid Kleopatra

In this section, we will discuss the simulation and results for asteroid Kleopatra. Asteroid Kleopatra is dog-bone shape metal asteroid. The gravitational field of the asteroid is highly variable and much stronger asteroid Eros and Bennu which will be reflected in control effort and poor tracking via feed-forward MPC control. The initial

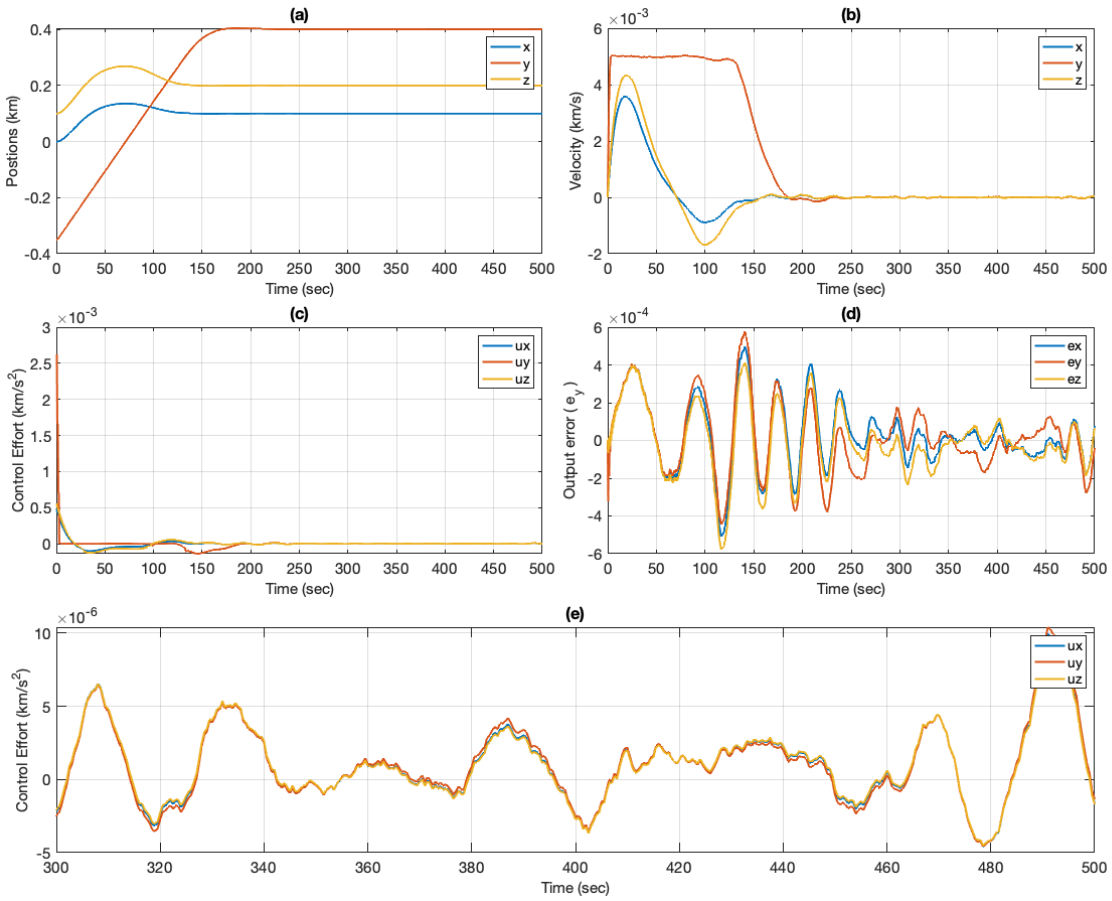


*Figure 6.18* Plots for DAMPC with noise case for asteroid Bennu, (a) position vs. time, (b) velocity vs. time, (c) control effort vs. time, (d) output error vs. time, (e) control effort zoomed in.

and final conditions are given as follows,

$$\mathbf{r}_{in} = [10 \ -100 \ 0 \ ]^T \text{ km}, \quad \dot{\mathbf{r}}_{in} = [0 \ 0 \ 0]^T \text{ km/s}$$
$$\mathbf{r}_f = [50 \ 60 \ 25 \ ]^T \text{ km}, \quad \dot{\mathbf{r}}_f = [0 \ 0 \ 0 \ ]^T \text{ km/s} \tag{6.7}$$

The NMPC conditions are given in Table 6.3 case. The adaptive control gains are initialized with zero initial condition and the adaptive tuning parameter is set to $\Gamma_e = \bar{\Gamma}_e = 10^3 I_{3\times 3}$.

Table 6.3

NMPC Parameters for Case 2 for asteroid Kleopatra

| | |
|---|---|
| N | 100 |
| **Q** | $1 \times 10^{-5} \begin{bmatrix} \mathbf{I}_{3\times3} & \mathbf{0}_{3\times3} \\ \mathbf{0}_{3\times3} & \mathbf{I}_{3\times3} \end{bmatrix}$ |
| **R** | $0.5\mathbf{I}_{3\times3}$ |
| $\Delta T$ | 0.2 |
| Control Constraint | $-0.007 \leq \mathbf{u} \leq 0.007\ km/s^2$ |
| Velocity Constraint | $-0.1 \leq \mathbf{u} \leq 0.1\ km/s$ |
| a | 150 km |
| b | 70 km |
| c | 50 km |

#### 6.3.3.1. Case 1: MPC Feed-forward Only

In this section, we present the results for the first case where we apply the NMPC control found in the previous chapter to asteroid Kleopatra with the "actual" system as presented in Chapter 3. The desired and actual trajectory after implementing MPC feed-forward only can be seen in Figure 6.19. In this case it can be seen clearly that the trajectories are diverging significantly. This is because the the two-body assumption used for calculating MPC trajectory. In case of Kleopatra, the gravitational model is better represented by a polyhedral gravity model due its shape and mass. Also, as the duration of mission get longer the divergence from the desired position also increases and causes even further drift. The output error can be seen in Figure 6.21 (d). As compared to the previous asteroid, the output error in this case is significantly high. The position and velocities are given in Figure 6.21 (a) and (b) respectively.

It can be seen that the positions do not converge to the desired position and velocities

do not converge to zero. The control effort from the feed-forward MPC is given in Figure 6.21 (c). It can also be noted that the ellipsoidal constraint for obstacle avoidance is not met and the spacecraft eventually ends up inside the ellipsoid. This can be seen in Figure 6.20.

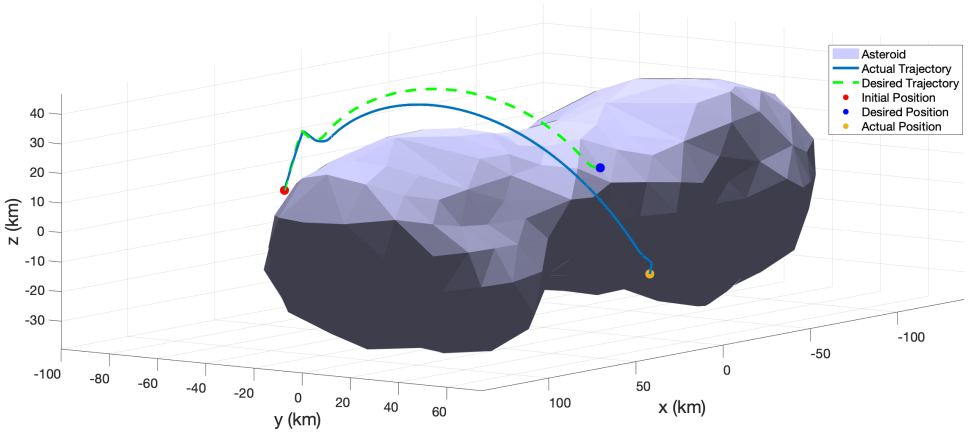


*Figure 6.19* Trajectory of spacecraft around asteroid Kleopatra for MPC feed-forward.

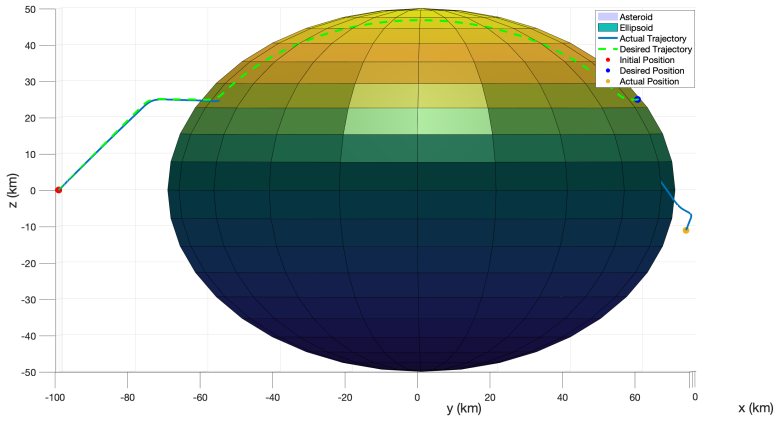


*Figure 6.20* Ellipsoidal constraint for MPC feed-forward case for Kleopatra.

### 6.3.3.2. Case 2: Adaptive Control

In this section we discuss the simulation and results for the case where the adaptive control is implemented to track the trajectories found using the NMPC methodology

from the previous chapter. The adaptive control will be tuned once and the tuning the parameters will be kept constant for other asteroids. This is to show the robustness of adaptive control to different asteroids and dynamical conditions.

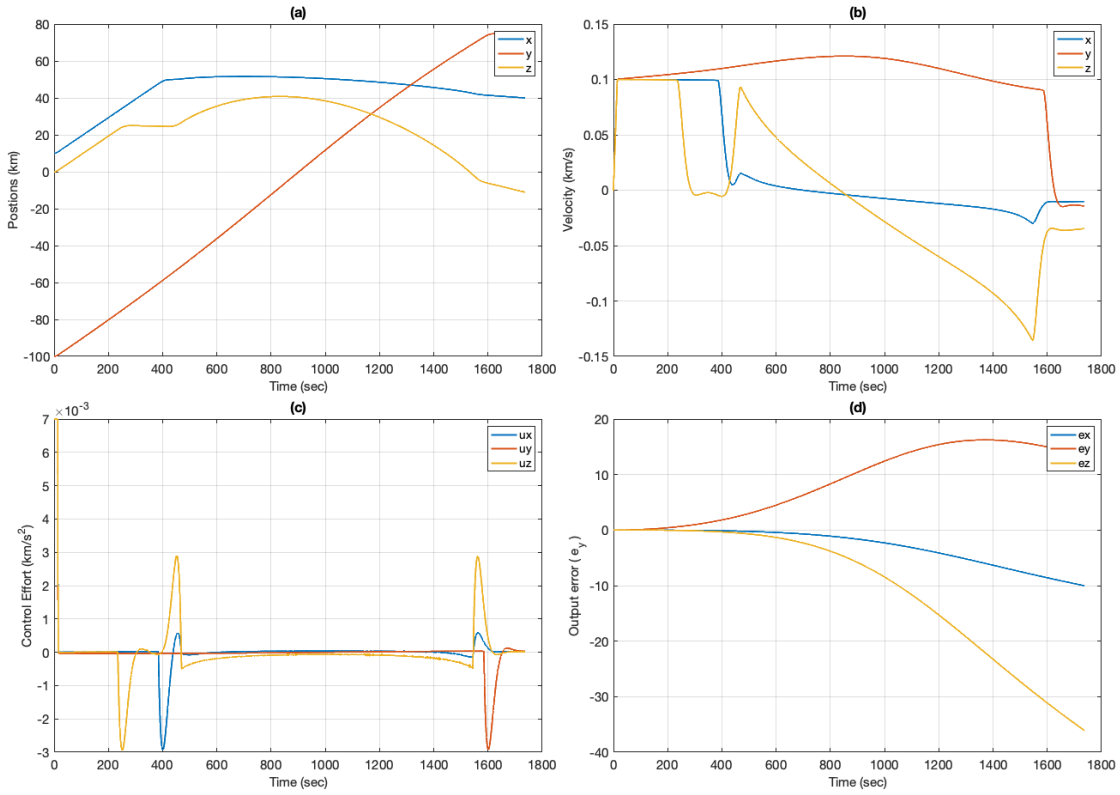


*Figure 6.21* Plots for MPC feed-forward case for asteroid Kleopatra, (a) position vs. time, (b) velocity vs. time, (c) control effort vs. time, (d) output error vs. time.

It can be seen from the Figure 6.22 that the adaptive control is able to successfully track the desired trajectory generated from the MPC and converge to the final desired position. Which shows that the adaptive control is robust to varying gravity field of the asteroid Kleopatra without re-tuning the adaptive control gains. Note that the adaptive control weighting gains are kept constant for all three asteroids. The position and velocities are shown in Figure 6.22 (a) and (b). The positions successfully converge to the

desired final position and the velocities converge to the zero. The adaptive control effort can be seen in Figure 6.22 (c).

The adaptive control can be further improved reducing the overshoot and chatter. The output error can be seen in Figure 6.22 (d). The output error is far less as compared to the previous case which shows that the adaptive control is able to track the trajectories in the presence of disturbances.

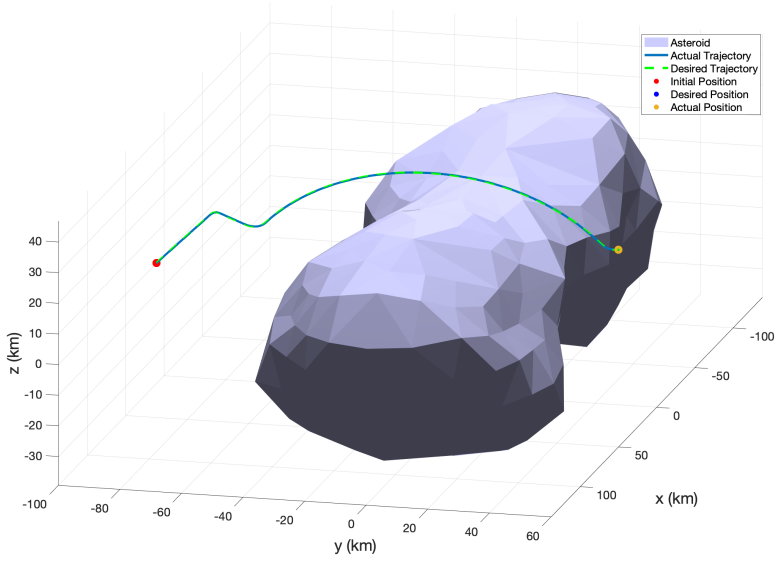


*Figure 6.22* Trajectory of spacecraft around the asteroid Kleopatra for the adaptive control case.

#### 6.3.3.3. Case 3: DAMPC Implementation

In this section we show the simulation and results for the combined control i.e. direct adaptive model predictive control (DAMPC). As mentioned before, the DAMPC is a combination of adaptive control and MPC, where the adaptive control is the feedback control and the NMPC is the feed-forward control.

The NMPC feedforward control values are similar to one used in Case 1 and in the

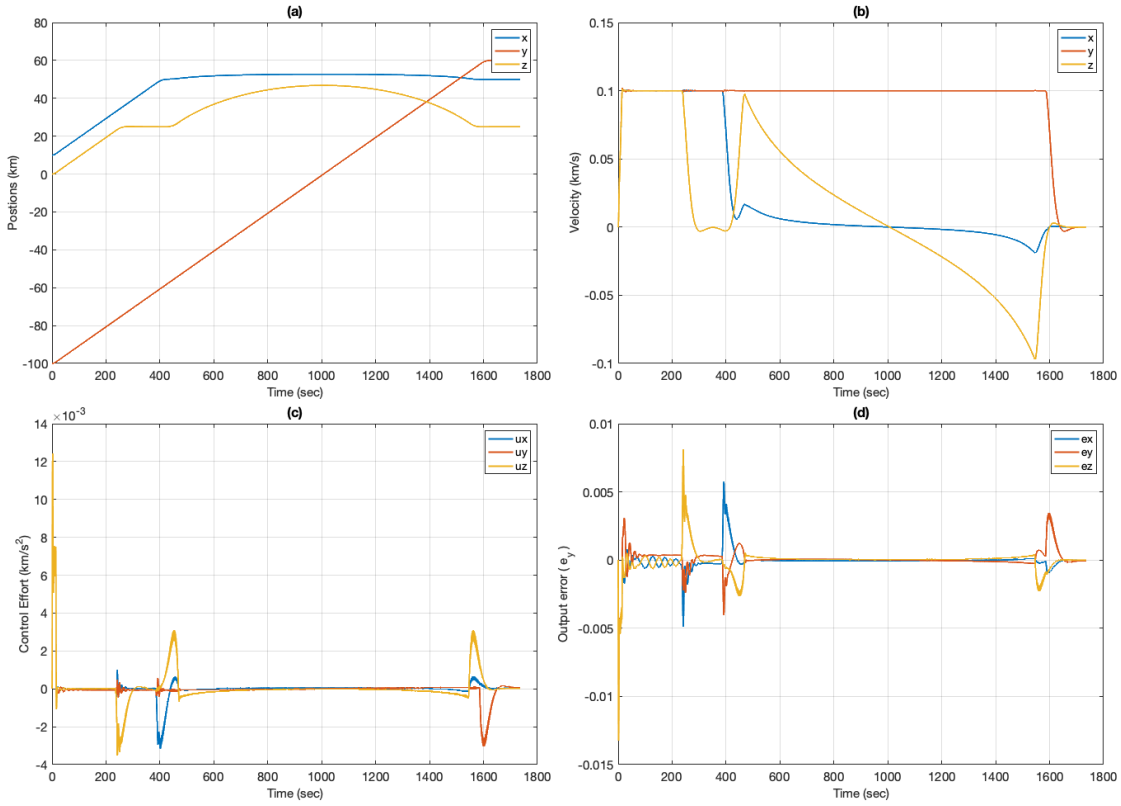


*Figure 6.23* Plots for adaptive control case for asteroid Kleopatra, (a) position vs. time, (b) velocity vs. time, (c) control effort vs. time, (d) output error vs. time.

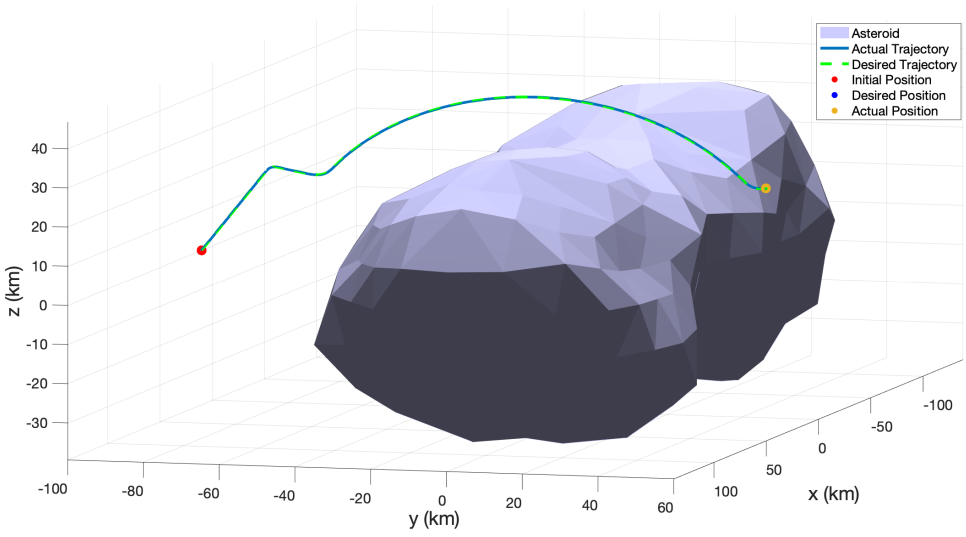


*Figure 6.24* Trajectory of spacecraft around asteroid Kleopatra for DAMPC case.

previous chapter. The actual and desired trajectories can be seen in Figure 6.24. It can be seen that the DAMPC is able to track the trajectories successfully.

However, the tracking performance of DAMPC is better as compared to the adaptive control which is shown in Figure 6.25 (d). The control of DAMPC is also better in terms of overshoot and chatter and can be seen in Figure 6.25 (c). The position and velocities and can be seen in Figure 6.25 (a) and (b).

#### 6.3.3.4. Case 4: Effects of Unknown Noise

In this section we discuss the effects of system noise on the DAMPC and compare it with the case adaptive control only. It was found that DAMPC offers a better tracking performance in the presence of noise and a reduced chatter in the control effort as compared to the adaptive control only. A random Gaussian noise of $(1 \times 10^{-4}\mathcal{N}(0,\, I_{3\times 3})$ is added to the system. The magnitude of the error is taken to be one order higher than the gravity to further test the robustness of the control system to unknown noise.

Figure 6.26 shows the plots for the case where only adaptive controller is implemented with noise and Figure 6.27 shows the plots for where DAMPC is implemented. It can be seen from the figures that the DAMPC is able to handle the noise better than adaptive control in terms of the output error and control effort. Figure 6.26 (e) and Figure 6.27 (e) shows the magnified control efforts and it can be seen that the DAMPC's control effort less in magnitude and chatter as compared to the adaptive control.

Minimum and maximum errors for each asteroid for all three cases are given in Table 6.4, Table 6.5 and Table 6.6. It can be seen that the minimum error is the lowest for DAMPC for asteroids and the maximum error is also the lowest for DAMPC for all the

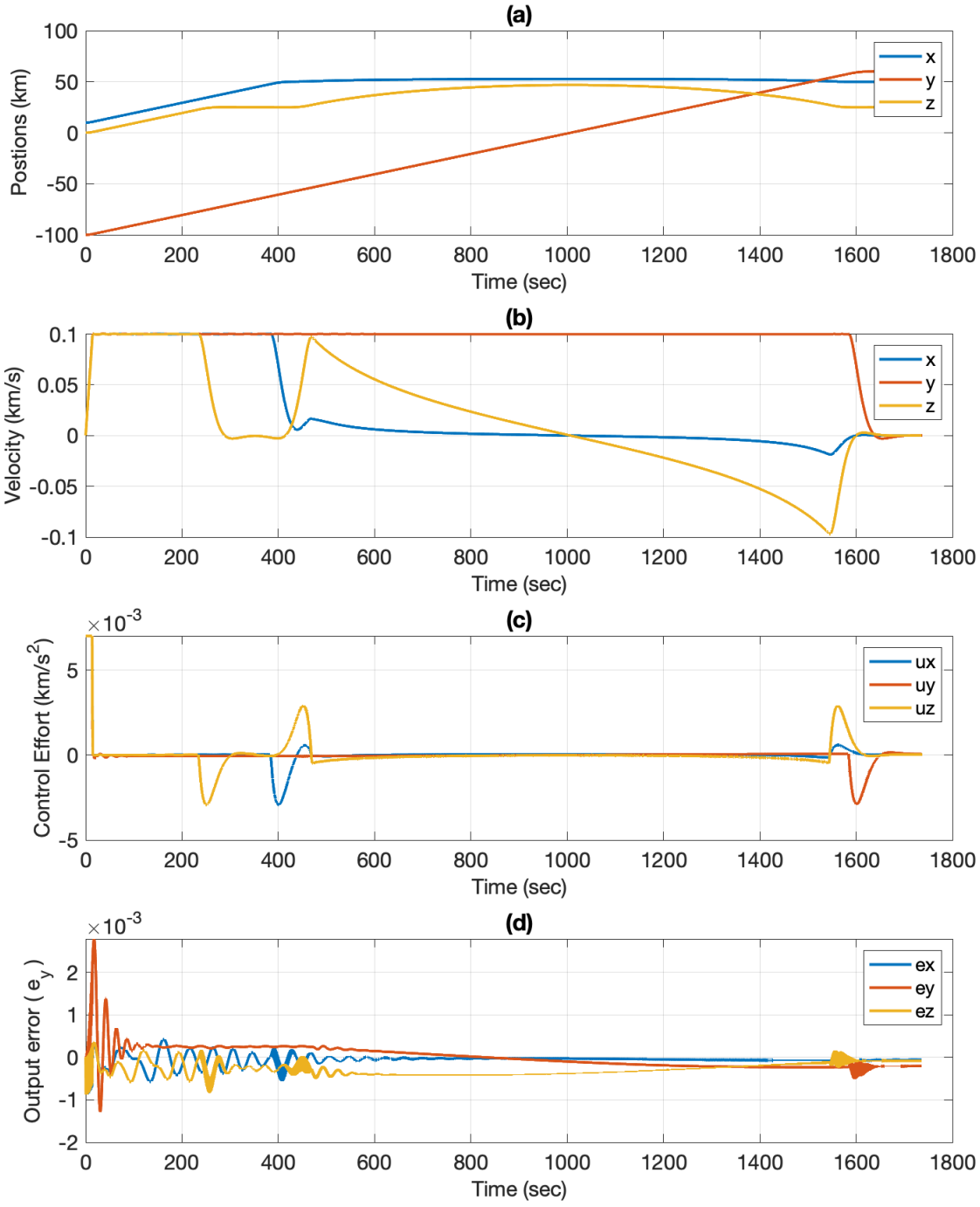


*Figure 6.25* Plots for DAMPC case for asteroid Kleopatra, (a) position vs. time, (b) velocity vs. time, (c) control effort vs. time, (d) output error vs. time.

asteroids. This shows that DAMPC outperforms adaptive control and MPC-feedforward control for all the cases.

It can be noted that the perforamance of MPC is also dependent on the type of numerical solver used and its various parameters. In this work, CASADI (Andersson et al., 2019) is used as a solver. However, several other types of solvers and methodologies can be implemented and more research needs to be in order to conclude the best case solver. It can also be noted that the DAMPC is also agnostic to type of optimal control technique applied. Therefore, for a linear system, a linear quadratic regular (LQR) or linear quadratic tracker can be also implemented.

Table 6.4

Output error for asteroid Eros

| Errors | MPC Only (km) | Adaptive (km) | DAMPC (km) |
|---|---|---|---|
| Min $e_x$ | 0 | -8.92e-4 | -3e-4 |
| Min $e_y$ | 0 | -0.0070 | -5.25e-4 |
| Min $e_z$ | -0.3367 | -0.0075 | -6.9e-4 |
| Max $e_x$ | 0.0104 | 7.5185e-4 | 2.32e-4 |
| Max $e_y$ | 0.0574 | 0.0028 | 7.16e-4 |
| Max $e_z$ | 0 | 0.007 | 4.19e-4 |

Table 6.5

Output error for asteroid Bennu

| Errors | MPC Only (km) | Adaptive (km) | DAMPC (km) |
|---|---|---|---|
| Min $e_x$ | -0.0014 | -0.0033 | -5.9e-5 |
| Min $e_y$ | -0.0011 | -0.01 | -3.25e-4 |
| Min $e_z$ | -0.0029 | -0.02 | -6e-5 |
| Max $e_x$ | 1e-5 | 0.03 | 2.32e-5 |
| Max $e_y$ | 2e-4 | 0.01 | 7.16e-5 |
| Max $e_z$ | 4.149 | 0 | 1.19e-5 |

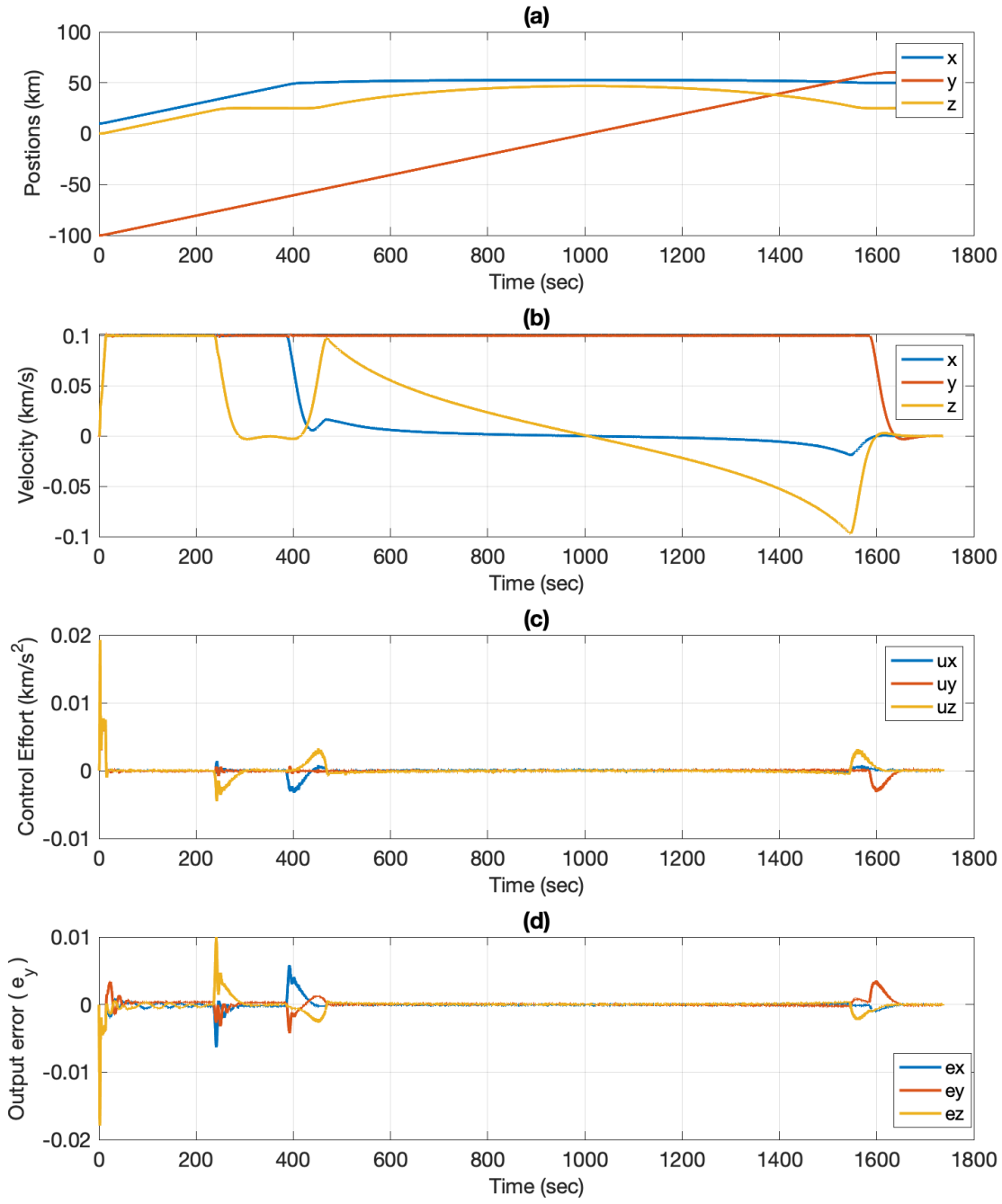


*Figure 6.26* Plots for adaptive control case with noise for asteroid Kleopatra, (a) position vs. time, (b) velocity vs. time, (c) control effort vs. time, (d) output error vs. time.

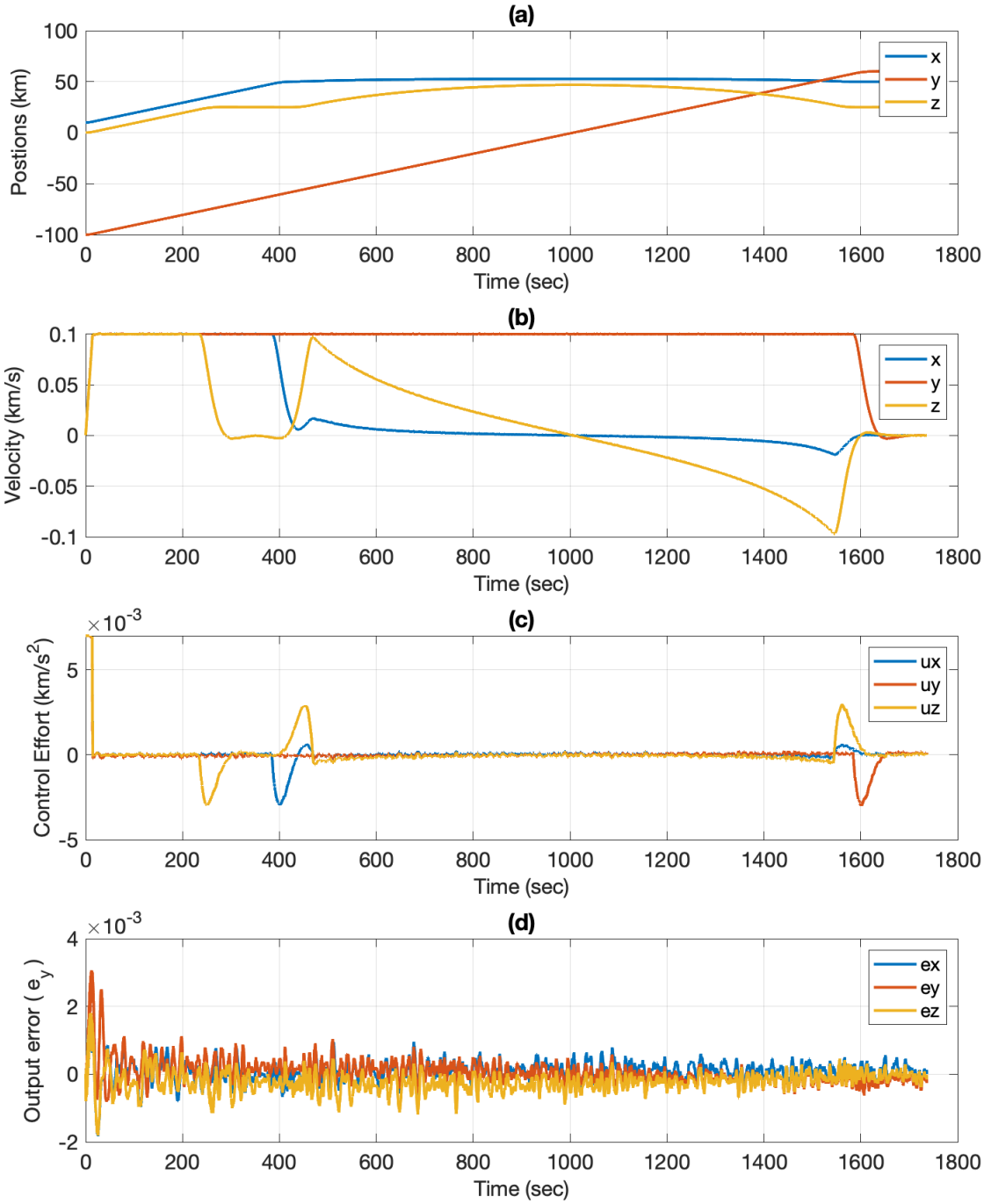


*Figure 6.27* Plots for DAMPC case with noise for asteroid Kleopatra, (a) position vs. time, (b) velocity vs. time, (c) control effort vs. time, (d) output error vs. time.

Table 6.6

Output error for asteroid Kleopatra

| Errors | MPC Only (km) | Adaptive (km) | DAMPC (km) |
|---|---|---|---|
| Min $e_x$ | -0.0132 | -0.0033 | -8e-4 |
| Min $e_y$ | -0.0132 | -0.01 | -0.0013 |
| Min $e_z$ | -0.0132 | -0.02 | -8e-5 |
| Max $e_x$ | 0 | 0.0058 | 4.2e-4 |
| Max $e_y$ | 16 | 0.0035 | 0.001 |
| Max $e_z$ | 0 | 0.0081 | 4e-4 |

# 7. Conclusions and Future Works

This work focused on developing and implementing adaptive control and model predictive control methodologies for spacecraft missions in the proximity of asteroids. Asteroid and spacecraft dynamical parameters were assumed to be unknown, and it was shown that the adaptive control could track user-given trajectories successfully. The work was divided into four main parts:

1. Spacecraft dynamics near the asteroid.
2. Adaptive control of the spacecraft near asteroid without system knowledge.
3. Nonlinear model predictive control formulation for sub-optimal trajectory generation.
4. Development of direct adaptive-model predictive control methodology.

The spacecraft dynamics near the vicinity of the asteroid were developed using a polyhedral gravity model and coupled orbit-attitude dynamics, which included forces from solar radiation pressure and gravity gradient.

The dynamical model was used to test the performance and robustness of the adaptive control system. A direct adaptive control based on simple adaptive control was developed and implemented. A robust control $e$ modification was developed to enhance further the adaptive control's ability to handle system and sensor noise. The adaptive control was tested numerically on three different asteroids with the varying gravitational field.

The adaptive control weighting matrices were kept constant for three cases to test the robustness of the adaptive control. The adaptive control was able to track user-given trajectories for orbital and hovering cases successfully. The controller was further tested

for robustness by adding random Gaussian noise and sinusoidal noise on the system and sensor. It was shown that the adaptive control was able to handle the unknown noise successfully. The $e$ modification was compared with the more popular $\mu$ modification, and it was shown that the $e$ modification performs superior to the $\mu$ modification.

A nonlinear model predictive control methodology was developed to add further autonomy to the control system. The NMPC was developed using multiple shooting. It was shown that the NMPC was able to successfully generate sub-optimal trajectories for the given initial and final state while successfully avoiding obstacles. An ellipsoidal constraint was implemented as a nonlinear constraint. The NMPC was also tested on three different asteroids.

Lastly, the nonlinear model predictive control was paired with direct adaptive control as a feed-forward control to add optimality and reduce overshooting resulting from the adaptive control. It was shown that the new control method named direct-adaptive model predictive control (DAMPC) was able to successfully track trajectories and significantly reduce the overshooting of the adaptive control. The DAMPC methodology was also tested with system noise, and it was shown that the DAMPC is able to better handle system noise compared to adaptive control, the only system. The DAMPC was also implemented on three different asteroids. Overall, this work showed the successful design and application of adaptive control and model predictive control to track trajectories in the vicinity of asteroids.

In the future, this work can be further improved in the following ways:

- Improve the adaptive control by adding self-tuning weighting matrices to increase the autonomy further.

- Further test the adaptive control with modeling and sensor noise.
- Modify the adaptive control to work input constraint.
- Enhance the capability of the control system to work in thrust failure scenarios. Which is a common problem for spacecrafts.
- Rigorously develop a stability proof for the DAMPC system.
- Add moving horizon estimator and test the performance of the control in various conditions.
- Experimentally test the viability of the DAMPC system.
- Numerically develop and test DAMPC system without other forms of MPC.
- Test the ability of DAMPC to handle thrust failure.
- Further develop the ability to handle moving obstacles in real-time.

# REFERENCES

AlandiHallaj, M., & Assadian, N. (2017). Soft landing on an irregular shape asteroid using Multiple-Horizon Multiple-Model predictive control. *Acta Astronaut.*, *140*, 225–234.

Andersson, J. A. E., Gillis, J., Horn, G., Rawlings, J. B., & Diehl, M. (2019). CasADi – A software framework for nonlinear optimization and optimal control. *Mathematical Programming Computation*, *11*(1), 1–36.

Barkana, I. (2010). Output feedback stabilizability and passivity in nonstationary and nonlinear systems. *Int. J. Adapt Control Signal Process.*

Barkana, I. (2016). Robustness and perfect tracking in simple adaptive control: Robustness and perfect tracking. *Int. J. Adapt Control Signal Process.*, *30*(8-10), 1118–1151.

Bolatti, D. A., & de Ruiter, A. H. (2016). Modeling spacecraft Orbit-Attitude coupled dynamics in close proximity to asteroids. *AIAA/AAS astrodynamics specialist conference*. American Institute of Aeronautics; Astronautics. Long Beach. 13-16 September.

Bolatti, D. A., & de Ruiter, A. H. J. (2020). Quantification of attitude effects on orbital dynamics near asteroids. *Acta Astronaut.*, *167*, 467–482.

Broschart, S. B., & Scheeres, D. J. (2005). Control of hovering spacecraft near small bodies: Application to asteroid 25143 itokawa. *J. Guid. Control Dyn.*, *28*(2), 343–354.

Grimm, G., Messina, M. J., Tuna, S. E., & Teel, A. R. (2004). Examples when nonlinear model predictive control is nonrobust. *Automatica*, *40*(10), 1729–1738.

Grüne, L., Pannek, J., Seehafer, M., & Worthmann, K. (2010). Analysis of unconstrained nonlinear MPC schemes with time varying control horizon.

Guelman, M. (2014). Closed-Loop control of close orbits around asteroids. *J. Guid. Control Dyn.*, *38*(5), 854–860.

Ioannou, P. A., & Kokotovic, P. V. (1984). Instability analysis and improvement of robustness of adaptive control. *Automatica*, *20*(5), 583–594.

Ioannou, P. A., & Kokotovic, P. V. (Eds.). (1983). *Adaptive systems with reduced models*. Springer, Berlin, Heidelberg.

Kaufman, H., Barkana, I., & Sobel, K. (1997a). *Direct adaptive control algorithms: Theory and applications*. Springer Science & Business Media.

Kaufman, H., Barkana, I., & Sobel, K. (1997b). Direct adaptive control algorithms: Theory and applications. Springer Science & Business Media.

Kikuchi, S., Howell, K. C., Tsuda, Y., & Kawaguchi, J. (2017). Orbit-attitude coupled motion around small bodies: Sun-synchronous orbits with sun-tracking attitude motion. *Acta Astronautica*.

Kumar, K. D., & Shah, M. (2007). Attitude dynamics and control of satellites orbiting rotating asteroids. *Canadian Conference on Electrical and Computer Engineering*, 1388–1391. Vancouver. 22-26 April.

LaSalle, J. P. (1976). Stability of nonautonomous systems. *Nonlinear Anal. Theory Methods Appl.*, *1*(1), 83–90.

Lee, D., Sanyal, A. K., Butcher, E. A., & Scheeres, D. J. (2015). Finite-time control for spacecraft body-fixed hovering over an asteroid. *IEEE Trans. Aerosp. Electron. Syst.*, *51*(1), 506–520.

Lee, D., & Vukovich, G. (2016). Adaptive finite-time control for spacecraft hovering over an asteroid. *IEEE Trans. Aerosp. Electron. Syst.*, *52*(3), 1183–1196.

Lee, D., & Vukovich, G. (2015). Adaptive sliding mode control for spacecraft body-fixed hovering in the proximity of an asteroid. *Aerosp. Sci. Technol.*, *46*, 471–483.

Lee, K., Moase, W. H., & Manzie, C. (2018). Mesh adaptation in direct collocated nonlinear model predictive control: Mesh adaptation in direct collocated nonlinear model predictive control. *Int. J. Robust Nonlinear Control*, *28*(15), 4624–4634.

Lee, K. W., & Singh, S. N. (2019). Noncertainty-equivalence adaptive attitude control of satellite orbiting around an asteroid. *Acta Astronaut.*, *161*, 24–39.

Li, X., Qiao, D., & Li, P. (2018). Bounded trajectory design and self-adaptive maintenance control near non-synchronized binary systems comprised of small irregular bodies. *Acta Astronaut.*, *152*, 768–781.

Li, X., Warier, R. R., Sanyal, A. K., & Qiao, D. (2019). Trajectory tracking near small bodies using only attitude control. *J. Guid. Control Dyn.*, *42*(1), 109–122.

Liao-McPherson, D., Dunham, W. D., & Kolmanovsky, I. (2016). Model predictive control strategies for constrained soft landing on an asteroid. *AIAA/AAS astrodynamics specialist conference*. American Institute of Aeronautics; Astronautics. Long Beach. 13-16 September.

Liu, K., Liu, F., Wang, S., & Li, Y. (2015). Finite-Time spacecraft's soft landing on asteroids using PD and nonsingular terminal sliding mode control. *Math. Probl. Eng.*, *2015*, 1–10.

Lu, E. T., & Love, S. G. (2005). Gravitational tractor for towing asteroids. *Nature*, *438*(7065), 177–178.

Mehrez Said, M. W. (2018). Optimization based solutions for control and state estimation in non-holonomic mobile robots: Stability, distributed control, and relative localization. Retrieved from: Http://arxiv.org/abs/1803.06928.

Misra, G., Izadi, M., Sanyal, A., & Scheeres, D. (2016). Coupled orbit–attitude dynamics and relative state estimation of spacecraft near small solar system bodies. *Adv. Space Res.*, *57*(8), 1747–1761.

Narendra, K., & Annaswamy, A. (1987). A new adaptive law for robust adaptation without persistent excitation. *IEEE Trans. Automat. Contr.*, *32*(2), 134–145.

NASA. (2020). PDS: Small bodies node home. Retrieved from: Https://pds-smallbodies.astro.umd.edu/.

Nazari, M., Wauson, R., Critz, T., Butcher, E., & Scheeres, D. J. (2014). Observer-based body-frame hovering control over a tumbling asteroid. *Acta Astronaut.*, *102*, 124–139.

Oguri, K., & McMahon, J. W. (2020). Solar radiation Pressure–Based orbit control with application to Small-Body landing. *J. Guid. Control Dyn.*, *43*(2), 195–211.

Ono, G., Terui, F., Ogawa, N., Kikuchi, S., Mimasu, Y., Yoshikawa, K., Ikeda, H., Takei, Y., Yasuda, S., Matsushima, K., Masuda, T., Saiki, T., & Tsuda, Y. (2020). GNC strategies and flight results of hayabusa2 first touchdown operation. *Acta Astronaut.*, *174*, 131–147.

Ostafew, C. J., Schoellig, A. P., Barfoot, T. D., & Collier, J. (2016). Learning-based nonlinear model predictive control to improve vision-based mobile robot path tracking: Learning-based nonlinear model predictive control to improve vision-based mobile robot path tracking. *J. field robot.*, *33*(1), 133–152.

Prabhakar, N., Painter, A., Prazenica, R., & Balas, M. (2018). Trajectory-Driven adaptive control of autonomous unmanned aerial vehicles with disturbance accommodation. *J. Guid. Control Dyn.*, *41*(9), 1976–1989.

Reyhanoglu, M., Kamran, N. N., & Takahiro, K. (2012). Orbital and attitude control of a spacecraft around an asteroid. *2012 12th International Conference on Control, Automation and Systems*, 1627–1632.

Reynolds, T., & Mesbahi, M. (2017). Small body precision landing via convex model predictive control. *AIAA SPACE and astronautics forum and exposition*. Orlando. 12-17 September.

Rybus, T., Seweryn, K., & Sasiadek, J. Z. (2017). Control system for Free-Floating space manipulator based on nonlinear model predictive control (NMPC). *J. Intell. Rob. Syst.*, *85*(3), 491–509.

Sanyal, A. K., Bloch, A., & McClamroch, N. H. (2004). Dynamics of multibody systems in planar motion in a central gravitational field. *Dyn. Syst. Appl.*, *19*(4), 303–343.

Schaub, H., & Junkins, J. L. (2018). *Analytical mechanics of space systems, fourth edition*. American Institute of Aeronautics; Astronautics, Inc.

Scheeres, D. (2006). Spacecraft at small NEO. Retrieved from: http://arxiv.org/abs/physics/0608158

Scheeres, D., & Schweickart, R. (2004). The mechanics of moving asteroids. *2004 planetary defense conference: Protecting earth from asteroids*. American Institute of Aeronautics; Astronautics.

Schlipf, D., Schlipf, D. J., & Kühn, M. (2013). Nonlinear model predictive control of wind turbines using LIDAR: Nonlinear model predictive control of wind turbines using LIDAR. *Wind Energy*, *16*(7), 1107–1129.

Shea, G. (2018). Beyond earth: A chronicle of deep space exploration. Retrieved from: http://www.nasa.gov/connect/ebooks/beyond_earth_detail.html

Shi, J.-F., Ulrich, S., & Allen, A. (n.d.). Spacecraft adaptive attitude control with application to space station Free-Flyer robotic capture. *AIAA 2015 scitech forum* (pp. 1–23). Orlando. 23 January.

Silva, T. M., Bouvier, J.-B., Xu, K., Hirabayashi, M., & Ho, K. (2020). Spacecraft trajectory tracking and parameter estimation around a splitting contact binary asteroid. *Acta Astronaut.*, *171*, 280–289.

Sincarsin, G., & Hughes, P. (1982). Gravitational orbit-attitude coupling for very large spacecraft. *AIAA astrodynamics conference*. San Diego. 9-11 August.

Stackhouse, W. T., Nazari, M., Henderson, T. et al. (2020). Adaptive control design using the Udwadia-Kalaba formulation for hovering over an asteroid with unknown gravitational parameters. *AIAA Scitech 2020 forum.* Orlando. 6-7 January.

Starek, J. A., & Kolmanovsky, I. V. (2014). Nonlinear model predictive control strategy for low thrust spacecraft missions: Low thrust nonlinear mpc strategy. *Optim. Control Appl. Methods*, *35*(1), 1–20.

Tiwari, M., Henderson, T., & Prazenica, R. J. (2020). Spacecraft body frame hovering over an asteroid using a direct apdative control strategy. *2020 AAS/AIAA astrodynamics specialist virtual lake tahoe conference.* Virtual. 7-13 August.

Tiwari, M., Prazenica, R. J., & Henderson, T. (2020). Tracking reference orbits around asteroids with unknown gravitational parameters using a nonlinear adaptive controller. *AIAA scitech 2020 forum*. Orlando. 6-11 January.

Tsuda, Y., Yoshikawa, M., Abe, M., Minamino, H., & Nakazawa, S. (2013). System design of the hayabusa 2—asteroid sample return mission to 1999 JU3. *Acta Astronaut.*, *91*, 356–362.

Tuna, S. E., Messina, M. J., & Teel, A. R. (2006). Shorter horizons for model predictive control. *2006 american control conference.* Minneapolis. 14-16 January.

Ulrich, S., & de Lafontaine, J. (2007). Autonomous atmospheric entry on mars: Performance improvement using a novel adaptive control algorithm. *The Journal of the Astronautical Sciences*, *55*(4), 431–449.

Ulrich, S., Saenz-Otero, A., & Barkana, I. (2016a). Passivity-Based adaptive control of robotic spacecraft for proximity operations under uncertainties. *J. Guid. Control Dyn.*, *39*(6), 1444–1453.

Ulrich, S., Saenz-Otero, A., & Barkana, I. (2016b). Passivity-Based adaptive control of robotic spacecraft for proximity operations under uncertainties. *J. Guid. Control Dyn.*, *39*(6), 1444–1453.

Ulrich, S., Sasiadek, J. Z., & Barkana, I. (2012). Modeling and direct adaptive control of a flexible- joint manipulator. *J. Guid. Control Dyn.*, *35*(1), 25–39.

Wang, L.-S., Krishnaprasad, P. S., & Maddocks, J. H. (1990). Hamiltonian dynamics of a rigid body in a central gravitational field. *Celest. Mech. Dyn. Astron.*, *50*(4), 349–386.

Wang, Y., Zhong, R., & Xu, S. (2018). Orbital perturbation due to orbit-attitude coupling near asteroids. *Aircraft Engineering and Aerospace Technology; Bradford*, *90*(1), 104–113.

Wang Yue, & Xu Shijie. (2014). Gravitational Orbit-Rotation coupling of a rigid satellite around a spheroid planet. *J. Aerosp. Eng.*, *27*(1), 140–150.

Werner, R. A., & Scheeres, D. J. (1996). Exterior gravitation of a polyhedron derived and compared with harmonic and mascon gravitation representations of asteroid 4769 castalia. *Celest. Mech. Dyn. Astron.*, *65*(3), 313–344.

Wong, H., de Queiroz, M. S., & Kapila, V. (2001). Adaptive tracking control using synthesized velocity from attitude measurements. *Automatica*, *37*(6), 947–953.

Worthmann, K. (2011). Stability analysis of unconstrained receding horizon control schemes. Retrieved from: https://epub.uni-bayreuth.de/273/

Yang, H., & Baoyin, H. (2015). Fuel-optimal control for soft landing on an irregular asteroid. *IEEE Trans. Aerosp. Electron. Syst.*, *51*(3), 1688–1697.

## PUBLICATIONS

Tiwari, M., Prazenica, R. J., and Henderson, T. (2021). A Novel Direct Adaptive-Model Predictive Control Technique with Application to Spacecraft Trajectory Tracking. *Journal of Guidance, Dynamics, and Control*.

Tiwari, M., Prazenica, R. J., and Henderson, T. (2021). Spacecraft Direct Adaptive Control in Asteroid Vicinity with Coupled Orbit-Attitude Dynamics. *Journal of Guidance, Dynamics, and Control.*

Zuehlke D., Tiwari, M., and Henderson, T. (2020). Autonomous Satellite Detection and Tracking using Optical Flow. *AIAA/AAS Astrodynamics 2020 Virtual Specialist Forum*. Virtual Conference. 9-12 August.

Tiwari, M., Prazenica, R. J., and Henderson, T. (2020). Autonomous Spacecraft Obstacle Avoidance and Trajectory Tracking in a Dense Debris Field. *AIAA/AAS Astrodynamics Specialist 2020 Virtual Forum*. Virtual Conference. 9-12 August.

Tiwari, M., Prazenica, R. J., and Henderson, T. (2020). Spacecraft body frame hovering over an asteroid using a direct adaptive control strategy. *AAS/AIAA Astrodynamics Specialist Virtual Lake Tahoe Conference*. Virtual Conference. 9-12 August.

Jacob J. K, Daniel Posada, Francisco J. Franquiz, Madhur Tiwari, and Troy Henderson. (2020). Modeling of An On-Orbit Maintenance Robotic Arm Test-Bed. *AAS/AIAA Scitech Forum 2020*. Orlando. 3-7 January.

Tiwari, M., Prazenica, R. J., and Henderson, T. (2020). Tracking Reference Orbits Around Asteroids with Unknown Gravitational Parameters Using a Nonlinear Adaptive Controller. *AIAA Scitech 2020 Forum*. Orlando. 3-7 January.

Tiwari, M., Zuehlke, D., and Henderson, T. (2019). Identifying Spacecraft Configuration Using Deep Neural Networks for Precise Orbit Estimation. *AAS/AIAA Spaceflight Mechanics Meeting, Ka', 2019*. Hawaii. 7-11 January.

Prabhakar, N., Tiwari, M., Henderson, T., and Prazenica, R. J. (2019). Application of Direct Adaptive Control to Autonomous Satellite Docking. *AIAA Scitech 2019 Forum, American Institute of Aeronautics and Astronautics.* San Diego. 7-11 January.

Vergara, P., Tiwari, M., Prazenica, R. J., and Henderson, T. (2019). Multiresolution-Based 3-D Terrain Estimation Algorithms for Complex Urban Environments. *AIAA Scitech 2019 Forum, American Institute of Aeronautics and Astronautics.* San Diego. 7-11 January.

Henderson and Tiwari. (2017). 3D Reconstruction, Representation, and Registration of Satellite Imagery for Improved Space Situational Awareness. *1st IAA Conference on Space Situational Awareness*. Orlando. 1-2 November.

## APPENDIX A - Adaptive Control Stability

Given the error dynamics equation below:

$$\mathbf{e}_x(t) = \mathbf{x}^*(t) - \mathbf{x}(t) \tag{1}$$

Substituting (4.1) and (4.29),

$$\dot{\mathbf{e}}_x(t) = \mathbf{A}^*\mathbf{x}^*(t) + \mathbf{B}^*\mathbf{u}^*(t) - \mathbf{A}\mathbf{x}(t) - \mathbf{B}\mathbf{u}(t) \tag{2}$$

Adding and subtracting $\mathbf{A}\mathbf{x}^*(t)$ in (2)

$$\dot{\mathbf{e}}_x(t) = \mathbf{A}^*\mathbf{x}^*(t) + \mathbf{B}^*\mathbf{u}^*(t) - \mathbf{A}\mathbf{x}(t) - \mathbf{B}\mathbf{u}(t) - \mathbf{A}\mathbf{x}^*(t) + \mathbf{A}\mathbf{x}^*(t) \tag{3}$$

Substituting the ideal system equation (4.31), ideal system control law (4.32), adding and subtracting $\mathbf{B}\tilde{\mathbf{K}}_{e_y}\mathbf{e}_y(t)$, $\mathbf{B}\tilde{\mathbf{K}}_{x_m}\mathbf{x}_m(t)$ and $\mathbf{B}\tilde{\mathbf{K}}_{u_m}\mathbf{u}_m(t)$, and substituting the compact adaptive control law from (4.11) in above equation (3),

$$\begin{aligned}\dot{\mathbf{e}}_x(t) = {} & \mathbf{A}(\mathbf{x}^*(t) - \mathbf{x}(t)) - \mathbf{A}(\mathbf{X}\mathbf{x}_m + \mathbf{U}\mathbf{u}_m) + \mathbf{A}^*(\mathbf{X}\mathbf{x}_m + \mathbf{U}\mathbf{u}_m) \\ & - \mathbf{B}\mathbf{K}(t)\mathbf{r}(t) + \mathbf{B}\tilde{\mathbf{K}}_{e_y}\mathbf{e}_y(t) + \mathbf{B}\tilde{\mathbf{K}}_{x_m} + \mathbf{B}\tilde{\mathbf{K}}_{u_m}\mathbf{u}_m(t) \\ & - \mathbf{B}\tilde{\mathbf{K}}_{e_y}\mathbf{e}_y(t) - \mathbf{B}\tilde{\mathbf{K}}_{x_m}\mathbf{x}_m(t) - \mathbf{B}\tilde{\mathbf{K}}_{u_m}\mathbf{u}_m(t) \\ & + \mathbf{B}^*(\tilde{\mathbf{K}}_{x_m}\mathbf{x}_m + \tilde{\mathbf{K}}_{u_m}\mathbf{u}_m)\end{aligned} \tag{4}$$

Combining terms and substituting system error equation $\mathbf{e}_x$ from (4.35) in (4)

$$\begin{aligned}\dot{\mathbf{e}}_x(t) = {} & \mathbf{A}\mathbf{e}_x - \mathbf{B}\tilde{\mathbf{K}}_{e_y}\mathbf{e}_y(t) - \mathbf{B}[\mathbf{K}(t) - \tilde{\mathbf{K}}]\mathbf{r}(t) + [(\mathbf{A}^* - \mathbf{A})\mathbf{X} \\ & + (\mathbf{B}^* - \mathbf{B})\tilde{\mathbf{K}}_{x_m}]\mathbf{x}_m(t) + [(\mathbf{A}^* - \mathbf{A})\mathbf{U} \\ & + (\mathbf{B}^* - \mathbf{B})\tilde{\mathbf{K}}_{u_m}]\mathbf{u}_m(t)\end{aligned} \tag{5}$$

Here,

$$\tilde{\mathbf{K}} = [\tilde{\mathbf{K}}_{e_y} \;\; \tilde{\mathbf{K}}_{x_m} \;\; \tilde{\mathbf{K}}_{u_m}] \tag{6}$$

Generally, system parameters vary slowly, therefore,

$$\mathbf{A}^* = \mathbf{A} \tag{7}$$

$$\mathbf{B}^* = \mathbf{B} \tag{8}$$

Substituting the the above equations. The final form of error dynamics is given as,

$$\dot{\mathbf{e}}_x(t) = \mathbf{A}\mathbf{e}_x(t) - \mathbf{B}\tilde{\mathbf{K}}_{e_y}\mathbf{e}_y(t) - \mathbf{B}[\mathbf{K}(t) - \tilde{\mathbf{K}}]\mathbf{r}(t) \tag{9}$$

$$\dot{\mathbf{e}}_x^T(t) = \mathbf{e}_x^T(t)\mathbf{A}^T - \mathbf{e}_y^T(t)\tilde{\mathbf{K}}_{e_y}^T\mathbf{B}^T - \mathbf{r}^T(t)[\mathbf{K}(t) - \tilde{\mathbf{K}}]^T\mathbf{B}^T \tag{10}$$

Rewriting the Lyapunov function from (4.16),

$$V(t) = \mathbf{e}_x^T\mathbf{P}\mathbf{e}_x + tr[\mathbf{K}_I - \tilde{\mathbf{K}}]\mathbf{\Gamma}^{-1}[\mathbf{K}_I - \tilde{\mathbf{K}}]^T \tag{11}$$

Differentiating $V(t)$,

$$\dot{V}(t) = \dot{\mathbf{e}}_x^T\mathbf{P}\mathbf{e}_x + \mathbf{e}_x^T\dot{\mathbf{P}}\mathbf{e}_x + \mathbf{e}_x^T\mathbf{P}\dot{\mathbf{e}}_x + tr[\dot{\mathbf{K}}_I\mathbf{\Gamma}^{-1}(\mathbf{K}_I - \tilde{\mathbf{K}})^T] + tr[(\mathbf{K}_I - \tilde{\mathbf{K}})\Gamma^{-1}\dot{\mathbf{K}}_I^T] \tag{12}$$

$\dot{\mathbf{K}}_I$ can be written as follows

$$\dot{\mathbf{K}}_I = [\dot{\mathbf{K}}_{Ie} \;\; \dot{\mathbf{K}}_{Ix} \;\; \dot{\mathbf{K}}_{Iu}] \tag{13}$$

Substituting the for each adaptive law

$$\dot{\mathbf{K}}_I = [\mathbf{e}_y(t)\mathbf{e}_y(t)^T\mathbf{\Gamma}_e - \mu\|\mathbf{e}_y(t)\|\mathbf{K}_{Ie}, \quad \mathbf{e}_y(t)\mathbf{x}_m(t)^T\mathbf{\Gamma}_x, \quad \mathbf{e}_y(t)\mathbf{u}_m(t)^T\mathbf{\Gamma}_u] \tag{14}$$

$$\dot{\mathbf{K}}_I = \mathbf{e}_y(t)\mathbf{r}(t)^T\mathbf{\Gamma} - [\mu\|\mathbf{e}_y(t)\|\mathbf{K}_{Ie}, \quad \mathbf{0}, \quad \mathbf{0}] \tag{15}$$

Substituting $\dot{\mathbf{e}}_x$ from (9) and $\dot{\mathbf{K}}_I$ from Equation (15) in Equation (12)

$$\begin{aligned}\dot{V}(t) = {} & [\mathbf{e}_x^T\mathbf{A}^T - \mathbf{e}_y^T\tilde{\mathbf{K}}_{e_y}^T\mathbf{B}^T - [\mathbf{B}(\mathbf{K} - \tilde{\mathbf{K}})\mathbf{r}(t)]^T]\mathbf{P}\mathbf{e}_x + \mathbf{e}_x^T\dot{\mathbf{P}}\mathbf{e}_x \\ & + \mathbf{e}_x^T\mathbf{P}[\mathbf{A}\mathbf{e}_x - \mathbf{B}\tilde{\mathbf{K}}_{e_y}\mathbf{e}_y - \mathbf{B}[\mathbf{K}(t) - \tilde{\mathbf{K}}]\mathbf{r}(t)] && (16) \\ & + tr[(\mathbf{e}_y\mathbf{r}^T\mathbf{\Gamma} - [\mu\|\mathbf{e}_y\|\mathbf{K}_{Ie}, \quad \mathbf{0}, \quad \mathbf{0}])\mathbf{\Gamma}^{-1}(\mathbf{K}_I - \tilde{\mathbf{K}})^T] && (17) \\ & + tr[(\mathbf{K}_I - \tilde{\mathbf{K}})\mathbf{\Gamma}^{-1}(\mathbf{e}_y(t)\mathbf{r}(t)^T\mathbf{\Gamma} - [\mu\|\mathbf{e}_y(t)\|\mathbf{K}_{Ie}, \quad \mathbf{0}, \quad \mathbf{0}])] && (18)\end{aligned}$$

Simplifying and rearranging terms

$$\begin{aligned}\dot{V}(t) = {} & \mathbf{e}_x^T[\dot{\mathbf{P}} + \mathbf{P}(\mathbf{A} - \mathbf{B}\tilde{\mathbf{K}}_{ey}\mathbf{C}) + (\mathbf{A} - \mathbf{B}\tilde{\mathbf{K}}_{ey}\mathbf{C})^T\mathbf{P}]\mathbf{e}_x \\ & - \mathbf{r}^T(t)[\mathbf{K}(t) - \tilde{\mathbf{K}}]^T\mathbf{B}^T\mathbf{P}\mathbf{e}_x - \mathbf{e}_x^T\mathbf{P}\mathbf{B}[\mathbf{K}(t) - \tilde{\mathbf{K}}]\mathbf{r}(t) \\ & + tr[\mathbf{e}_y\mathbf{r}^T(\mathbf{K}_I - \tilde{\mathbf{K}})^T] && (19) \\ & + tr[(\mathbf{K}_I - \tilde{\mathbf{K}})\mathbf{r}\mathbf{e}_y^T] && (20) \\ & - tr[[\mu\|\mathbf{e}_y(t)\|\mathbf{K}_{Ie}, \quad \mathbf{0}, \quad \mathbf{0}]\mathbf{\Gamma}^{-1}(\mathbf{K}_I - \tilde{\mathbf{K}})^T] && (21) \\ & - tr[(\mathbf{K} - \tilde{\mathbf{K}})\mathbf{\Gamma}^{-1}[\mu\|\mathbf{e}_y(t)\|\mathbf{K}_{Ie}, \quad \mathbf{0}, \quad \mathbf{0}]^T] && (22)\end{aligned}$$

Using trace property $tr(\mathbf{b}(\mathbf{a}_1\mathbf{a}_2)^T) = \mathbf{a}_2^T\mathbf{a}_1^T\mathbf{b}$ and substituting $\mathbf{K}_I(t) = \mathbf{K}(t) - \mathbf{K}_p(t) = \mathbf{K}(t) - \mathbf{e}_y(t)\mathbf{r}^T(t)\bar{\mathbf{\Gamma}}$,

$$\dot{V}(t) = \mathbf{e}_x^T[\dot{\mathbf{P}} + \mathbf{P}(\mathbf{A} - \mathbf{B}\tilde{\mathbf{K}}_{ey}\mathbf{C}) + (\mathbf{A} - \mathbf{B}\tilde{\mathbf{K}}_{ey}\mathbf{C})^T\mathbf{P}]\mathbf{e}_x$$

$$- \mathbf{r}^T(t)[\mathbf{K}(t) - \tilde{\mathbf{K}}]^T\mathbf{B}^T\mathbf{P}\mathbf{e}_x - \mathbf{e}_x^T\mathbf{P}\mathbf{B}[\mathbf{K}(t) - \tilde{\mathbf{K}}]\mathbf{r}(t)$$

$$+ \mathbf{r}^T(\mathbf{K}(t) - \mathbf{e}_y(t)\mathbf{r}^T(t)\bar{\mathbf{\Gamma}} - \tilde{\mathbf{K}})^T\mathbf{e}_y \tag{23}$$

$$+ \mathbf{e}_y^T(\mathbf{K}(t) - \mathbf{e}_y(t)\mathbf{r}^T(t)\bar{\mathbf{\Gamma}} - \tilde{\mathbf{K}})\mathbf{r} \tag{24}$$

$$- tr[[\mu\|\mathbf{e}_y(t)\|\mathbf{K}_{Ie}, \quad \mathbf{0}, \quad \mathbf{0}]\mathbf{\Gamma}^{-1}(\mathbf{K} - \tilde{\mathbf{K}})^T] \tag{25}$$

$$- tr[(\mathbf{K} - \tilde{\mathbf{K}})\mathbf{\Gamma}^{-1}[\mu\|\mathbf{e}_y(t)\|\mathbf{K}_{Ie}, \quad \mathbf{0}, \quad \mathbf{0}]^T] \tag{26}$$

Using ASP property $\mathbf{PB} = \mathbf{C}^T$ and substituting $\mathbf{e}_y = \mathbf{C}\mathbf{e}_x$ and cancelling like terms

$$\dot{V}(t) = \mathbf{e}_x^T[\dot{\mathbf{P}} + \mathbf{P}(\mathbf{A} - \mathbf{B}\tilde{\mathbf{K}}_{ey}\mathbf{C}) + (\mathbf{A} - \mathbf{B}\tilde{\mathbf{K}}_{ey}\mathbf{C})^T\mathbf{P}]\mathbf{e}_x$$

$$- \mathbf{r}^T\bar{\mathbf{\Gamma}}\mathbf{r}\mathbf{e}_y^T\mathbf{e}_y - \mathbf{e}_y^T\mathbf{e}_y\mathbf{r}^T\bar{\mathbf{\Gamma}}\mathbf{r} \tag{27}$$

$$- 2tr[(\mathbf{K} - \tilde{\mathbf{K}})\mathbf{\Gamma}^{-1}[\mu\|\mathbf{e}_y(t)\|\mathbf{K}_{Ie}, \quad \mathbf{0}, \quad \mathbf{0}]^T] \tag{28}$$

Adding like terms and substituting ASP property from Equation (4.18)

$$\dot{V}(t) = -\mathbf{e}_x^T(t)\mathbf{Q}(t)\mathbf{e}_x(t) - 2\mathbf{e}_y^T(t)\mathbf{e}_y(t)\mathbf{r}(t)^T\bar{\mathbf{\Gamma}}\mathbf{r}(t) - 2tr[(\mathbf{K}_I - \tilde{\mathbf{K}})\mathbf{\Gamma}^{-1}[\mu\|\mathbf{e}_y(t)\|\mathbf{K}_{Ie}, \quad \mathbf{0}, \quad \mathbf{0}]^T] \tag{29}$$